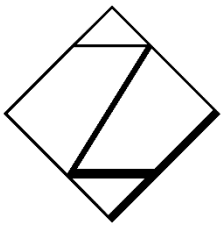

Westsächsische Hochschule Zwickau
University of Applied Sciences

nanolab

Characterization of a novel method to coat 2- and 3-dimensional surfaces with photoresist

Masterthesis

Issued: 03.12.2021

Submitted: 02.05.2022

Author:	Benedikt Vatter
Matriculation number:	35538
Institute:	Physikalische Technik/Informatik
Course:	Nanotechnology
Course number:	191212
University:	Westsächsische Hochschule Zwickau- University of Applied Science Zwickau Am Kornmarkt 1, 08056 Zwickau
Primary Supervisor:	Prof. Dr. rer. nat. Daniel Schondelmaier
Second Supervisor:	Prof. Dr. rer. nat. Stefan Braun

Acknowledgment

I would like to thank everyone who contributed to this work.

Firstly, I would like to thank Prof. Dr. rer. nat. Daniel Schondelmaier for supervising this work and his helpful input in discussions.

Special thank go to Jens Saupe and Robert Heimburger for their introduction to this topic and helpful guidance at the beginning of my work.

I would also like to thank Dominik Weber for his support and Toni Junghans for helpful insights and contributions in discussion of this work.

Furthermore, I would like to thank my wife Nadine for her patience and support during this time, not to forget her parents Ines and Heiko and their support to our family.

Abstract

This work aimed to apply the Floating Film Transfer Method (FTM), developed by Kaneto et.al., as a new way of coating planar and nonplanar substrates with photoresist. Focus laid on the creation of a workflow to coat the substrate and process it by UV-Lithography and Nanoimprint lithography. Conventional coating methods like spin-, spray- or dip coating are well established in today's industry but are limited in their capabilities to coat curved and structured surfaces. FTM offers the possibility to overcome these limitations. Therefore, two negative resists AR-N-4400 and AR-N-4600-10 as well as two positive resists AR-P-3110 and AZ-MIR 701 were drop cast on deionized water. The resist spreads into a thin film that can be transferred to a planar or curved substrate. Profilometric and ellipsometric measurements were conducted to evaluate the topography of the resist. A non-uniform thickness distribution was found depending on the resist and parameters like solid content, water temperature, and the amount of surfactant. UV-Lithography and Nanoimprintl ithography were successfully performed with these films. Resolutions as low as 2,3±0,4 µm were achieved by UV-Lithography of AR-P-3110. A periodic pattern with a pitch of 1,51 µm was transferred by thermal nanoimprint lithography to AR-N-4400-10. As proof of concept Laser Direct Writing was performed to structure AZ-MIR 701coated on a glass vial.

Table of contents

TABLE OF CONTENTS ..... **I**

FIGURE INDEX ..... **III**

TABLES ..... **V**

LIST OF ABBREVIATIONS ..... **VI**

LIST OF SYMBOLS ..... **VII**

1 MOTIVATION ..... **- 1 -**

2 STATE OF THE ART ..... **- 3 -**

2.1 Chemistry behind Photoresists ..... - 3 -
2.1.1 Positive resist ..... *- 3 -*
2.1.2 Negative Resists ..... *- 5 -*
2.1.3 Development ..... *- 5 -*
2.2 Resist Coating methods ..... - 7 -
2.2.1 Spin-Coating ..... *- 7 -*
2.2.2 Solution-based Spray-Coating ..... *- 9 -*
2.2.3 Dip-Coating ..... *- 11 -*
2.2.4 Langmuir-Blodgett ..... *- 12 -*
2.3 Nanoimprint and UV-Lithography ..... - 13 -
2.4 Marangoni-Effect and Floating Film Transfer Method ..... - 14 -

3 EXPERIMENTAL ..... **- 19 -**

3.1 Substrate preparation ..... - 19 -
3.2 Coating methods ..... - 19 -
3.3 Preliminary examination ..... - 22 -
3.3.1 Resist choice ..... *- 22 -*
3.3.2 Casting tool ..... *- 23 -*
3.3.3 Determination of lithographic process parameters ..... *- 23 -*
3.4 Sample preparation with varying FTM process parameters ..... - 25 -
3.4.1 Variation of the Water temperature ..... *- 25 -*
3.4.2 FTM with a variety of Photoresists ..... *- 26 -*
3.4.3 Variation of the surface tension ..... *- 26 -*
3.4.4 Preparation of hydrophobic and hydrophilic samples ..... *- 27 -*
3.5 Fabrication of nonplanar FTM coated Samples ..... - 29 -
3.5.1 FTM coats as a protection layer for microstructured substrates ..... *- 30 -*
3.5.2 NIL on planar and nonplanar substrates ..... *- 30 -*
3.5.3 Process parameter for UV-Lithography on nonplanar substrates ..... *- 32 -*
3.6 Characterization methods ..... - 32 -
3.6.1 Profilometry ..... *- 32 -*
3.6.2 Ellipsometry ..... *- 34 -*
3.6.3 Contact angle measurement ..... *- 35 -*
3.6.4 Light microscopy and focus stacking ..... *- 35 -*

4 RESULTS AND DISCUSSION ..... **- 37 -**

4.1 Depiction of the Film formation process ..... - 37 -
4.2 Results from preliminary examinations ..... - 39 -

4.2.1 Choice of resists ..... *- 39 -*
4.2.2 Choice of casting method ..... *- 40 -*
4.2.3 Determination of lithographic process parameters ..... *- 41 -*
4.3 CHARACTERIZATION OF THE FILM FORMATION UNDER VARIOUS CONDITIONS ..... - 49 -
4.3.1 Temperature influence ..... *- 49 -*
4.3.2 Resist influence ..... *- 53 -*
4.3.3 Influence of Surfactants on the Film ..... *- 59 -*
4.3.4 Impact of the substrate surface energy on the coating mechanism ..... *- 61 -*
4.4 FTM ON NONPLANAR SAMPLES ..... - 63 -
4.4.1 FTM coat as a protection layer ..... *- 63 -*
4.4.2 NIL on nonplanar surfaces ..... *- 65 -*
4.4.3 UV lithography on nonplanar substrates ..... *- 71 -*

5 SUMMARY ..... - 72 -

5.1 FTM FILM MORPHOLOGY ..... - 72 -
5.2 UV-LITHOGRAPHY AND NIL ..... - 73 -
5.3 ADVANTAGES AND DISADVANTAGES ..... - 74 -

6 OUTLOOK ..... - 75 -

REFERENCES ..... - 76 -

Figure Index

Figure 1: Positive and negative image after UV-Lithography on a Si substrate (reproduced from [25, p. 34]) ..... - 4 -
Figure 2: Süss-reaction mechanism of DNQ after UV exposure. I) release of Nitrogen after absorption, II) intermediate radical, III) Wolff rearrangement to a ketene and IV) reaction with H_2O to form a carboxlyc acid (reproduced from [24]) ..... - 4 -
Figure 3: a) 2-(4-Methoxystyryl)-4,6-bis-(trichloromethyl)-1,3,5-triazine and b) Triphenylsulfonium triflate as an example for a photosensitive acid generator (PAG) ..... - 5 -
Figure 4: Form of the sidewall after exposure and development. Positive resists show an overcut whereas negative resists show an undercut caused by the reduced absorption towards the bottom of the resist (reproduced from [1, p. 684]). ..... - 6 -
Figure 5: Schematic of the spin coating process. a) deploying the solution on the substrate b) spin-up phase c) spin-off phase d) finished thin film. Evaporation of the solvent in every stage. (reproduced from [30, p. 287]). ..... - 8 -
Figure 6: a) Spin curve for SU8-50 and SU8-100. b) Expected film thickness for certain viscosity and spin speed of SU8. Images were taken from [33, p. 2] ..... - 9 -
Figure 7: Increase in resist thickness with increasing radial position on a curved substrate with 20 mm curvature (reproduced from [5]) ..... - 9 -
Figure 8: a) Spray coating process with a nozzle and Nitrogen as carrier gas. b) Pattern of the nozzle movement above the wafer. Images were taken from [34, p. 3] ..... - 10 -
Figure 9: Spray coated AZ4999 a) after deposition and b) after softbake. high temperatures allowed the resist to flow and accumulated at the bottom (reproduced from [34, p. 4]) ..... - 10 -
Figure 10: Dip coating process for flat substrates. The substrate is immersed in a tank of photoresist. Controlled withdrawal at constant or varying speed generates desired thicknesses. Optional rotating during withdrawal can enhance thickness uniformity (reproduced from [36]) . ..... - 11 -
Figure 11:Langmuir film formation. a) Self orientation of an amphiphilic substance on liquid. Compressing the bars to form a closed monolayer. b) Langmuir-Blodgett method to transfer several monolayers to a hydrophilic substrate. c) Coating mechanism of a define amount of monolayers (reproduced from [11]) ..... - 12 -
Figure 12: Process steps for thermal nanoimprint lithography (t-NIL). a) positioning the stamp/mold on the coated substrate, b) applying heat and additional pressure to transfer the pattern, c) cooling and demolding (reproduced from [39, p. 11]) ..... - 13 -
Figure 13: Surface tension at the interface of oil, water and air (reproduced from [41, p. 83]). ..... - 15 -
Figure 14: Visiualization of the marangoni effect as proposed in [43]. A bowl of water with pepper a) before adding soap b) in the middle of the spreading and c) the end result ..... - 15 -
Figure 15: FTM process to create thin poly[2,5-bis(3-tetradecylthiophen-2-yl)thieno[3,2-b]thiophene] (pBTTT C-14). a) schematic of the spreading process, b) photography of the process in a petri dish at 0 s, 1/8 s and 1/4 s and c) self ordering mechanism of the polymer (reproduced from [13]) ..... - 16 -
Figure 16: Parameter effecting the alignment during FTM measured by a) Absorption spectrum and DR at varying solid contents, b) absorption spectrum and DR at varying liquid substrate temperatures, c) film thickness and DR at varying viscosity of the liquid substrate and d) absorption spectrum and DR at varying annealing temperatures (reproduced from [46]). ..... - 18 -
Figure 17: Schematic of the FTM process in this work. a) submerging the substrate under water and drop casting a single resist drop, b) formation of a thin resist film, c) coating the substrate by lowering the water level and d) drying in a vacuum oven. ..... - 20 -
Figure 18: a) Result of placing the resist on a 95°C hotplate for tempering and b) uniform resist film after drying in the vacuum oven for 2 h at 40 °C. ..... - 21 -
Figure 19: a) Temperature profile of the drying process in a vacuum oven for 2 h with an end temperature of 40 °C. b) Roughness R_Q of FTM coated AR-N-4600-10 on microscope slides at 4 different dry times. ..... - 22 -
Figure 20: Preparation steps to fabricate a Dynasylan solution ready to coat on Si-substrates as proposed in [50, p. 122]. Instead of a mesh Si wafer slices were used. ..... - 28 -

Figure 21: Chemical reaction to coat Dynasylan on Si substrates."First the silane (Dynasylan® R8261) undergoes hydrolysis reaction in the presence of an acid (HCl in our study) to produce silanol and three moles of ethanol. Then, three silanol molecules condense, and two moles of water is produced. […] [In] this stage, hydrogen bonds form between the oxygen and hydrogen molecules on hydroxyl groups and those on the adsorbed silanol molecules. Finally, upon heating, covalent bonds are formed (grafted) between the silane and SS surface". Reproduced from [50, p. 124] ..... - 29 -
Figure 22: Temperature profile for t-NIL process, imprinting a lens array coated with AR-N-4600-10 ..... - 31 -
Figure 23: Profilometer measurement on a Si wafer. Thickness and roughness obtained from a length of 500 µM in compliance with ISO 4287 and ISO 4288. ..... - 34 -
Figure 24: Resistor through hole soldered on a PCB a) before and b) after focus stacking, colorized to increase 3D character ..... - 36 -
Figure 25: Resist film AR-N-4600-10 after a) drop cast on deionized water and b) coating on a 4" Si wafer and drying for 2 h at 40 °C in a vacuum drying oven. ..... - 37 -
Figure 26: a) Source zone, transparent zone and outer zone as observed from Rochê et.al. b) Locally resolved radial velocity u as a function of radius r. (reproduced from [49, p. 3]) ..... - 38 -
Figure 27: First successful pattern transfer via UV-Lithography with FTM coated AR-N-4400-05 on a microscope slide. ..... - 39 -
Figure 28: Consistency in drop volume generation by Eppendorf and fine dosing syringe ..... - 40 -
Figure 29: Microscopic Images of structures after development with various Acetone:DI Water concentrations. Development time: 2 min. UV dose 250 mJ/cm² ..... - 42 -
Figure 30: Development of AR-N-4600-10 in 8:1 Acetone :DI-H_2O after exposure with varying doses of a) 100 mJ/cm², b) 250 mJ/cm² and c) 500 mJ/cm² ..... - 43 -
Figure 31: Development results of AR-N-4400-05 at varying concentration and t_{DEV}. ..... - 44 -
Figure 32: Development result for AR-N-4400-10 at t_{DEV}= 2 min 30 s, 4 min, and 8 min. ..... - 45 -
Figure 33: Development of AR-P-3110 in AR-300-47 5:1 after t_{DEV} =30 s, 45 s, 60 s and 75 s. ..... - 46 -
Figure 34: a) Line width measurement of row 1 to 5. b) measurement spots on row 1 to 5(left to right) of sample 1 with AR-P-3110. ..... - 47 -
Figure 35: Average line width d of AR-P-3110 at varying t_{DEV} ..... - 47 -
Figure 36: 3D Plot and derived line profile of lines fabricated by UV-Lithography of AR-P-3110. ..... - 48 -
Figure 37: Smallest achieved structure for each resist and maximum resolution according to Allresist [48]. ..... - 48 -
Figure 38: Si wafer FTM coated with AR-N-4600-10 at a) T_{H2O}=21 °C and b) T_{H2O}=40 °C. Red circle injection zone, yellow circle inner zone blue square outer zone. ..... - 50 -
Figure 39: Microscopic images of a) sample 1 and b) sample 2. c) and d) are and contour plots derived from profilometric measurements for each temperature T_{H2O} and e) and f) show the corresponding roughness plots. ..... - 50 -
Figure 40: Thickness distribution of AR-N-4600-10 at T_{H2O}=21°C measured by ellipsometry without UV-Lithography. - 51 -
Figure 41: Topographic profile a) spin coated AR-N-4600-10 as well as b) FTM coated AR-N-4600-10 at 21 °C and c) 40°C water temperature measured by profilometry. ..... - 52 -
Figure 42: a) Surface tension oscillation and b) surface velocity oscillation over time caused by Marangoni instability (reproduced from [57, p. 1432]) ..... - 53 -
Figure 43: Images and thickness distribution of 3 FTM coated AR-N-4400-05 samples on 4" Si wafer. ..... - 54 -
Figure 44: Minimum, maximum and average thickness of FTM coated AR-N-4400-05. ..... - 55 -
Figure 45: 3D Map of AR-N-400-10 measured by DektakXT. Area: 300x300µM resolution: 5µM/trace ..... - 56 -
Figure 46: Images and thickness distribution of 3 FTM coated AR-N-4400-10 samples on 4" Si wafer. ..... - 57 -
Figure 47:a) AR-P-3110 before and after UV-Lithography, b) contour plot derived from Dektak measurements.. - 58 -
Figure 48: 3D-Map of AR-P-3110 over 300x300µM and height distribution along the black arrow derived from Profilometer measurement. ..... - 58 -
Figure 49: 3D-Map of AR-P-3110 and extracted line profile with visible oscillation. ..... - 59 -

Figure 50: Images and Height distribution gained from ellipsometric and profilometric measurement of FTM coated AR-N-4600-10 with surfactant ("Fit").. ..... - 60 -
Figure 51: a) Contact angle measurement on Si with Dynasylan confirming the hydrophobic character. b) FTM coated AR-N-4600-10 on a Dynasylan coated Si substrate after tempering at 95 °C on a hotplate...... - 61 -
Figure 52: Contact angle measurement on a TiO_2 sample without UV exposure and after 20 min UV exposure...... - 62 -
Figure 53: UV-exposed TiO_2 coated with AR-N-4600-10 after UV-Lithography. ..... - 63 -
Figure 54: Proposed mechanism of coating edges with FTM resulting in a uniform coat..... - 64 -
Figure 55: Microstructure in AR-P-3220 coated with AR-N-4600-10 after exposure and development, a) without defects caused by the developer and b) structure with visible development. ..... - 64 -
Figure 56: Topology of the wall of the square structure with 10,4 µM thick AR-P 3220...... - 65 -
Figure 57: a) Nanoimprinted Si wafer with 1,5µM pitch and visible rainbow effect caused by the pattern. b) Profilometer measurement confirming a 1,5 µM pattern...... - 66 -
Figure 58: FTM coated Glass lens with AR-N-4600-10. The resist is strong enough to create a hollow space over several mm without tearing. Wrinkles are visible indicating stress caused by deformation. ..... - 67 -
Figure 59: a) Lens coated with AR-N-4600-10 imprinted with holographic structure. Image is stitched together from eight pictures at 5-x magnification. b) Distorted dot pattern after radiating through the lens with a green laser beam...... - 67 -
Figure 60: a) PDMS master stamp with a holographic pattern. b) Imprinted pattern in AR-N-4600-10. Black rectangles show the same pattern...... - 67 -
Figure 61: Lens array coated with AR-N-4400-10 and visible imprinted hologram. b) Bessy Logo and c) dot grid visualized by radiating through the lens with a green laser beam...... - 68 -
Figure 62: a) Stacked microscopic image showing the periodic pattern in AR-N-4400-10. The inlet image displays the FFT of the image used to measure the pitch to 1,51 µM. b) Interference pattern after radiating through the lens with a green laser beam. c) Original height data acquired by profilometry and circle fit to determine the radius of the lens. d)..... - 70 -
Figure 63: Height profile after curvature subtraction derived from Figure 62 c). The inlet shows the periodic pattern observable over the entire length...... - 70 -
Figure 64: 3D Map of the lens array FTM coated with AR-N-4400-10 and imprinted with a periodic 1,5 µM pattern. (Pattern might not be visible in the printed version)..... - 71 -
Figure 65: a) AR-P 3110 FTM coated on a lens array and processed by UV-Lithography in contact mode. b) Amber glass vial FTM coated with AZ MIR 701 and processed by Direct Laser writing. ..... - 71 -

Tables

Table 1: Determination of process parameters for UV-Lithography..... - 24 -
Table 2: Process parameters 21°C and 40°C..... - 25 -
Table 3: Process conditions for FTM and UV-Lithography..... - 26 -
Table 4: Process parameter of surface modified samples ..... - 28 -
Table 5: Processing conditions creating microstructured sample..... - 30 -
Table 6: Process parameters for t-NIL..... - 31 -
Table 7: DektakXT measurement settings..... - 33 -
Table 8: Min, Max and Avg Thickness and Roughness of each Resist..... - 73 -

List of abbreviations

Abbreviation	Meaning
ArF	Argon fluoride
CAR	Chemically amplified resist
DI	Deionized
DNQ	Diazonaphthoquinone
EUV	Extreme ultraviolett
FTM	Floating film transfer method
GBL	Gammabutylacton
H_2O	Water
MEMS	Micro-electro-mechanical system
NaOH	Sodium hydroxide
N_2	Nitrogen
PAG	Photo-activated acid generator
PEB	Post exposure bake
PMA/PGMEA	1-methoxy-2-propyl-acetate
PMMA	Poly(methyl-2-methylpropenoate)
Si	Silicon
SiO_2	Silicon dioxide
TiO_2	Titanium dioxide
t-NIL	Thermal Nanoimprint Lithography
TMAH	Tetramethyl-amonium hydroxide
UV	Ultraviolett
UV-NIL	Ultraviolett Nanoimprint Lithography

List of symbols

Abbreviation	Meaning	Unit
c	Concentration	Wt-% or Vol-%
C_P	Heat capacity	J/K
d	Linewidth	nm
DR	Dichroic ratio	/
D_{UV}	UV-dose	mJ/cm^2
I	Absorption	%
n	Refractive index	/
$N_{1/2/3}$	Cauchy coefficients	/
P	Resist thickness	nm
R_q	Root mean square roughness	nm
r	Radial position	mm
R	Curvature	mm
Q_a	Flow rate	µL/s
s	Standard Deviation	nm
T_{H2O}	Water temperature	°C
T_{Oven}	Oven temperature	°C
T_{PEB}	PEB temperature	°C
t_{PEB}	PEB time	min
t_{Dev}	Development time	min
t_{Oven}	Tempering time	h:min
t_{UV}	UV-exposure time	s
u	Radial velocity	m/s
V	Volume	m^3
X,Y,Z	Coordinates	mm,mm,nm
λ	Wavelength	nm
η	Viscosity	mPa*s
ω	Angular velocity	RPM
ρ	Density	g/cm^3
σ	Surface tension	N/m
θ	Angle	°

1 Motivation

Fabrication of integrated circuits, circuit boards, or displays relies heavily on lithographic processes. One key part of this process is the photoresist, a photosensitive material used for patterning structures and traces or as a component in micro-electro-mechanical systems (MEMS) [1].

The history of photoresists can be traced back to the early 19th century with the invention of photography. Joseph Nicéphore Niépce used Bitumen of Judea to create an image of his courtyard[1]. More light-sensitive materials like dichromate gelatin discovered by William Henry Fox Talbot paved the way to the success of photography and photolithography. Unfortunately, gelatin did not prove to be resistant to etching. It became apparent that light-induced crosslinking and polymerization of etch-resistant materials is the key to manufacturing integrated circuits. On behalf of Bell Laboratories development of resist materials at Kodak started, leading to the formulation of Kodak Thin Film Resist. This mix of bis-azide and low molecular weight rubber was the working horse of the industry for nearly 2 decades until 1972 a combination of novolac and diazonaphthoquinone (DNQ) hit the market quickly changing the entire industry [2]

Novolac-based resins are still in use today however shrinking transistor sizes and increased requirements in resolution as well as the development of MEMS and nanopatterning technologies led to a variety of different manufacturers and resists. The chemical composition of the resist must be fine-tuned to the process in question [3]. In 2019 a bad batch of resist caused 550 Mio USD damage to a production site of TSMC which shows how important it is to carefully select and process the resist [4].

Up until today, most substrates coated with photoresist must be planar due to limitations in the coating process. Spin coating as the most prominent coating technique leads to striations and inhomogeneous thickness on nonplanar substrates [5]. Technologies like spray coating or electrodeposition might show better results but inhere limitations as well. Spray coating of thin

[1] Exposure to sunlight took at least 8 hours. The original photo is displayed in the Harry Ransom Center/University of Texas, Austin, Texas.

films shows poor uniformity. Electrodeposition typically requires conducting substrates and special photoresists limiting the application[6–8]. With Langmuir-Blodgett precise and uniform coatings can be achieved but the experimental conditions must be controlled precisely and thicker layers require several repetitions, therefore, increasing the chance for defects and processing time [9–11].

In this work, planar and nonplanar substrates are coated with photoresist by the floating film transfer method (FTM). First introduced in 2009 by Morita et.al. this technique promises to create a uniform polymer film on a liquid substrate [12–14]. Jens Saupe and Robert Heimburger developed the idea to use photoresist as a polymer solution. This photoresist film will be transferred to solid planar and nonplanar substrates.

This work aims to show the morphology and UV-Lithographic performance of the resist after FTM. Several positive and negative resists will be examined. These findings will be used to coat nonplanar substrates. Patterning of those substrates will be performed by Nanoimprint lithography pathing the way for future applications such as improving the optical properties of glass lenses.

2 State of the Art

In this chapter, common and established coating methods will be presented. The advantages and disadvantages of the different methods will be discussed, especially regarding coating nonplanar surfaces.

2.1 Chemistry behind Photoresists

A photoresist, or short resist, is a composition of polymers and other chemicals sensitive to light exposure. It is mostly used in semiconductor technology to transfer patterns and fabricate integrated circuits by UV-Lithography. Exposure to the UV regime requires special light sources. In the past wavelengths in use were the the g-, h- or i-line (436 nm, 407 and 404 nm and 365 nm) of a mercury lamp [2,15]. With shrinking nodes, smaller wavelengths were needed and industry switched to the 193 nm wavelength produced by ArF excimer lasers. Recent advances lead to even smaller wavelengths of 13,5 nm applied in commercial products like the ASML system Twinscan NXE:3600D [16]. Special lasers vaporize small tin drops and start a plasma that irridates EUV-light [17]. Besides UV-Lithography direct laser writing, e-beam lithography or nanoimprint lithography gained more and more attention in recent years [18–22]. Multitude and complex photoresists each specifically developed for different technologies are in existence. Therefore, only a small excerpt of the products will be presented since the focus in this work lies on solvent-based positive and negative photoresists sensitive to the g-h- and i-line.

2.1.1 Positive resist

Two main principles in pattern transfer can be distinguished: negative and positive imaging (see Figure 1). In the case of positive resists solvability after exposure is enhanced leaving only unexposed portions resulting in a positive image. Typical positive resists contain a resin called novolac, a photoactive substance like diazonaphtoquinone sulfate (DNQ), and solvent. The chain length of the resin is dependent on the polymerization process. An acid-catalyzed

condensation of phenol compounds with an aldehyde results in a resin with varying chain length and side chains. This effects adhesion on the substrate and the desired properties of the resist during and after processing such as dark erosion or glass transition temperature. DNQ is a photosensitive substance and raises the solvability of the resist after exposure by 3 to 4 orders of magnitude [15, p. 7]. UV absorption results in the release of nitrogen and the formation of a carboxylic acid called Süss reaction which is responsible for the increased solvability. Solutions are commonly solved in an organic solvent like 1-Methoxy-2-propyl-acetate (PMA or PGMEA) with viscosities matched to the desired thickness of the resist after coating [15,23,24].

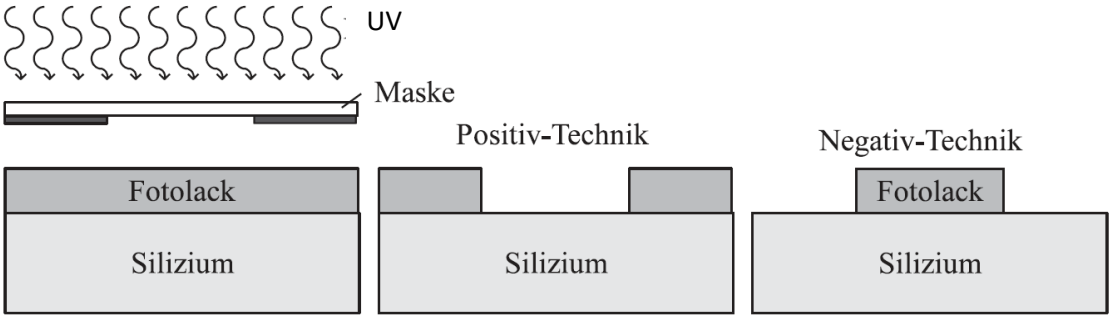

Figure 1: Positive and negative image after UV-Lithography on a Si substrate (reproduced from [25, p. 34])

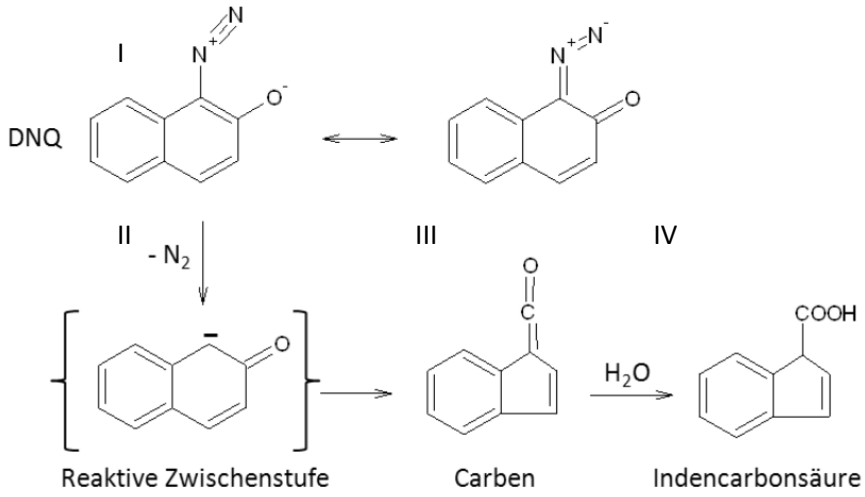

Figure 2: Süss-reaction mechanism of DNQ after UV exposure. I) release of Nitrogen after absorption, II) intermediate radical, III) Wolff rearrangement to a ketene and IV) reaction with H_2O to form a carboxlyc acid (reproduced from [24])

2.1.2 Negative Resists

In contrast to the discussed positive resist a negative image will be achieved after exposure and crosslinking of a negative resist. Negative resists contain the following components: a resin (novolac, PMMA), a photo-activated acid generator (PAG), and a crosslinking agent. UV-light is absorbed by the PAG (examples shown in Figure 3) and forms an acid. The absorption can be enhanced by absorption amplifiers like metal nanoparticles or by integrating the PAG in the polymer chain of the resin. A better conversion rate of photons along with enhanced sensitivity can be observed and exposure time can be reduced [3]. Under heat, the acids crosslink with crosslinking agents like melamine in chemically amplified resists (CAR) introducing an additional step called post-exposure bake (PEB). Precise control of PEB time and temperature is mandatory to achieve the highest resolution. The solvability of crosslinked resist after PEB is dramatically lowered [15].

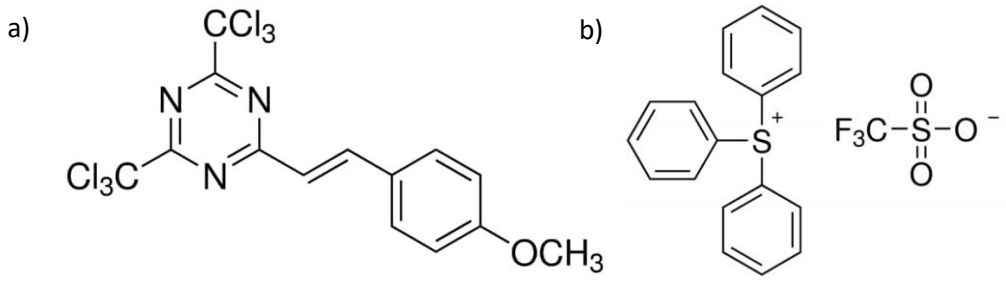

Figure 3: a) 2-(4-Methoxystyryl)-4,6-bis-(trichloromethyl)-1,3,5-triazine and b) Triphenylsulfonium triflate as an example for a photosensitive acid generator (PAG)

2.1.3 Development

Development after exposure and optional PEB is done in a liquid or aqueous solution. Developers can be distinguished into two categories: developers with metal ions like NaOH-based aqueous solutions and metal ion free developers like organic solutions e.g. acetone-based

developers or tetramethyl ammonium hydroxide (TMAH). In positive resists DNQ acids deprotonate the resin increasing the solvability whereas in negative resist solvability of unexposed regions is sufficient. Key parameters to guarantee good results are developer concentration, development time, temperature, and degradation of the developer after time and usage. Careful choice of photoresist in combination with precise tuned exposure, softbake, postbake, and development is key to fabricate small and high-resolution structures[15,24]. The form of the developed structure depends on the type of resist (see Figure 4). Positive resists show sidewalls with slopes less than 90° or overcut whereas an undercut can be observed for negative resists [1, p. 684].

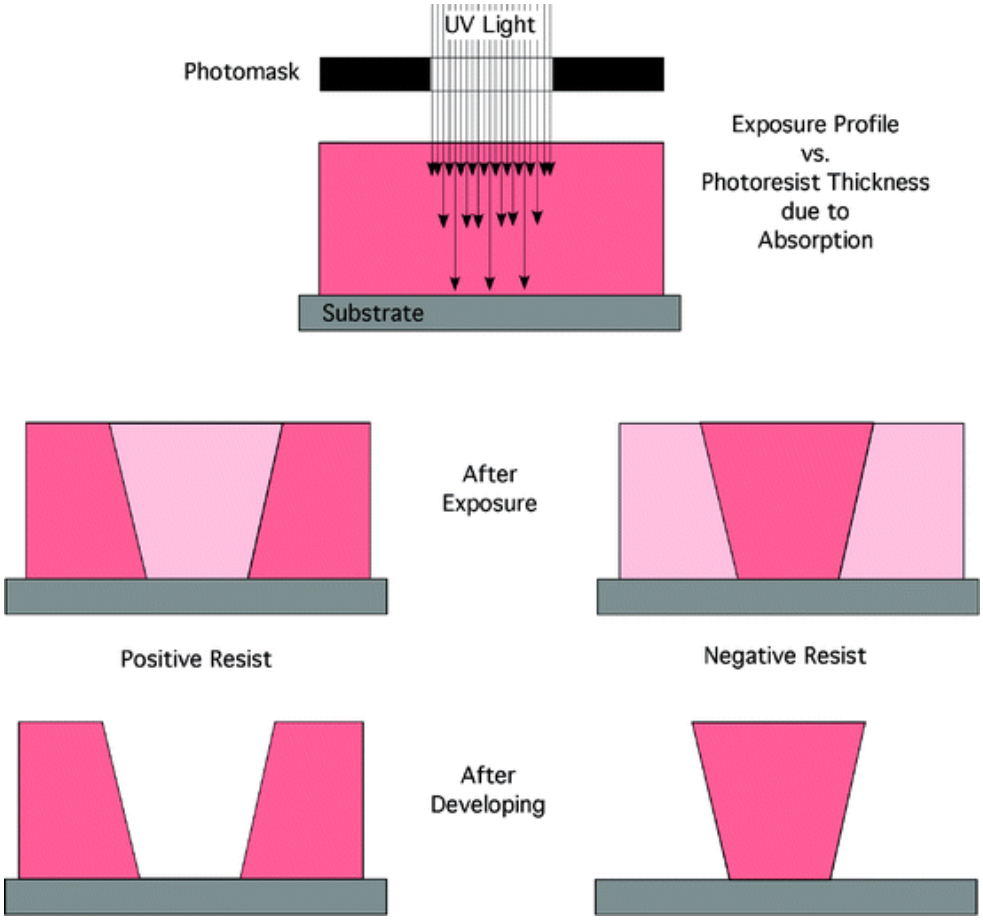

Figure 4: Form of the sidewall after exposure and development. Positive resists show an overcut whereas negative resists show an undercut caused by the reduced absorption towards the bottom of the resist (reproduced from [1, p. 684]).

2.2 Resist Coating methods

In the previous part, the chemical composition of photoresists and reactions after UV exposure were presented. The development process was depictured. Now techniques to coat substrates with said photoresists will be presented.

2.2.1 Spin-Coating

The method of choice for coating planar substrates is spin-coating. It is widely used in research and industrial environments [26–28]. An illustration of the process is shown in Figure 5. The substrate is attached to a spinning vacuum chuck and a polymer solution, e.g. photoresist is applied by dispensing it in the center of the spinning substrate (Figure 5 a). Rotational forces spread the resist evenly over the whole substrate (Figure 5 b and c) and allow high conformity of resist thickness over the whole substrate. Variation of thickness is possible by changing the viscosity of the resist as well as by variation of the spinning speed and time and temperature. In [29], Chen et. al. discuss the most critical parameters and determine an expression for calculating the film thickness P:

$$P = k' \cdot \omega^{\alpha} \cdot \eta^{\beta} \cdot \left(\frac{E \cdot \lambda}{C_p}\right)^{\gamma} \tag{1}$$

In formula (1) ω is the angular velocity, "k´ is an [experimental derived] proportionality constant, η is the viscosity of the initial solution, […] C_p is the heat capacity of the solvent, E is the average rate of evaporation and λ is the latent heat of evaporation" [30, pp. 288–289]. Typical values for α, β and γ are given in [30, p. 289] with α = -0,5 , β = 0,36 and γ = 0,6. According to formula (1), the film thickness decreases with higher angular velocity and evaporation rate and lower viscosity of the initial polymer solution. Manufacturers of photoresists typically provide values for certain viscosities and spin speed to achieve a specific film thickness. The spinning curve (film thickness as a function of spin speed) for SU-8 50 and SU-8 100 is shown in Figure 6. The process, once all parameters are set, delivers "a highly controllable and reproducible film thickness"[26, p. 174] and is applicable for a wide range of commonly available photoresists. Best results are achieved with clean and planar surfaces. If the surface is covered with structures as deep as 10 µm (in some cases as high as 15 µm),

spin-coating can be used to apply photoresist. It is not suitable for substrates with deeply etched structures like v-grooves or etched through holes. Those structures are obstacles to the resist flow while spinning thus leading to defects like striation and variation of resist thickness [15]. Another problem is the concentration of photoresist at the bottom of grooves. In [31] Yu et.al. report failures of their device connected to poor coverage of the sidewalls thus not protecting the substrate during the etch process. To overcome these problems one can use polymer solution with high solid count and low viscosity as presented in [32]. These materials cover deep trenches and have good self-leveling attributes. However, the difference in film thickness makes it difficult to process small structures with photolithography. Regions with thick resist film might get underdeveloped while regions with thin resist film get overexposed leading to undesired problems during the etching process. Spin coating on curved substrates inheres also some Limitations. Resist thickness is nonuniform with increasing thickness at increasing radial position (see Figure 7). Feng et. al. formulated a limit for uniform thickness distribution by the ratio of radial position r and curvature R to r/R=0,816 [5]. Furthermore, spin-coating leads to small bumps at the edge of the wafer that need to be removed before exposure. Only 3% to 5% of the applied resist forms the film at the end of the spinning process. The rest will fly off the substrate. This leads to high costs and waste of resist and is problematic in regards to environmental aspects like material waste and recycling of the non-used resist for certain types of resists [15].

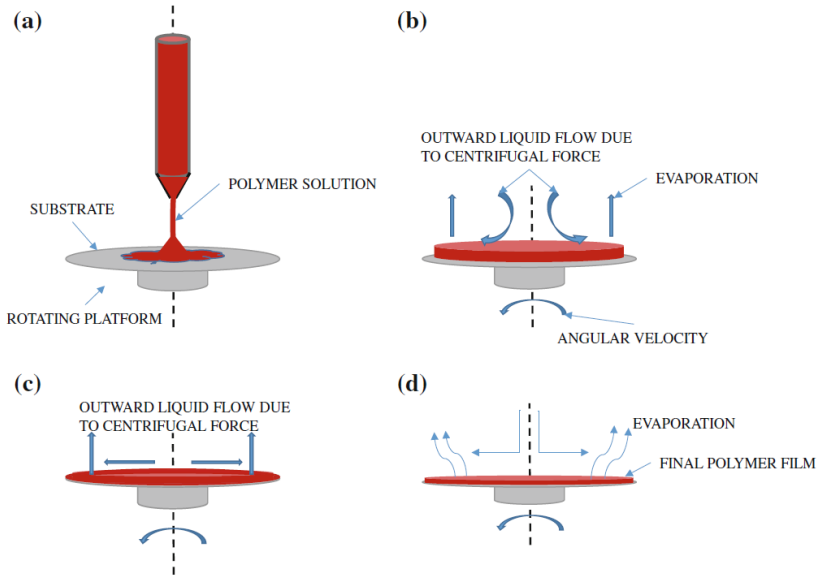

Figure 5: Schematic of the spin coating process. a) deploying the solution on the substrate b) spin-up phase c) spin-off phase d) finished thin film. Evaporation of the solvent in every stage. (reproduced from [30, p. 287]).

a)

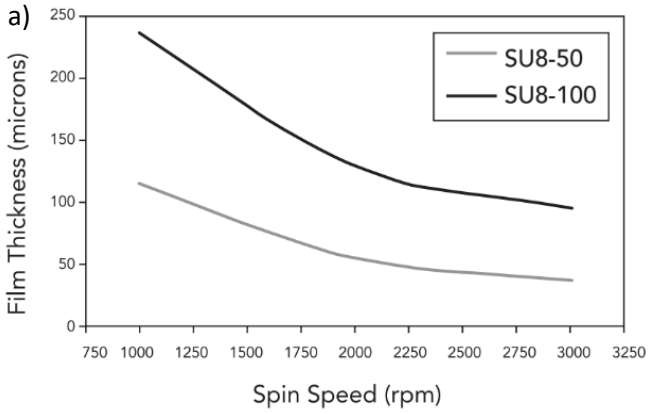

b)

PRODUCT	VISCOSITY cSt	THICKNESS microns	SPIN SPEED rpm
SU-8 50	12250	40	3000
		50	2000
		100	1000
SU-8 100	51500	100	3000
		150	2000
		250	1000

Figure 6: a) Spin curve for SU8-50 and SU8-100. b) Expected film thickness for certain viscosity and spin speed of SU8. Images were taken from [33, p. 2]

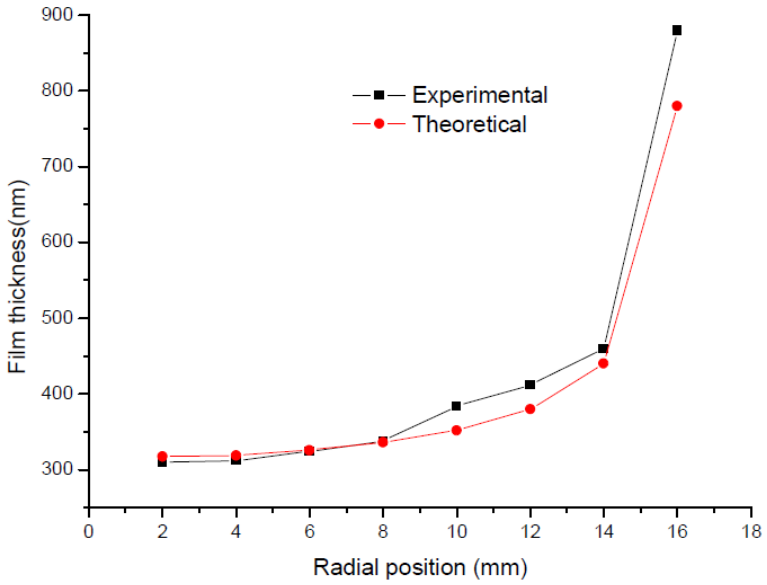

Figure 7: Increase in resist thickness with increasing radial position on a curved substrate with 20 mm curvature (reproduced from [5])

2.2.2 Solution-based Spray-Coating

To overcome the limitations of spin coating, especially when talking about 3D structured substrates, spray coating can be applied. The resist is atomized through a fin nozzle by

ultrasonic atomization and sprayed on the substrate. Nitrogen N_2 is commonly used as a carrier gas. The resist droplets with diameters in the range of µm land on the substrate and form a uniform film. This process is pictured in Figure 8 a). There are several ways of positioning and movement of the nozzle to achieve a uniform layer on the substrate. One example is given in Figure 8 b). It shows an example of the spray coating process and pattern used by SÜSS MicroTec Lithography GmbH [34]. In praxis, each process where spray coating is deployed needs its own test series, compared to spin coating where process parameters are often given by the manufacturer [1, p. 690].

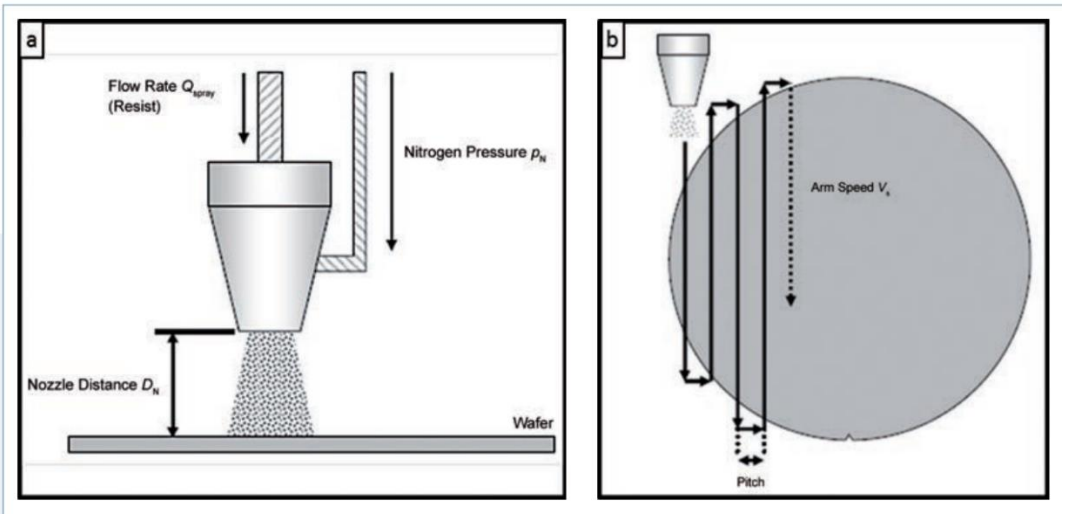

Figure 8: a) Spray coating process with a nozzle and Nitrogen as carrier gas. b) Pattern of the nozzle movement above the wafer. Images were taken from [34, p. 3]

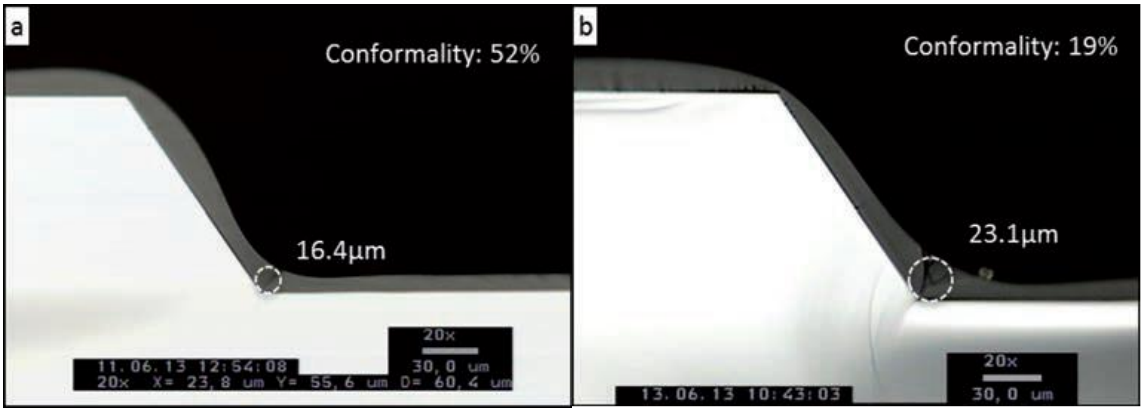

Figure 9: Spray coated AZ4999 a) after deposition and b) after softbake. high temperatures allowed the resist to flow and accumulated at the bottom (reproduced from [34, p. 4])

While in theory textured substrate can be coated in praxis nonuniform coatings are observed. Sidewalls are inhomogeneously covered and the resist thins out while accumulations at the bottom of the groove are observed (see Figure 9) [35]. To coat a closed film high amounts of resist are necessary. Thin films under 1 µm are hard to achieve. Low viscous resists will result in a smooth surface but increase the chance of uncoated edges while high viscous resists increase the roughness and negatively impact the UV-lithographic process [15,24].

2.2.3 Dip-Coating

In the case of dip-coating, the substrate is immersed inside a reservoir filled with resist. By moving it out slowly and controlled, the substrate gets coated with a thin and uniform film (Figure 10 a)). The method is regarded as easy to set up and maintain. Curved substrates can be coated by rotation during the withdrawal process as it is shown in Figure 10 b). Nevertheless, the withdrawal speed, as well as resist temperature, viscosity, ambient temperature, pressure, and the surface energy of the substrate, must be controlled precisely to achieve the desired thickness and repeatable results. Clean working environments and meticulously cleaned substrates are mandatory. Contaminations on the substrate or aggregation of particles in the resist solution can lead to pinholes and craters [36,37]

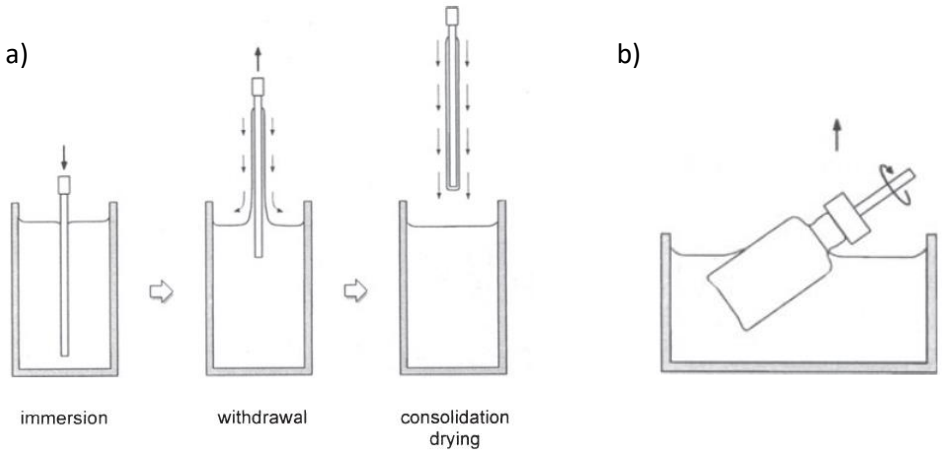

Figure 10: Dip coating process for flat substrates. The substrate is immersed in a tank of photoresist. Controlled withdrawal at constant or varying speed generates desired thicknesses. Optional rotating during withdrawal can enhance thickness uniformity (reproduced from [36]) .

2.2.4 Langmuir-Blodgett

The Langmuir-Blodgett method is a special way of coating, allowing it to create monolayers from a solution-based process. A definite amount of a solution is cast with a microsyringe on a liquid substrate like water. The liquid surface must be perfectly clean. Amphiphilic substances with hydrophilic and hydrophobic tails are often used. The solution quickly spreads and the solvent evaporates or diffuses into the liquid, leaving loose molecules on the surface. Two plates compress the surfaces molecules until the maximum surface tension is reached (Figure 11 a). The molecules thereby get condensed into a uniform monolayer. The monolayer can be transferred to a substrate by the Langmuir-Blodgett (vertical submersion) or Langmuir-Schäfer (horizontal stamping) method. During submersion, the hydrophilic or hydrophobic group connects to the substrate via physisorption depending on the surface energy and topology of the substrate (Figure 11 b). A second layer connects to the first monolayer when the substrate emerges. Repeating the process leads to a definite number of monolayers (Figure 11 c). Since only 10-20 Å are coated with each run it is a time-consuming process. The surface tension measured by the Wilhelmy plate method must be constant during the process. It was shown that this process can be successfully applied to DNQ and novolac-based photoresists [9–11].

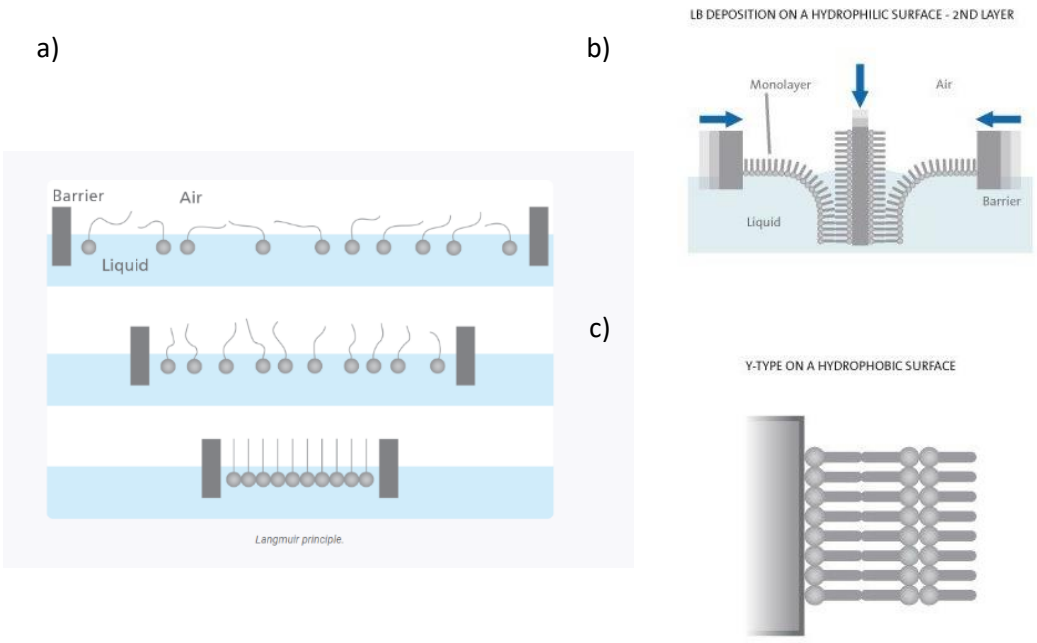

Figure 11:Langmuir film formation. a) Self orientation of an amphiphilic substance on liquid. Compressing the bars to form a closed monolayer. b) Langmuir-Blodgett method to transfer several monolayers to a hydrophilic substrate. c) Coating mechanism of a define amount of monolayers (reproduced from [11])

2.3 Nanoimprint and UV-Lithography

Two methods of structuring the resist were investigated in this work and will therefore be mentioned here: nanoimprint lithography (NIL) and UV photolithography.

Nanoimprint lithography

NIL can be performed in a variety of ways (thermal NIL, UV-NIL, thermal UV-NIL) but only thermal imprinting (t-NIL) was used in this work. The processes is shown in Figure 12The substrate is placed inside a nanoimprinting device at room temperature. After positioning the stamp on top of the coated substrate it is heated above the glass transition temperature of the resist. At this point, the resist can be formed and the structure from the mold is transferred to the resist. Additionally, pressure on top of the weight of the mold can be applied to support the imprinting process. After a defined retention time, typically in the range of minutes, the chamber is cooled down and the stamp can be demolded. The structure is now cast into the resist [38, pp. 215–232].

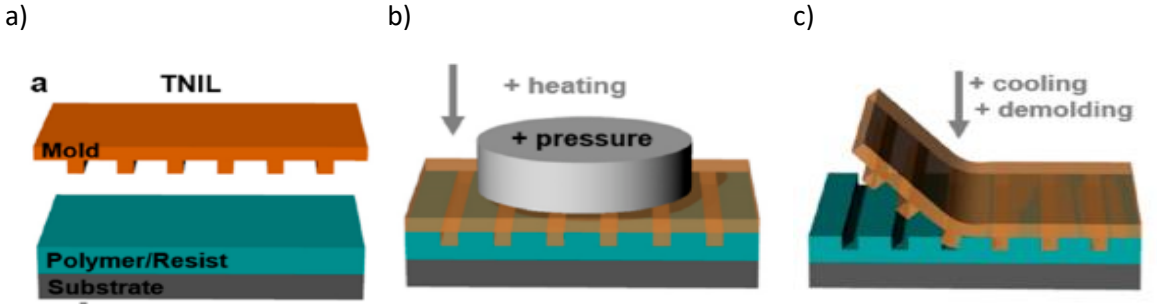

Figure 12: Process steps for thermal nanoimprint lithography (t-NIL). a) positioning the stamp/mold on the coated substrate, b) applying heat and additional pressure to transfer the pattern, c) cooling and demolding (reproduced from [39, p. 11])

UV-Lithography

UV-Lithography is a broadly used method to structure resist coated samples in the µm to nm scale. A softbake following before mentioned coating methods ensures a minimum amount of solvent remains in the resist. Since not only solvent but also water evaporates, a dehydration step for DNQ-based positive resist must be implemented. Softbake and Dehydration are crucial for high resolutions and require exact control of temperature and time. Substances in the resist like Diazonaphthoquinone (DNQ) in novolac-based positive resists absorb the light and lead to

increased solvability during a development step. In the case of negative resists crosslinking agents catalyze the crosslinking after exposure and a consecutive post exposure bake, resulting in a vastly reduced solvability. The resist is exposed to UV light typically to the i-, g-, and h-line of a mercury vapor lamp or in the case of Deep UV (DUV) to an excimer laser. Extreme UV (EUV) demands even more sophisticated light sources where tin droplets get evaporated by one laser and a plasma ignition is induced by a second pulsed laser. Parameters like wavelength λ, focus, exposure time t_{UV} , and dose D_{UV} effect the result and therefore must be precisely controlled. Pattern transfer can be achieved by using a photomask in direct contact or proximity mode or by a laser direct writing system. Following the exposure a post exposure bake (PEB) at a specific temperature TPEB for a period of time tPEB is necessary to enhance the photo-initialized crosslinking. Development of the exposed sample in perfectly matched developers like alkali-based NaOH solution (AZ 351B for AZ positive resists from Microchemicals) or TMAH (AR 300-47 developer for AR negative and positive resists from Allresist) leads to µm/nm thin patterns. More in-depth information on that topic and state-of-the-art lithography technologies[2] can be found in [16,25,38,40].

2.4 Marangoni-Effect and Floating Film Transfer Method

Inside a substance, each molecule interacts with its neighbor due to weak and strong forces like van der Waals forces or dipole-dipole interactions [41]. The molecular forces are in equilibrium as long as other molecules of the same type surround them. At phase boundaries like liquid-air or liquid-liquid, this equilibrium is disturbed. A net force occurs which leads to the phenomenon we call surface tension or interfacial tension (Figure 13). It is well known in nature and enables water striders to stay on top of a liquid surface and is the reason oil spreads on water [41]. According to equation (2) the surface tension can be calculated as:

$$\sigma_{WD} \cdot \cos\theta_1 = \sigma_{OD} \cdot \cos\theta_2 + \sigma_{WO} \cdot \cos\theta_3 \qquad (2)$$

[2] Introducing the world's first 2 nm node chip (333 Mio Transistor/mm^2): https://research.ibm.com/blog/2-nm-chip (14.04.2022 13:08)

Where σ_{WD} is the surface tension between water and air, $\theta_1$the angle enclosed by the water surface and the vector of σ_{WD}, σ_{OD} is the surface tension between oil and air, $\theta_1$the angle enclosed by the water surface and the vector of σ_{OD} , σ_{WO} is the surface tension between oil and water and $\theta_3$is the angle enclosed by the water surface and vector σ_{WO}. $\theta_2$determines whether a liquid spreads on a surface ($\theta_2 < 90°$) or dewetting occurs ($\theta_2 > 90°$) [41].

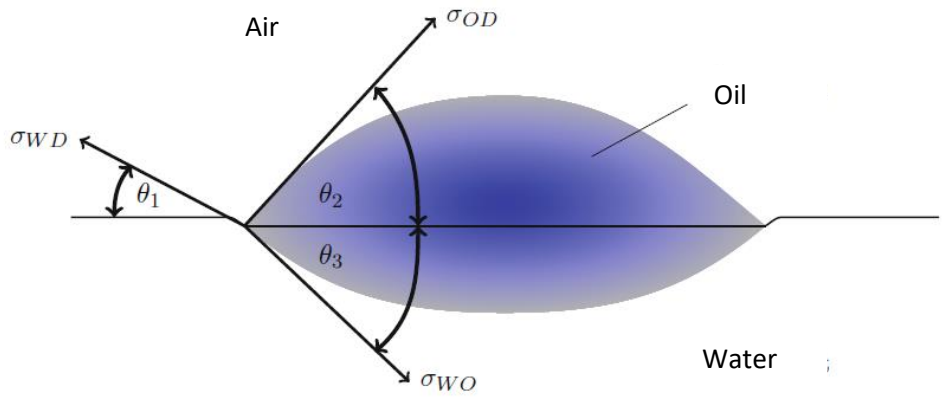

Figure 13: Surface tension at the interface of oil, water and air (reproduced from [41, p. 83]).

In the case of temperature or mass concentration gradient in a liquid, convection on the interface can be seen. This phenomenon was first described by James Thomson in 1855 [42] and later called Marangoni Effect named after the Italian physicist Carlo Giuseppe Matteo Marangoni. A concentration gradient leads to a surface tension gradient. Mass will flow towards regions of higher surface tension. The mass convection can be shown with a simple experiment. In a bowl of water pepper flakes spread out evenly on the surface. By adding one drop of dish soap (Fit) a concentration gradient occurs and moves the flakes omnidirectional to the edge of the bowl following the surface tension gradient [43].

a) b) c)

Figure 14: Visiualization of the marangoni effect as proposed in [43]. A bowl of water with pepper a) before adding soap b) in the middle of the spreading and c) the end result

This behavior was found to be very useful in creating thin, uniform, and self-organizing polymer films as described in [12,13,44,45]. Kaneto et.al. named their method Floating Film Transfer Method (FTM). They describe the process of coating substrates with thin polymer films like P3HT used in the production of organic transistors. A drop of the polymer solution is cast on a liquid substrate, here ethane-1,2-diol in a petri dish. Attributed to surface tension gradients Marangoni flow occurs and transports material away from the injection region, resulting in an evenly distributed thin film. The film is then transferred to a solid substrate by stamping. The film formation and self ordering process of poly[2,5-bis(3-tetradecylthiophen-2-yl)thieno[3,2-b]thiophene] (pBTTT C-14) on a mixture of ethane-1,2-diol and propane-1,2,3-triol as a liquid substrate is displayed in Figure 15. Depending on the polymer solution the shape of the film can be different. Starlike formations like in Figure 15 b) or circular shapes were observed.

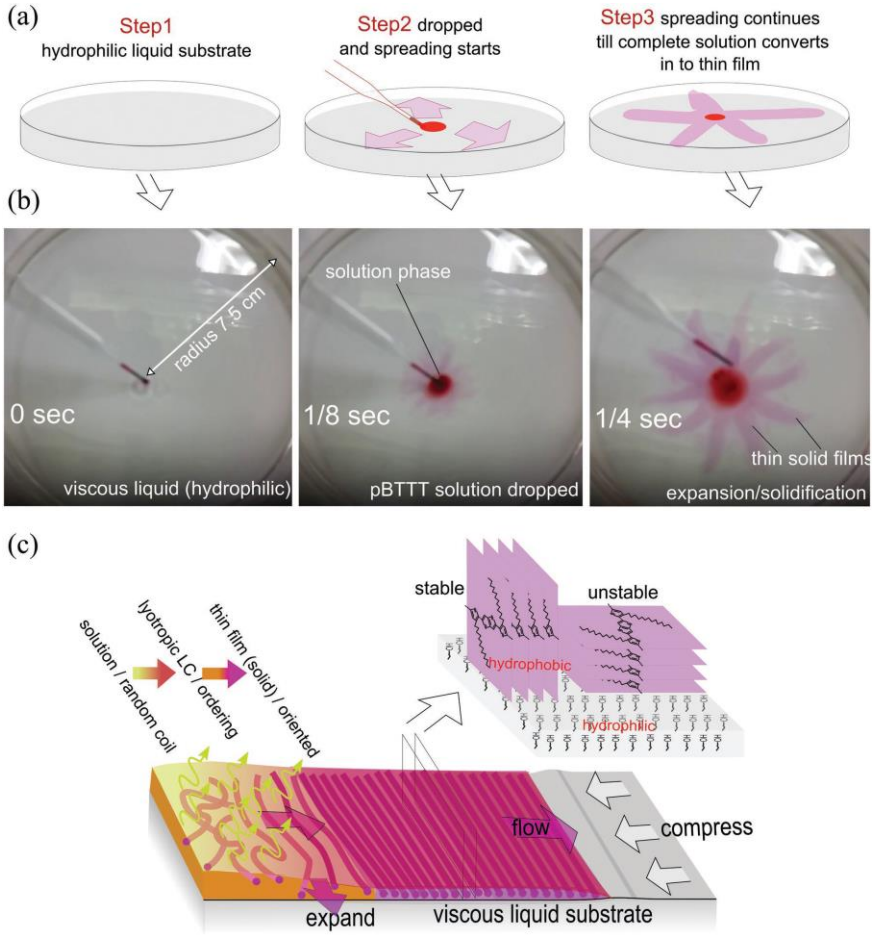

Figure 15: FTM process to create thin poly[2,5-bis(3-tetradecylthiophen-2-yl)thieno[3,2-b]thiophene] (pBTTT C-14). a) schematic of the spreading process, b) photography of the process in a petri dish at 0 s, 1/8 s and 1/4 s and c) self ordering mechanism of the polymer (reproduced from [13])

Pandey proposed that the alignment of the polymer chains is contributed to Marangoni flow-driven expansion and simultaneous compression due to the hydrophobic character of the polymer on a hydrophilic liquid substrate as pictured in Figure 15 c) [46]. Furthermore, he found that the alignment and thickness of the casted polymer correlate with the following parameters:

1. **Concentration of the polymer solution**: An increase in solid content inherently comes with a decrease in solvent. This results in rapid solidification by solvent evaporation and diffusion which hinders the spreading. Polymers with high solid content show less aligned chains and non-uniform surfaces. Too low solid content on the other hand hinders solidification also resulting in less aligned chains.

2. **Temperature of the liquid substrate:** Diffusion of solvent into the liquid substrate is enhanced at higher temperatures. With increased temperatures, shorter spreading can be observed due to shorter expansion periods.

3. **Viscosity of the liquid substrate:** Enhanced viscosity creates higher compression forces on the polymer and therefore increases the thickness of the film.

4. **Annealing temperature:** The rearrangement of polymer chains can be further improved by annealing at the right temperature.

Figure 16 shows the effect on the alignment by measuring the absorption of parallel ($I_{\parallel}$) and perpendicular ($I_{\perp}$) polarized light. The optical dichroic ratio (DR) can be calculated from these values. Higher DR directly correlates with the higher alignment of the polymer.

$$DR = \frac{I_{\parallel}}{I_{\perp}} \tag{3}$$

Although the Marangoni effect is known for more than a century, FTM is a fairly new technology. Thus information on the film formation process of polymers on liquid substrates is somewhat limited, especially on photoresist materials.

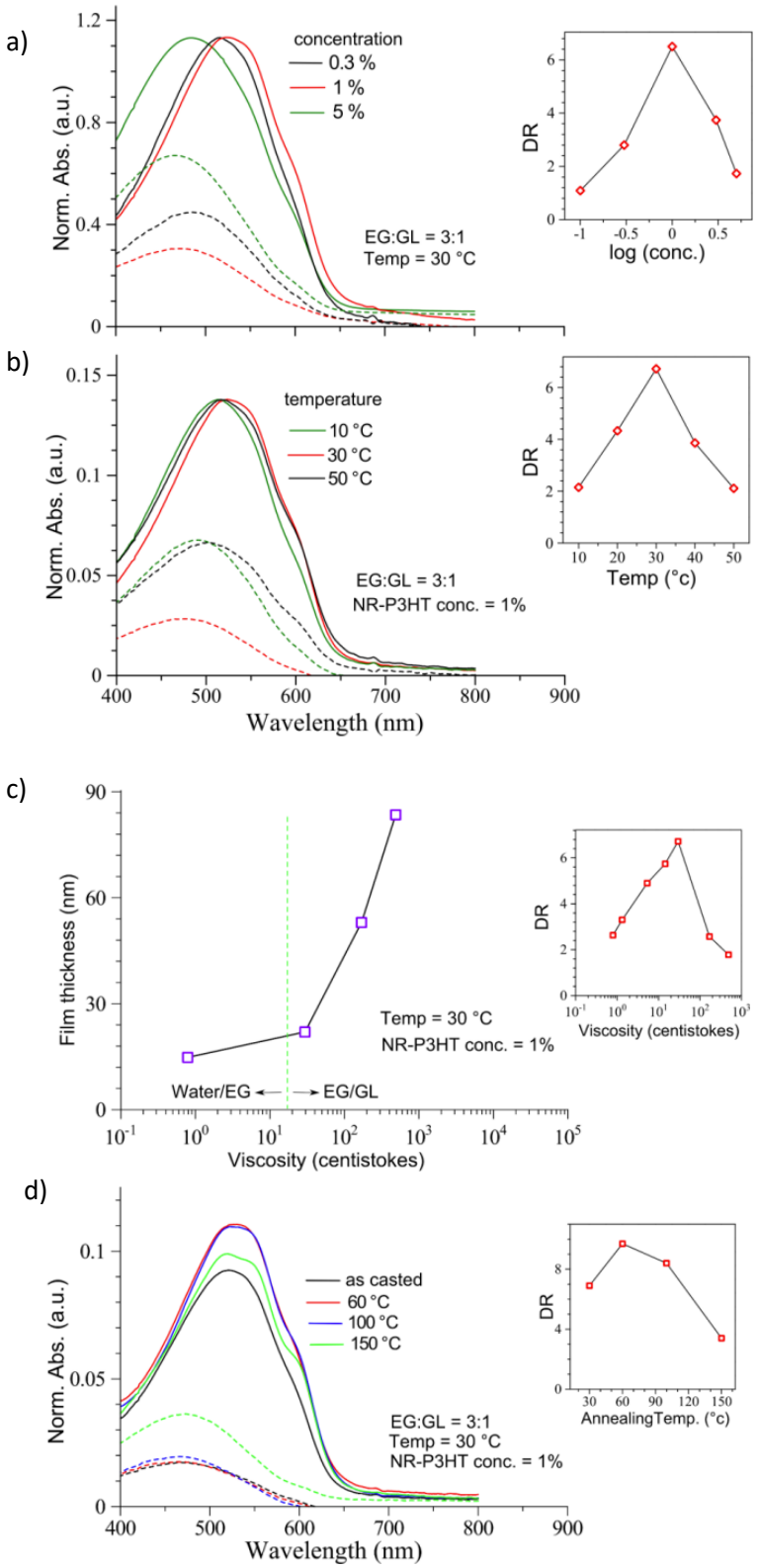

Figure 16: Parameter effecting the alignment during FTM measured by a) Absorption spectrum and DR at varying solid contents, b) absorption spectrum and DR at varying liquid substrate temperatures, c) film thickness and DR at varying viscosity of the liquid substrate and d) absorption spectrum and DR at varying annealing temperatures (reproduced from [46]).

3 Experimental

At the beginning of the experimental work, it was necessary to create a workflow and suitable starting parameters. This chapter depicts the possible procedure and setup of this new coating process, environmental conditions as well as used chemicals, resists, and process parameters. Process steps leading to planar and nonplanar structured samples are presented. All coatings were performed under cleanroom conditions and yellow light. Constant ambient conditions with air temperature T_{Air}=21 °C and relative humidity r.H.=45-50% were maintained.

3.1 Substrate preparation

4” Silicon (Si) wafers were used as planar substrates and Glass lenses and vials were used as non-planar substrates. The substrates are cleaned in three steps each for 5 min in an ultrasonic bath at 80 °C: 1. deionized water with an alkali cleaning solution, 2. acetone to remove organic compounds, and 3. propane-2-ol to remove excess acetone. If the substrate is further processed by spin coating a drying step for 30 min at 150 °C on the hotplate follows removing excess water on the surface of the substrate.

3.2 Coating methods

In this work, two main methods for resist coating were used: Spin Coating and Floating Film Transfer Method (FTM).

As described in 2.2.1 spin coating is a well-known method and is used for creating a thin layer of adhesion promoter or resist on a planar substrate. In this work, a spin coater from Lab Spin 6 TT Süss Microtec was used. Settings for each experiment are given separately in later chapters.

The second method is the new FTM. A temperature controllable water bath Julabo Pura 10 is filled with 1,7 l deionized water. The substrate is placed inside a steel grid and emerged under water. In literature FTM is often performed on ethane-1,2-diol [12,13,44]. Due to its high

viscosity, very low vapor pressure, and flammable character it was found not suitable for our process line, especially the drying step. 15-30 min wait time to ensure homogenous temperature are advised. The photoresist was then dispensed on the water surface. Two different dispensing methods were investigated: a) a 1 mL Eppendorf syringes and b) a software-controlled fine dosing syringe with a variable cannula size. A single drop of resist is enough to form a thin film on the water surface. After reaching a static state, the substrate is coated with the floating film by slowly lowering the water level. The resist will displace the water and cover the substrate in a comparable process to Langmuir-Blodgett (see 2.2.4). The bath was cleaned after each step with acetone, propan-2-ol, and deionized water. This ensured following experiments were unaffected by any resist remains

In another variant, like the one just described, the substrate is placed above the water surface and the film. By raising the water level, the substrate is exposed to the thin film and is coated due to its good adhesion properties. The same can be done by stamping the substrate on the film and consecutively pulling it through the liquid substrate (Langmuir-Schäfer method). Although it was shown that this method can be performed with P3HT on small samples [46][47], first trials showed poor results with this method and 4” wafers hence dismissing the method in this work.

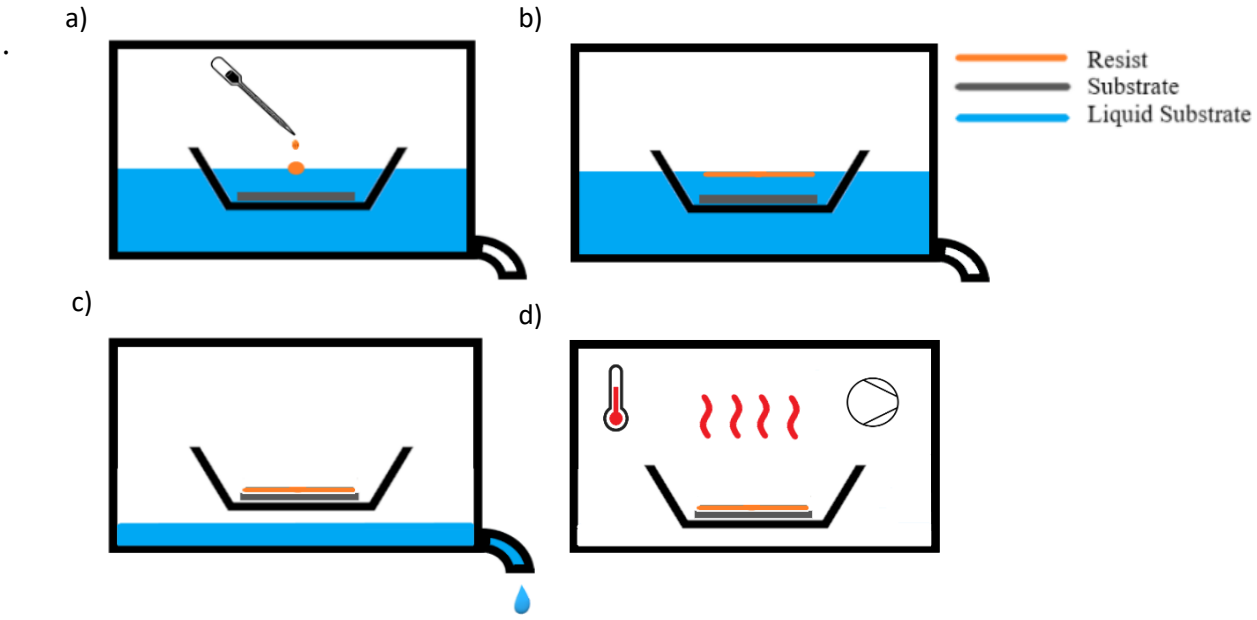

Figure 17: Schematic of the FTM process in this work. a) submerging the substrate under water and drop casting a single resist drop, b) formation of a thin resist film, c) coating the substrate by lowering the water level and d) drying in a vacuum oven.

Before drying excess water is manually removed by tilting the substrate a few degrees. This allows most of the water to flow away underneath the resist film. Drying can be done on a hotplate. This step is necessary since water is still trapped between the thin film and the substrate and can cause serious issues during the exposure and PEB. In the case of using a hotplate (HP 8 TT from Süss Microtec), only moderate temperatures below 40 °C and long drying times ensure acceptable results. High temperatures lead to the destruction of the resist layer (see *Figure 18*). Better results can be achieved when the substrate is dried in a vacuum dry oven (Binder VDL 53) at an ambient pressure of about 50 to 80 mbar (*Figure 18* b). An example of the temperature profile is displayed in Figure 19. Both ramping and preheating are viable options. A good indicator when the drying process is done is the disappearance of fog on the inside of the glass door of the oven. Depending on the amount of water that must be evaporated drying times can vary. Typical times t_{Oven} were 2-3 h at temperatures T_{Oven} of up to 50 °C. At moderate loads drying time over 3 h did not show any influence on the sample. The drying process serves as a sotftbake step too, so UV exposure can be done subsequently.

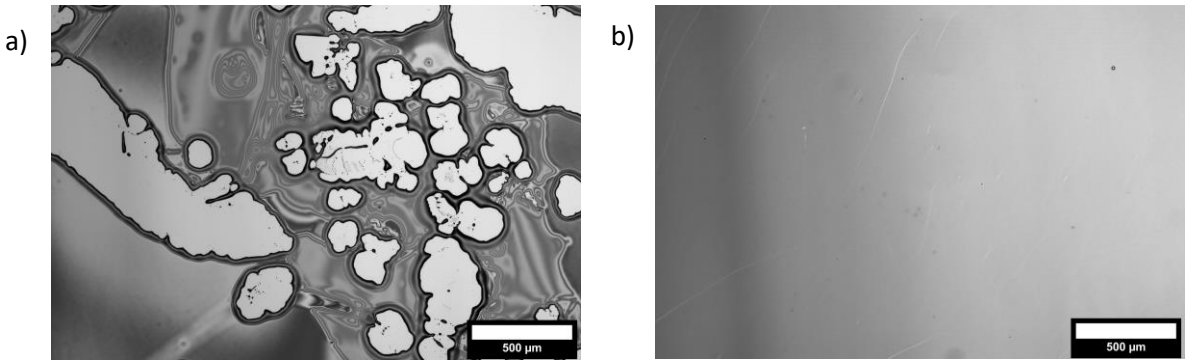

Figure 18: a) Result of placing the resist on a 95°C hotplate for tempering and b) uniform resist film after drying in the vacuum oven for 2 h at 40 °C.

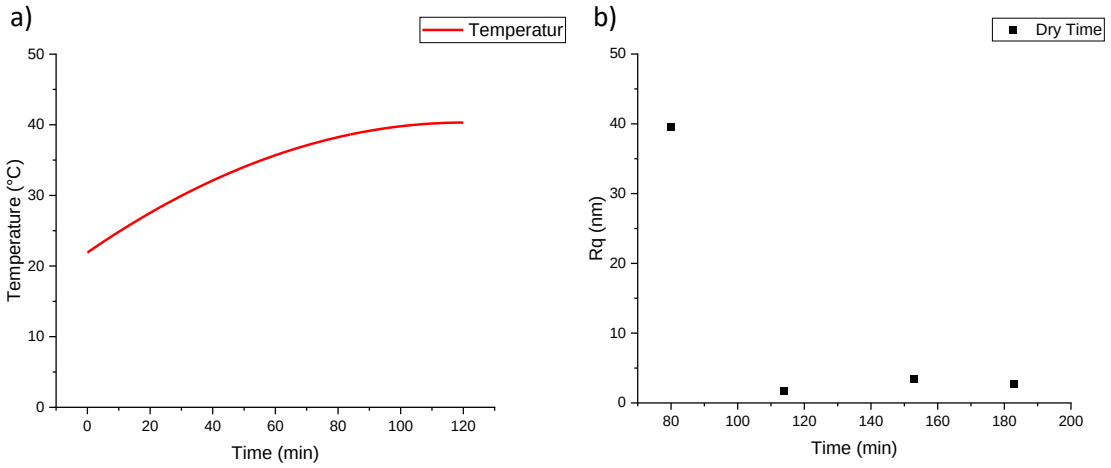

Figure 19: a) Temperature profile of the drying process in a vacuum oven for 2 h with an end temperature of 40 °C. b) Roughness R_q of FTM coated AR-N-4600-10 on microscope slides at 4 different dry times.

3.3 Preliminary examination

3.3.1 Resist choice

The choice of the investigated photoresist material is driven by various factors:

- The resist must be not soluble in water, but the solvent has to be.
- When hitting the water surface, the resist must spread out forming a thin film. This corresponds to a specific viscosity regime.
- The film must be mechanical robust while raising the substrate out of the water bath.
- The photoresist film must stick to the substrate.
- The solid content of the photoresist must not be too low or too high.

Positive and negative resists containing novolac meet these requirements. Novolac are in general unsolvable in water. The viscosity and solid content of the resist can be changed by adding solvent. Adhesion of novolac on Si is acceptable and can be enhanced if necessary by adhesion promoters. Several resists from Microchemicals and Allresist were chosen: AZ 1505, AZ 1512, AZ MIR 701, AR-N-4400, AR-N-4600, AR-P-3110, AR-P-3220 and SU-8-25. A

petri dish was filled with deionized water at T_{H2O}=21 °C. One drop of resist was cast on the smooth surface at approximately 2 cm distance. A 1 mL Eppendorf syringe was used to cast the drop. Film formation or in some cases lack of was observed. Depending on the result the film was then transferred to a glass substrate and dried in a vacuum oven for 2 h at 60 °C ramping from room temperature. The sample was inspected by light microscopy. If the result was promising further experiments were conducted with the resist in question. Main objective was to create and observe smooth and intact surfaces for later experiments.

3.3.2 Casting tool

To maintain comparable experiments it was necessary to evaluate the consistency in drop volume cast from the Eppendorf syringe and the micro-dosing syringe. Drops produced by the Eppendorf syringe were weighed on a precision scale and volume was derived from the density of the resist, whereas the volume of the drops from the micro-dosing syringe was measured by the contact angle measurement system. The software Advanced from Krüss can define the shape of the drop and measure the volume from 2-dimensional images after calibration. To calibrate the system measurement of the diameter of the steel cannula with an outside micrometer was necessary. The outside of the steel cannula must be cleaned with propan-2-ol or if necessary with acetone since resist remains negatively impact the drop formation, shape and volume. After longer periods without usage the first few drops cannot be considered due to the evaporation of the solvent at the tip of the cannula. The volume of each drop is primarily dependent on the cannula diameter although high enough flow rates must be applied. Otherwise, evaporation of the solvent leads to film formation on the surface of the drop. This film can lead to deformation of the shape and an increase in volume.

3.3.3 Determination of lithographic process parameters

The correct UV dose D_{UV} , developer and development time t_{Dev}, PEB temperature T_{PEB}, and time t_{PEB} for each resist had to be determined experimentally using manufacturer guidelines as starting points [47,48]. Samples were FTM coated as described in 3.2 with 4 different resists: AR-N-4600-10, AR-N-4400-05, AR-N-4400-10 and AR-P-3110. Each coat was done at 21 °C T_{H2O}. Process parameters for each process and resist are shown in Table 1. UV-Lithography was performed with mask aligner MA56 (Karl Süss, Germany) with varying D_{UV} depending on

the resist and thickness. The negative resist was post-exposure baked (PEB) on a hotplate before development. In the case of AR-P-3110 a PEB is not necessary. Exposure, PEB, and development settings for each resist are given in Table 1. A Chrom mask was used to create test structures of varying sizes down to 1 µm in width. Microscope images were used to evaluate the results. Criteria for good process parameters include: Complete development without remains, line width uniformity in compliance with the mask, and minimal dark erosion. Line widths were obtained from microscopic images. The resist thickness of a sample with AR-N-4600-10 before UV-Lithography was obtained by ellipsometry and from another sample after Lithography by profilometry.

Table 1: Determination of process parameters for UV-Lithography

Resist / Parameter	AR-N-4400-05	AR-N-4400-10	AR-N-4600-10	AR-P-3110
T_{Oven} / t_{Oven}	40 °C / 2h	50 °C/ 3 h	40 °C / 2 h	40 °C / 2 h
D_{UV}	100 mJ/cm^2	100 mJ/cm^2	100/250/500 mJ/cm^2	250 mJ/cm^2
PEB T_{PEB} / t_{PEB}	100 °C / 5 min	100 °C / 5 min	105 °C / 5 min	/
Developer / t_{Dev}	AR-N-300-47 1:1 / 10 min 3:2 / 5 min 7:3 / 3:30 min 9:3 / 2,5 /4 min	AR-N-300-47 9:3 2,5/4/8 min	Aceton:H_2O 5:1 … 10:1 2:30 min	AR-N-300-47 5:1 30/45/60/75 s,

3.4 Sample preparation with varying FTM process parameters

With the results found in 4.2.3, it is now possible to investigate the influence of temperature, resist choice, additives to the liquid substrate, and substrate preparation on FTM in combination with UV-Lithography.

Optical inspection was used to gain knowledge about the capabilities of each resist for UV-photolithography. Images from before and after the lithography process were obtained and compared to spin-coated samples. Defects, and resolution of the processed films were investigated by light microscopy. Profilometry paired with ellipsometry as described in 3.6.1 and 3.6.2 provides information about thickness uniformity and roughness distribution over the entire wafer.

3.4.1 Variation of the Water temperature

It is known that the Marangoni effect depends on the viscosity of the liquid substrate and the chemical properties and composition of the polymer solution [46, p. 40,49]. The viscosity is highly dependent on the temperature, which means by controlling the temperature the film formation process can be influenced. Si-Wafer were FTM coated with AR-N-4600-10 at 21 °C and 40 °C water temperature. AR-N-4600-10 was chosen based on the results in 4.2.1. UV-Lithography (see Table 2) was performed to create test structures which were then compared by microscopy and profilometry.

Table 2: Process parameters 21°C and 40°C

Process Parameter	AR-N-4600-10
Coating	FTM T_{H2O}=21°C and 40 °C
Drying	Vacuum Oven: 2:30 h:min, 40 °C
D_{UV}	250 mJ/cm^2
T_{PEB}, t_{PEB}	105 °C 5 min
Developer t_{Dev}	Aceton/H_2O 8:1 2:30 min

3.4.2 FTM with a variety of Photoresists

4” Wafer were FTM coated with AR-P-3110, AR-N-4400-05 and AR-N-4400-10 at T_{H2O}=21 °C. UV-Lithography was performed with process conditions displayed in Table 3. The influence of the type of resist, solid content, and viscosity on the spreading process was observed. Profilometry was conducted to gain knowledge about the thickness distribution over the whole wafer. The resolution of each resist was measured on the smallest achieved structure and compared to the mask dimension.

Table 3: Process conditions for FTM and UV-Lithography

Process Parameter	AR-N-4400-05	AR-N-4400-10	AR-P-3110
Coating	FTM T_{H2O}=21°C	FTM T_{H2O}=21°C	FTM T_{H2O}=21°C
Drying	Vacuum Oven: 2:00 h:min, 40 °C	Vacuum Oven: 2:00 h:min, 40 °C 0:45 h:min, 45 °C	Vacuum Oven: 2:00 h:min, 40 °C
D_{UV}	100 mJ/cm^2	100 mJ/cm^2	250 mJ/cm^2
T_{PEB}, t_{PEB}	100 °C 5 min	100 °C 5 min	/
Developer t_{Dev}	AR 300-47 3:1 2,5 min	AR 300-47 3:1 2,5 min	AR 300-47 5:1 1:00 min

3.4.3 Variation of the surface tension

A key factor in film spreading is the surface tension of the liquid substrate. By adding a surfactant one can lower the surface tension significantly, thus inhibit the spread of the polymer film. As surfactant 25, 50, and 100 mg of dishwashing soap “Fit” diluted in 1,7 l deionized water at T_{H2O}=21 °C was used. AR-N-4600-10 was FTM coated on a Si wafer and processed by UV-Lithography as described in Table 2. Samples were evaluated by profilometry and ellipsometry.

3.4.4 Preparation of hydrophobic and hydrophilic samples

Adhesion of the resist to the substrate is very important to achieve a uniform and defect-free coating. Adhesive promoters can be used to improve adhesion. With FTM it was found that adhesion of the resist to Si-wafers or glass was not a problem, but water trapped between the substrate and the thin film was. To avoid this the substrate was prepared with a very thin layer of fluoroalkyl silane. The fluorinated chains of the long-chain alkyl silane Dynasylan F8261 turn the substrate hydrophobic. In Figure *20* the preparation of the coating solution is described [50, pp. 122–123]. The substrates were successively cleaned in acetone, propan-2-ol, and deionized water. Meanwhile 30 ml of a solution of 1 % Dynasylan, 90 % propane-2-ol, 8,8 % H_2O and 0,2 % HCL (all percentages in %wt) was stirred for 4 h with a magnetic stirrer at room temperature. Following the preparation steps, the substrates were emerged into the solution and coated for 15 min in an ultrasonic bath at room temperature. After drying the substrate with a blast of compressed air followed by a curing step for 1 h at 120 °C on the hotplate, Dynasylan formed a covalent bond with the substrate. The mechanism of this process can be seen in Figure 21.

The coating was verified by the measurement of the contact angle. Contact angle measurements were performed by Krüss Drop Shape Analyzer DSA 25 with deionized water and diiodmethane. The sample was then FTM coated with AR-N-4600-10 at T_{H2O}=21 °C and dried in a vacuum oven overnight for 15,5 h at 21 °C followed by a Softback at 95 °C.

In a different approach, Si substrates with a thin sputtered TiO_2 layer were used. Samples were provided by Prof. Braun and Toni Junghans from WHZ/PTI department. By exposing TiO_2 to UV light it turns superhydrophilic [51]. Samples were exposed to UV for 20 min in a UV exposure chamber created by Dr. Robert Heimburger. Contact angles were measured with the DSA 25. Samples were then FTM coated with AR-N-4600-10 and UV-Lithographically processed (see Table 4).

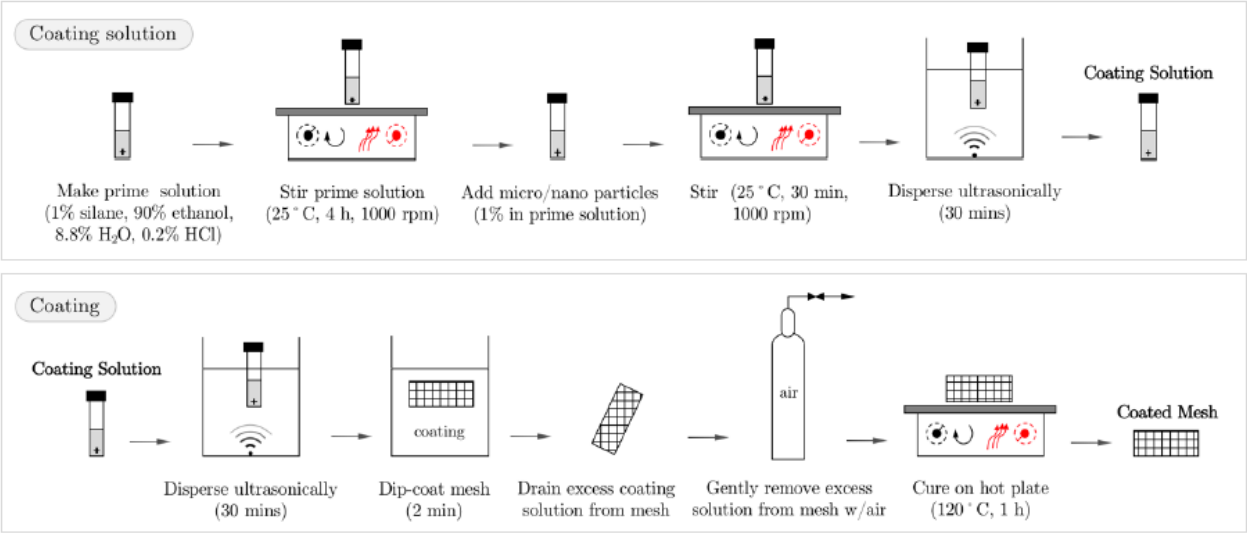

Figure 20: Preparation steps to fabricate a Dynasylan solution ready to coat on Si-substrates as proposed in [50, p. 122]. Instead of a mesh Si wafer slices were used.

Table 4: Process parameter of surface modified samples

Process Parameter	AR-N-4600-10
Coating	FTM T_{H2O}=21°C
Drying	Vacuum Oven: 2:30 h:min, 40 °C
D_{UV}	250 mJ/cm^2
T_{PEB}, t_{PEB}	105 °C 5 min
Developer t_{Dev}	Aceton/H_2O 8:1 2:30 min

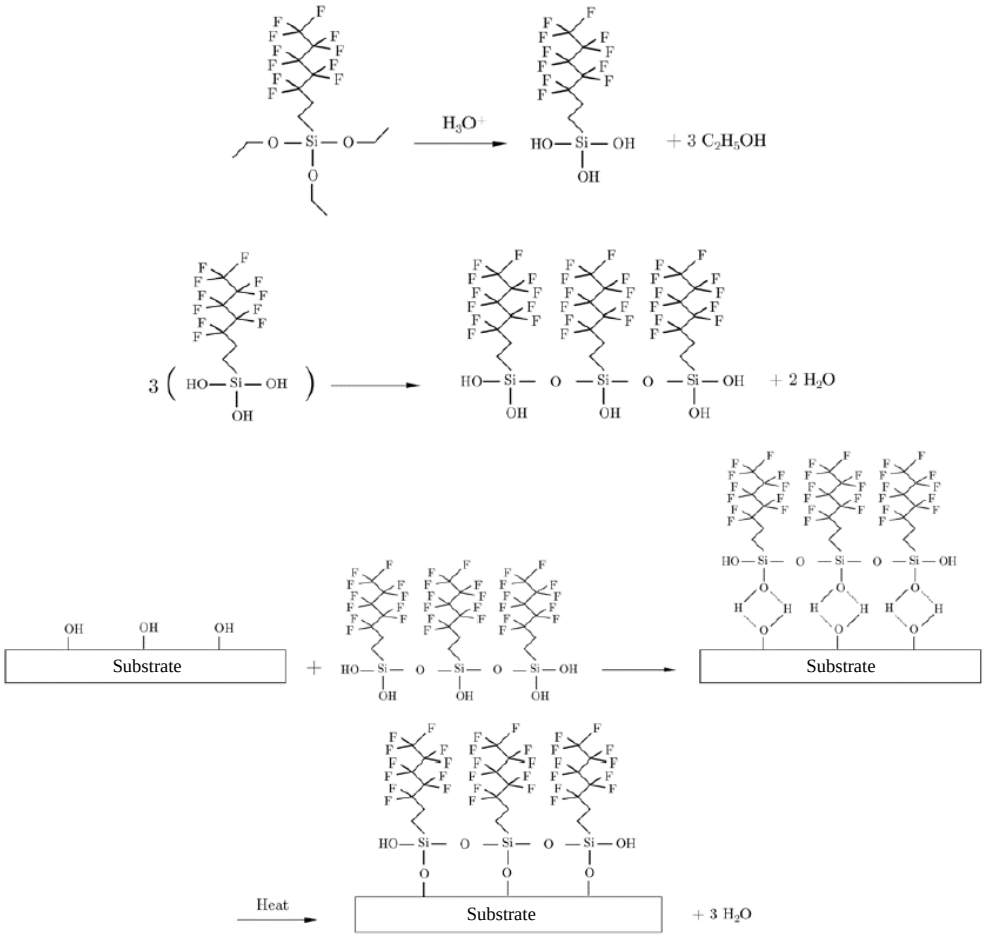

Figure 21: Chemical reaction to coat Dynasylan on Si substrates."First the silane (Dynasylan® R8261) undergoes hydrolysis reaction in the presence of an acid (HCl in our study) to produce silanol and three moles of ethanol. Then, three silanol molecules condense, and two moles of water is produced. […] [In] this stage, hydrogen bonds form between the oxygen and hydrogen molecules on hydroxyl groups and those on the adsorbed silanol molecules. Finally, upon heating, covalent bonds are formed (grafted) between the silane and SS surface". Reproduced from [50, p. 124]

3.5 Fabrication of nonplanar FTM coated Samples

Previous experiments were designed to understand the film formation, the lithographic properties of these films on planar substrates, and possible ways to manipulate the film formation process. Experiments detailed in this chapter aim to coat nonplanar surfaces and process them by UV-Lithography and NIL.

3.5.1 FTM coats as a protection layer for microstructured substrates

The possibility to coat microstructured surfaces with a FTM photoresist film was investigated. A Si wafer was spin-coated with AR-300-80 as an adhesion promoter followed by a layer of positive resist AR-P-3220 (Processing described in Table 5). The resist was structured via UV-Lithography using the MA 56 and a mask with square patterns. Resist thickness after UV-Lithography was determined by profilometry. In a next step, the structured resist was FTM coated with AR-N-4600-10 and dried. UV exposure was performed on a UV flood exposure (UV Belichtungsgerät 2 from GIE-TEC GmbH) working at wavelengths from 350 to 400 nm. The bilayer system was UV exposed with a D_{UV} of 1000 mJ/cm^2 followed by a PEB at T_{PEB} 105 °C for 5 min and subsequent immersion in AZ 351B 1:1. Microscopic images after rinsing and drying were obtained to evaluate the result.

Table 5: Processing conditions creating microstructured sample

Process Parameter	AR-300-80	AR-P-3220	AR-N-4600-10
Coating	5 s 500 RPM 20 s 4000 RPM	30 s 600 RPM 90 s 4000 RPM	FTM T_{H2O}=21°C
Tempering	Hotplate: 2 min 60 °C	Hotplate: 95 °C 4 min	Vacuum Oven: 2 h, 40 °C
D_{UV}	/	500 mJ/cm^2	1000 mJ/cm^2
T_{PEB}, t_{PEB}	/	/	105 °C 5 min
Developer t_{Dev}	/	AZ 351 B 1:1 2 min	AZ 351 B 1:1 2:30 min

3.5.2 NIL on planar and nonplanar substrates

3-dimensional substrates e.g., a glass lens 8 mm in diameter and two lens arrays were cleaned and coated with AR-4600-10 and AR-N-4400-10 as described in 3.2. FTM was performed at T_{H2O}=21 °C on deionized water without any additives. Samples were dried for 2 h at 40 °C in a vacuum oven. Simultaneous a Si wafer slice was equally processed. Two master PDMS stamps, one with a 1,5 µm pitch and one with holographic structures were used for t-NIL. Imprinting was performed with the imprinting tool Contact Nanoimprint Tool CNI1 from NIL

Technologies. Process conditions are displayed in Table 6 as well as Figure 22. Higher temperature, hold time and pressure apply to the imprinting of the lens array whereas lower values were used to imprint the Si sample. Profilometer measurements were acquired to confirm the imprint and calculate the curvature of the lens. Results were verified by light microscopy. Images of the curved substrate were stacked. Stacking was necessary due to the curvature of the sample. The method will be discussed in detail in 3.6.4. A green laser beam was radiated through the glass lens to observe the interference and holographic images caused by the imprinted structures.

Table 6: Process parameters for t-NIL

Process Parameter	Value
Pressure Low	1 bar
Initial Temperature	30 °C
Pressure High	2 (Si) and 4 bar (lens)
Temperature High	110 °C (Si) and 115 °C (lens)
Hold Time	10 min (Si) and 20 min (lens)

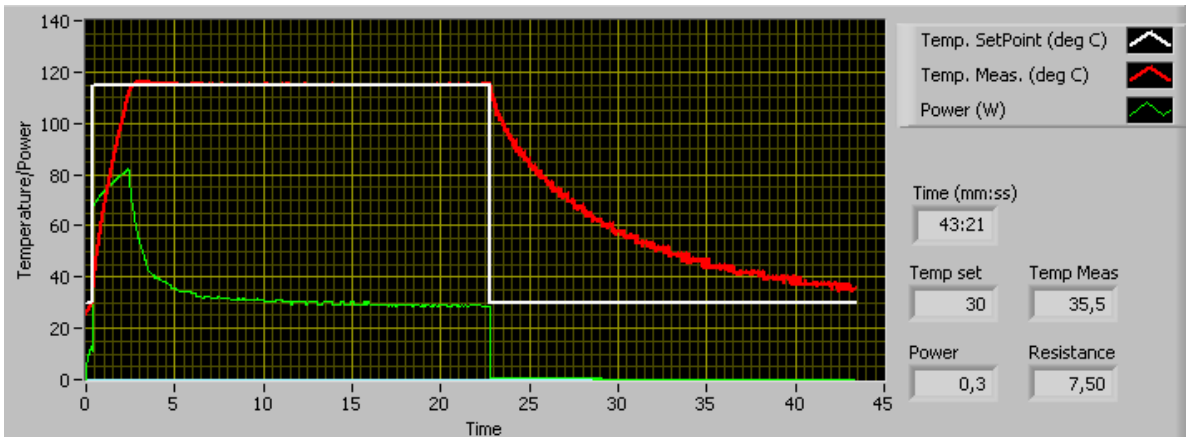

Figure 22: Temperature profile for t-NIL process, imprinting a lens array coated with AR-N-4600-10

3.5.3 Process parameter for UV-Lithography on nonplanar substrates

An amber glass vial 27,5 mm in diameter and a glass lens 61,7 mm in diameter were cleaned as described in 3.1. The vial was then FTM coated with AZ-MIR-701 and dried in a vacuum oven for 2 h at 40 °C. AR-N-4400 and 4600 are not sensitive to this wavelength so the positive AZ resist AZ 701 MIR was used instead. UV exposure was performed by a UV-diode laser working at 420 nm wavelength with a maximum power of 120 mW. The laser module LaserPro 3000 is part of the Bungard CCD. The dose, determined by the velocity of the laser and the diameter of the focus point, was calculated to D_{UV}= 380 mJ/cm^2. Since the spot size is a function of the working distance the dose can vary over a 3D substrate. To circumvent this the vial was exposed orthogonal to the curvature and the working distance was adjusted to create equal spot sizes for each line. Development was done in NaOH based developer AZ 351B diluted 1:1 in deionized H_2O for 10 s.

The glass lens was FTM coated with AR-P-3110 and dried on a hotplate for 30 min at 60 °C followed by UV exposure with 500 mJ/cm^2 by the flood exposure system with the square pattern mask. Development was performed in 5:1 AR-300-47 for 60 s.

3.6 Characterization methods

3.6.1 Profilometry

The first method of choice is the determination of the layer thickness and roughness with the profilometer DektakXT from Bruker. General settings are shown in Table 7. For faster data generation an automated routine was implemented to measure step heights and root mean square roughness values P_{Avg} and R_q at 64 points in an 8x8 pattern. This delivers a good overview of the height distribution and uniformity of the resist layer. Because of imperfections of the tip shape (diameter of 2 µm) and the measurement system in general an S and F-filter in Gaussian regression filter mode was applied. It acts as a low-pass filter with a short cutoff wavelength of 0,8 µm and a highpass filter with a long cutoff wavelength of 80 µm. P_{Avg} and R_q are calculated by the Vision 64 software provided by Bruker in compliance with ISO 4287

and ISO 4288 over a distance of 500 µm (see Figure 23). Layer thickness is measured between the substrate level and resist level. The complete dataset for every measurement is available upon request, but a small excerpt is shown in the following chapters. To measure the resist layer thickness it was necessary to process and structure the sample, therefore, creating clear steps over a minimal measuring distance. Otherwise, effects like wafer bow, roughness, waviness, or an uneven underground show an increased impact on the measurement. The software Origin was used to create contour maps out of the gained datasets. Due to the limited amount of data points with roughly 8 mm distance between each point the maps only represent an overview. Defects are not shown as well as smaller variations in resists thickness and roughness between each point. Therefore, additional 3D maps created by the Profilometer itself over 300x300 µm were obtained.

The uniformity 1%σ of the resist distribution was calculated from the average thickness P_{Avg} and standard deviation s:

$$1\%\sigma = \frac{s}{P_{Avg}} \tag{4}$$

Table 7: DektakXT measurement settings

Scan type	Standard Scan
Profile	Hills and Valleys
Stylus	2 µm
Stylus Force	3 mg
Speed	50 µm/s
Resolution	0,167 µm/pt

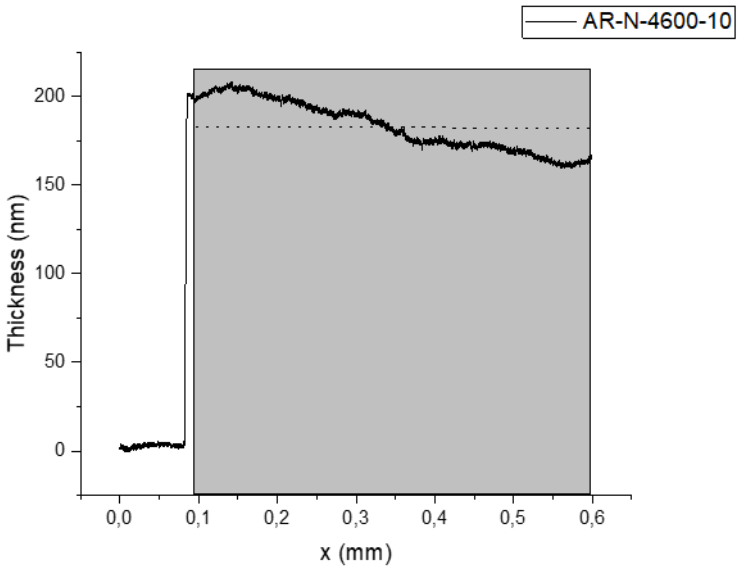

Figure 23: Profilometer measurement on a Si wafer. Thickness and roughness obtained from a length of 500 µm in compliance with ISO 4287 and ISO 4288.

Lithography might have reduced the resist layer thickness and varied the roughness. To determine the influence of the lithographic step a second noninvasive method called ellipsometry was employed followed by roughness measurements with the DektakXT.

3.6.2 Ellipsometry

Ellipsometry was performed to measure the resist thickness of unprocessed wafers after FTM coating. It is based on the alteration of the polarization plane caused by an interaction with the sample. The theory behind ellipsometry is already extensively described in the literature and should therefore not be part of this work [52].

Measurements were performed with the spectroscopic ellipsometer SE 800 “based on the Step Scan Analyzer measurement mode” [53]. To fit the experimental data to a mathematical model a multilayer consisting of Si substrate, 2 nm SiO_2, and resist with an unknown thickness was assumed. For the mathematical model Cauchy coefficients(N_1, N_2, N_3) provided by the manufacturer for different resists as well as preexisting datasets for Si (100) and SiO_2 were used. The coefficients allow it to mathematically describe the refraction index n as a function of the wavelength λ.

$$n = N_1 + \frac{N_2}{\lambda^2} + \frac{N_3}{\lambda^4} \quad (5)$$

High roughness values at the measuring spot can alter the result considerably. Since ellipsometry is dependent on smooth and defect-free surfaces the number of samples and available spots on them was somewhat limited. Up to 16 points per wafer were measured and merged to a contour map by Origin.

3.6.3 Contact angle measurement

Contact angle measurements to determine the hydrophilic or hydrophobic character of the sample surface were conducted with a Drop Shape Analyzer DSA 25 from Krüss. Contact angles were measured with deionized water with the sessile drop method and averaged over at least 5 measurements.

3.6.4 Light microscopy and focus stacking

Light microscopy was performed with a Zeiss Axioplan A1 to image, evaluate and measure structures present after processing. Images were taken by the high-resolution monochromatic camera ZWO ASI 183 MM Pro. For distance measurements, an object micrometer was used to calibrate the image for each magnification from 5x to 100x.

Microscopic images of non-planar objects are quite difficult to evaluate due to the limitations of focus depth when it comes to curved surfaces. A sub-micrometer structure on a curved glass lens for example is nearly impossible to see. This limitation can be overcome by using focus stacking. Focus stacking is commonly used in macro photography to create stunning pictures of insects and is often seen in fields like astronomy or light microscopy. Several images in different focus planes can be combined using stacking software like Helicon Focus or Focus projects 3 Professional which was used in this work. An example of the process is shown in Figure 24. The software determines sharp regions in each image, crops those regions, and stacks the images creating one sharp image in the process. There are several ways to calculate sharp regions and the user can mark sharp portions of the image manually. Photo-editing can be

performed before and after stacking to adjust brightness and contrast or create a depth impression as shown in Figure 24 [54,55].

Figure 24: Resistor through hole soldered on a PCB a) before and b) after focus stacking, colorized to increase 3D character

Microscope images may show a darker bar at the left side like *Figure 18* a) and b). This bar is the result of an inaccurate focussing of the halogen lamp after maintenance. It does not reflect the nature of the sample. However no negative impact was observed.

4 Results and Discussion

This chapter will present the results of the experiments described in chapter 3. The film formation of photoresists on deionized water will be discussed. Furthermore, UV-Lithography and t-NIL on planar and nonplanar substrates was conducted and the results will be presented.

4.1 Depiction of the Film formation process

The macroscopic observation of the film formation process on deionized water as a liquid substrate is described here. Starting from the injection zone a fast and omnidirectional spreading can be observed until the resist hits the wall of the bath or its maximum size. Resist is transferred to the outer zone by Marangoni flow caused by concentration gradients of the solvent in water [56]. The solvent dissolves into water resulting in a thin resist film. Depending on the resist and process parameters this results in either circular or randomly shaped films. Figure 25 a) shows such a film after formation of AR-N-4600-10 on water and after coating on a Si wafer and drying in a vacuum oven. A red dot in the middle in Figure 25 b) indicates the injection zone, where the drop hit the water surface and started to spread out. Secondary and subsequent spots might occur resulting from larger mass transfer. These spots act as a spreading center and can disturb the wave-like spreading.

a) b)

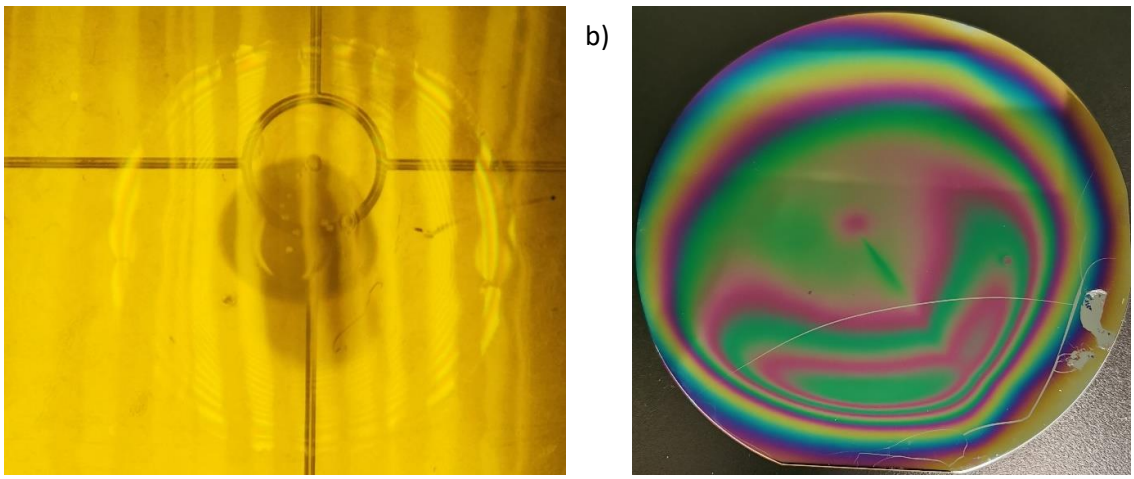

Figure 25: Resist film AR-N-4600-10 after a) drop cast on deionized water and b) coating on a 4" Si wafer and drying for 2 h at 40 °C in a vacuum drying oven.

In the case of AR-N-4400, AR-N-4600 and AR-P-3110 it was found that the spreading can be split up into three domains: 1. An injection zone, 2. Inner zone and 3. Outer zone. Similar behavior was observed in [49]. Roché et. al. investigated the shape of a thin film formed by a continuous flow of surfactant on ultrapure water [49]. As surfactants, they used alkyl trimethylammonium halides (C_nTAB; C_nTAC) and sodium alkyl sulfate (C_nNaSO4) with n=10-16 mixed with olive oil as a tracer. The oil droplets reflect light and indicate the concentration of surfactants at the surface. In Figure 26 a) the formation of three different zones is illustrated: 1. Source zone, 2. Transparent zone and 3. Outer zone. The radius of the source zone corresponds to the size of the injection needle. The transparent zone showed very low oil concentration in correspondence to the low light reflection, whereas the outer zone showed much higher oil concentrations and the formation of outward moving vortexes. According to their findings presented in Figure 26 b), Marangoni flow only occurs in the transparent zone with a defined radius following the formula (5) [49]:

$$r_* = B\left(\frac{\eta\rho}{(\sigma_w - \sigma_s)^2 D_{Diff}^3}\right)^{1/8}\left(\frac{Q_a}{c_*}\right)^{3/4} \tag{6}$$

B=dimensionless prefactor, η= dynamic viscosity, ρ= density, $\sigma_{w/s}$= surface tension of water/surfactant, D_{Diff}=diffusion coefficient, Q_a=flowrate, c_*= concentration of the surfactant.

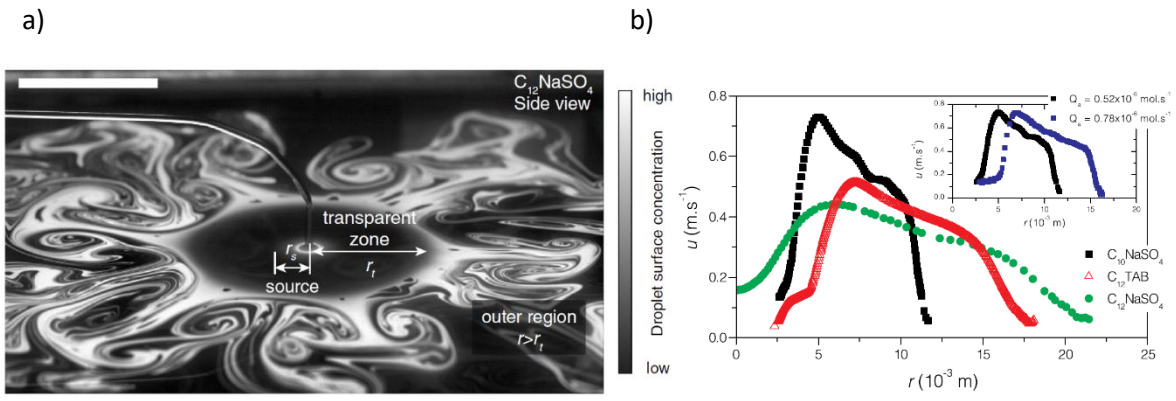

Figure 26: a) Source zone, transparent zone and outer zone as observed from Rochê et.al. b) Locally resolved radial velocity u as a function of radius r. (reproduced from [49, p. 3])

In the case of a drop, there is no steady flow rate. The Marangoni flow is only present until surface tension gradients are gone associated with the dissolution of solvent into water. This results in a thin film after a short period (1 to 2 seconds). Increasing film sizes were not observed even after minutes.

4.2 Results from preliminary examinations

4.2.1 Choice of resists

Several available positive and negative photoresists were investigated as described in 3.3.1. SU8-50 thinned with Gammabutylacton (GBL) was found to be suitable but produced nonuniform films of 250 nm to over 1300 nm and was therefore dismissed. Electra, an electroconductive negative photoresist from Microresist, was not forming a film on the liquid substrate as well as the positive resist AZ1505 from Microchemicals, but AZ1512 and AZ MIR 701 with a higher solid content did. Good first results were obtained with the negative Resist AR-N-4400 and AR-N-4600 and positive resist AR-P-3110 which are now further investigated. The first successfully UV lithographical processed sample coated with AR-N-4400-05 is shown in Figure 27, with the obvious need for further improvements of UV lithography parameters.

Figure 27: First successful pattern transfer via UV-Lithography with FTM coated AR-N-4400-05 on a microscope slide.

4.2.2 Choice of casting method

Two different methods for drop generation were investigated, a manually driven 1 mL Eppendorf syringe and a software and motor-controlled fine dosing syringe. Eppendorf syringes are often used in the literature for drop casting assumably due to their easy handling and fast swapping capabilities between different substances [12,13,46]. The fine dosing syringe in comparison requires a more complex system consisting of a syringe, a dosing unit, a controller, and a PC. The diameter of the syringe was measured to 1,851 µm. The consistency in drop volume is shown in Figure 28. One can see that the fine dosing syringe produced consistent drop volumes of V_{Fine}=10,2±0,2 µL whereas the Eppendorf syringe heavily varies with an average volume of $V_{Eppendorf}$=14,3±3,3 µL. While the handling with an Eppendorf syringe is much easier, further experiments were conducted using the fine dosing syringe to ensure consistent and comparable coatings.

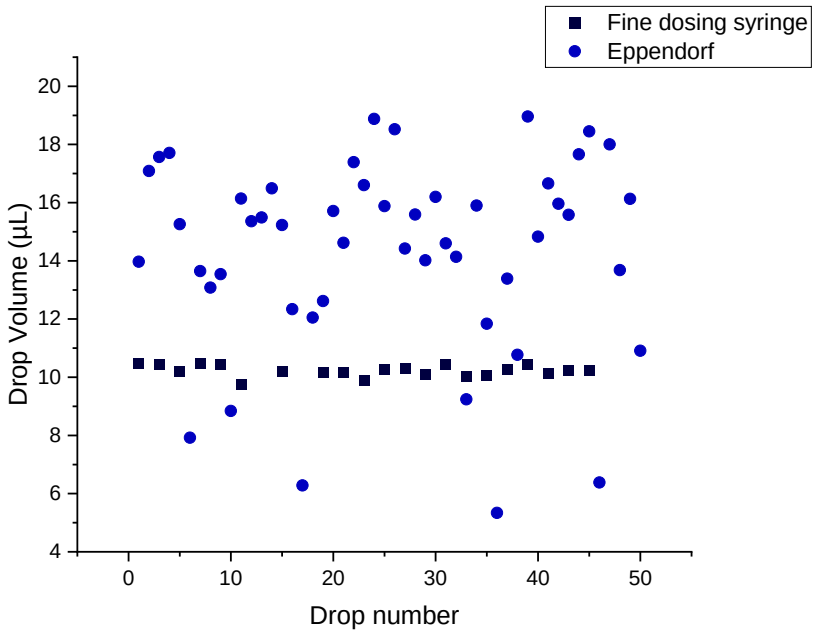

Figure 28: Consistency in drop volume generation by Eppendorf and fine dosing syringe

4.2.3 Determination of lithographic process parameters

AR-N-4600-10

Starting with AR-N-4600-10 the development time t_{Dev} was set to 2 min, as specified by the manufacturer, after UV exposure with 250 mJ/cm^2. Higher UV doses were chosen instead of the recommended D_{UV}= 120 mJ/cm^2, since not only the resist thickness was unknown but also the FTM process could have altered the chemical composition influencing the lithographic process. Standard developer AR 300 12 from Allresist could not be used due to its very high development rates. Instead, a mixture of Acetone and deionized water at varying concentrations was used to perform development. This was also the reason to increase the PEB time from 2 min to 5 min after temperature ramping from 60 °C to 105 °C to create more stable structures caused by increased crosslinking. This also increases the possibility of thermal crosslinking in unexposed regions [15,24]. Figure 29 shows microscopic images of the developed structures and corresponding resist thicknesses. Darker portions show the resist and brighter spots correspond to the substrate level. At concentrations below 8:1, the developer is underperforming showing signs of resist remains even in larger areas and small features are insufficiently developed. 8:1 turned out to be the go-to concentration as it showed the best results at an acceptable developing rate. However, corners were still rounded and edges were not completely developed indicating the need for further improvements. A high concentration with 10:1 led to merging lines as shown in Figure 29 indicating dark erosion. Resist thickness does seem to impact the result since thicker layers need more time for full development down to the substrate level. Nonetheless, the resist is processable by UV-Lithography.

The UV dose for 10 µm AR-N-4600-10 is given by the manufacturer with D_{UV}= 120 mJ/cm^2 [47]. Therefore, three identical coated substrates were exposed to UV at varying doses of 100, 250, and 500 mJ/cm^2. None of them show perfect results as all three show rounded edges and imperfect walls (see Figure 30). However, only at 250 mJ/cm^2 the small structures at the bottom (black square) of the image in Figure 30 b) were developed and edges showed minimal signs of underdevelopment. This test led to the decision to use 250 mJ/cm^2 for oncoming samples coated with Atlas 46.

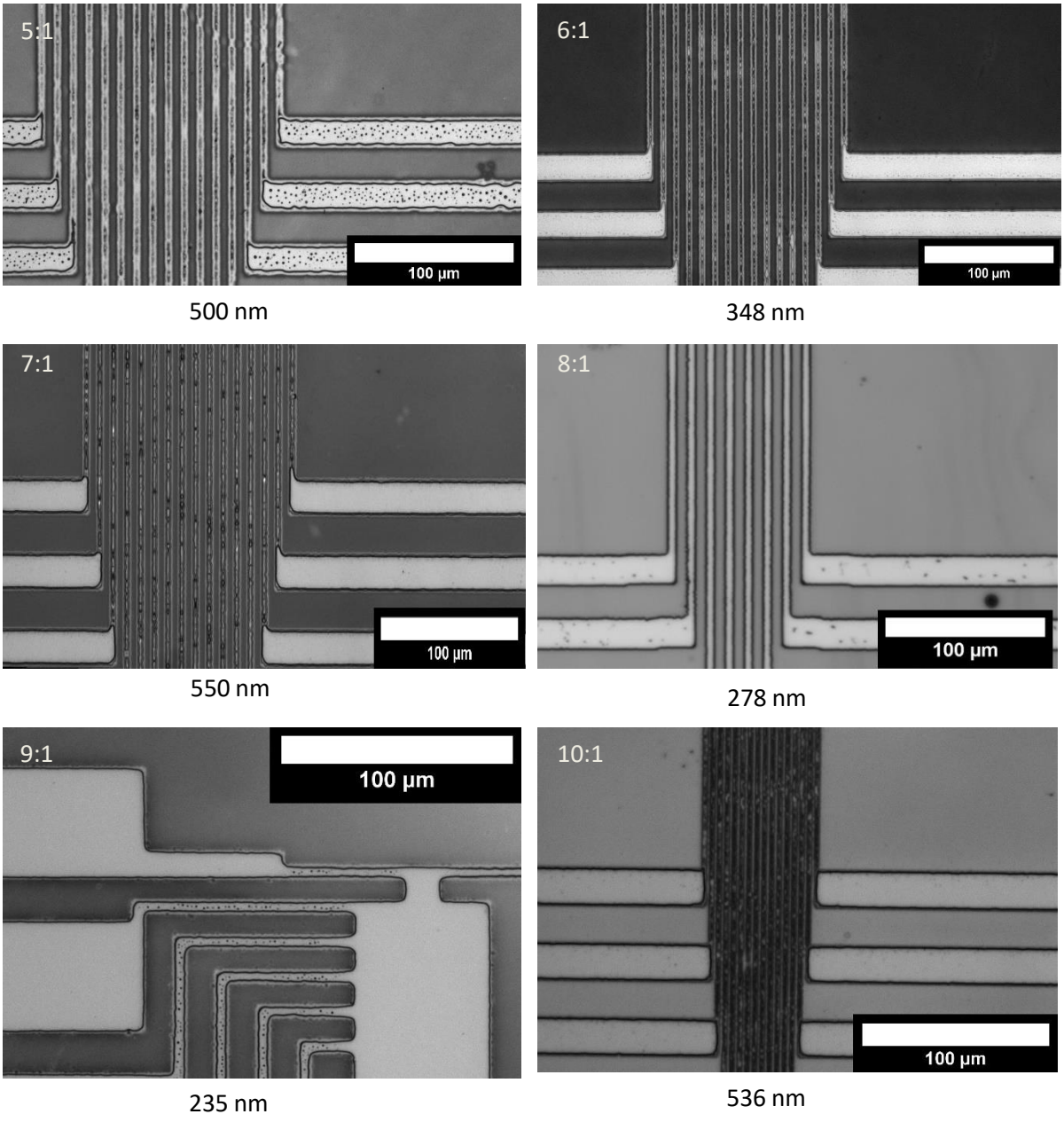

Figure 29: Microscopic Images of structures after development with various Acetone:DI Water concentrations. Development time: 2 min. UV dose 250 mJ/cm²

A developer with a slow development rate had to be applied. The reason for this is probably a reduced resist thickness which will be further investigated in later chapters. An increase in UV dose over manufacture guidelines indicates less sensitivity of the resist [47]. Reasons for this are unknown and subject to further research. It is imaginable that during the spreading and drying process water is absorbed into the bottom part of the resist film. Due to slow diffusion rates through the resist high concentration of water might be still present after drying, absorbing some of the UV light. Also, as will be shown in 4.1, the surface is non-uniform, causing

inhomogeneous exposure and Rayleigh scattering which negatively impact a uniform exposure. As described above the composition of the resist might have changed during FTM coating impacting the UV-Lithography.

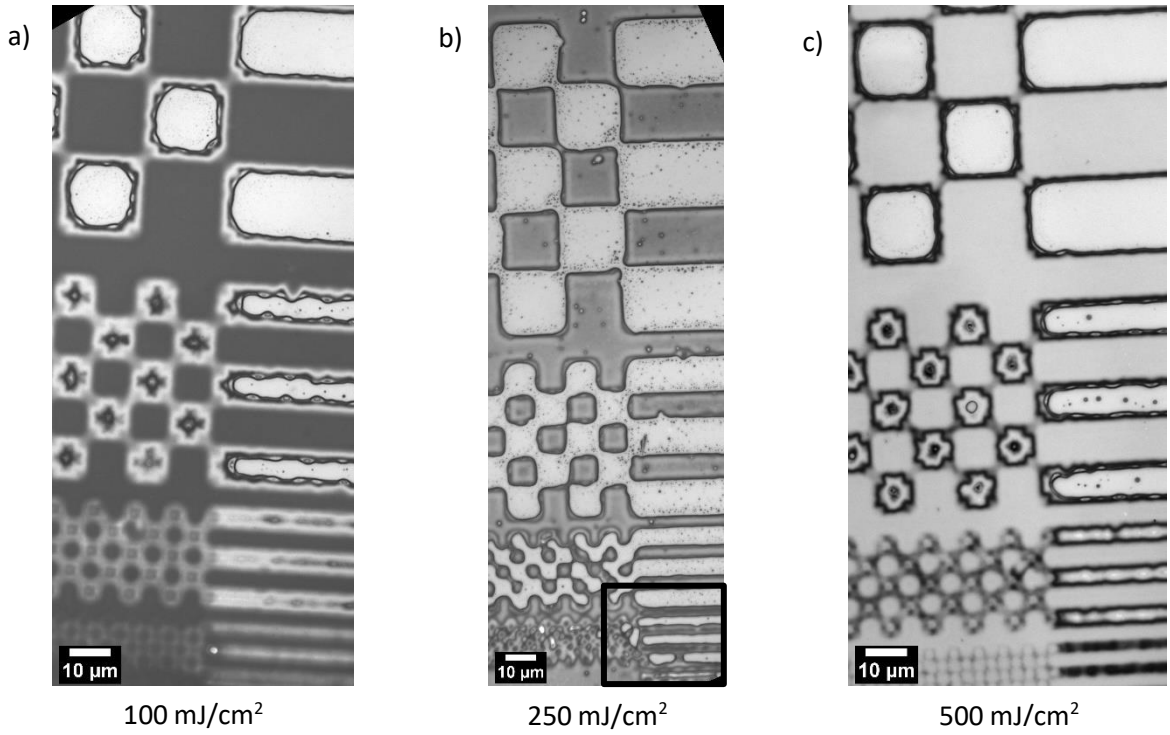

Figure 30: Development of AR-N-4600-10 in 8:1 Acetone :DI-H_2O after exposure with varying doses of a) 100 mJ/cm², b) 250 mJ/cm² and c) 500 mJ/cm²

AR-N 4400

AR-N-4400-05 and AR-N-4400-10 showed some conflicting results that will be discussed here. Standard developer AR-300-47 was used in a variety of concentrations and with different t_{Dev} at constant UV dose. Allresist recommends concentrations from pure AR-300-47 up to 6:1 diluted in deionized H_2O. We started at 1:1 and t_{Dev}=10 min with 100 mJ/cm² for AR-N-4400-05, resulting in mediocre structures as seen in Figure 31. Increasing the concentration up to 3:1 led to a significant decrease in t_{Dev} to 2 min 30 s with better linewidth d uniformity and d_{Avg}=3,3±0,3 µm. The line width from all 5 samples was obtained from microscope images at minimum of 20 points. Shapiro-Wilk test with a significance level α=0,05 shows that all groups were normally distributed with p>0,05. One factorial ANOVA delivered p=0,000284<0,05 which means inequality in variances. Line widths therefore significantly differ for each sample. Decreasing the t_{Dev} and simultaneous increase in developer

concentration led to smaller and more accurate line widths. Sample 5 shows signs of dark erosion causing an increase in line width at t_{Dev}=4 min.

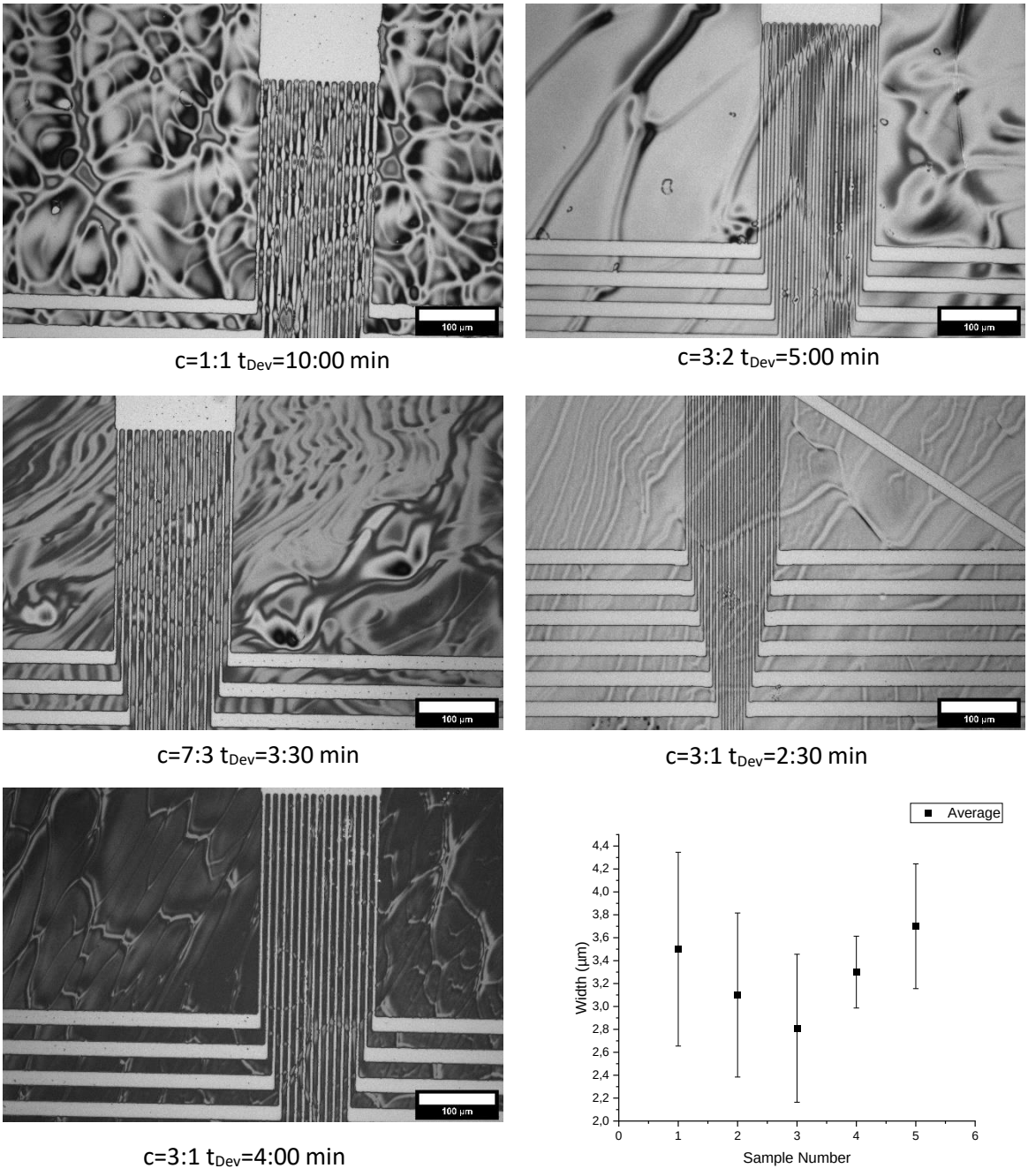

Figure 31: Development results of AR-N-4400-05 at varying concentration and t_{Dev}.

AR-N-4400-10 is, apart from a higher solid content, basically the same resist so it was assumed that AR-N-4400-05 development settings can be applied. Sample 1 in Figure 32 shows

comparable results to sample 4 in Figure 31 whereas samples 2 and 3 are severely underdeveloped even with nearly 3 times t_{Dev}. As of now, the cause is unknown. Possible explanations might be a nonuniform distribution of resist, aged developer, or locally occurring effects in the resist leading to crosslinking therefore inhibiting the dissolution.

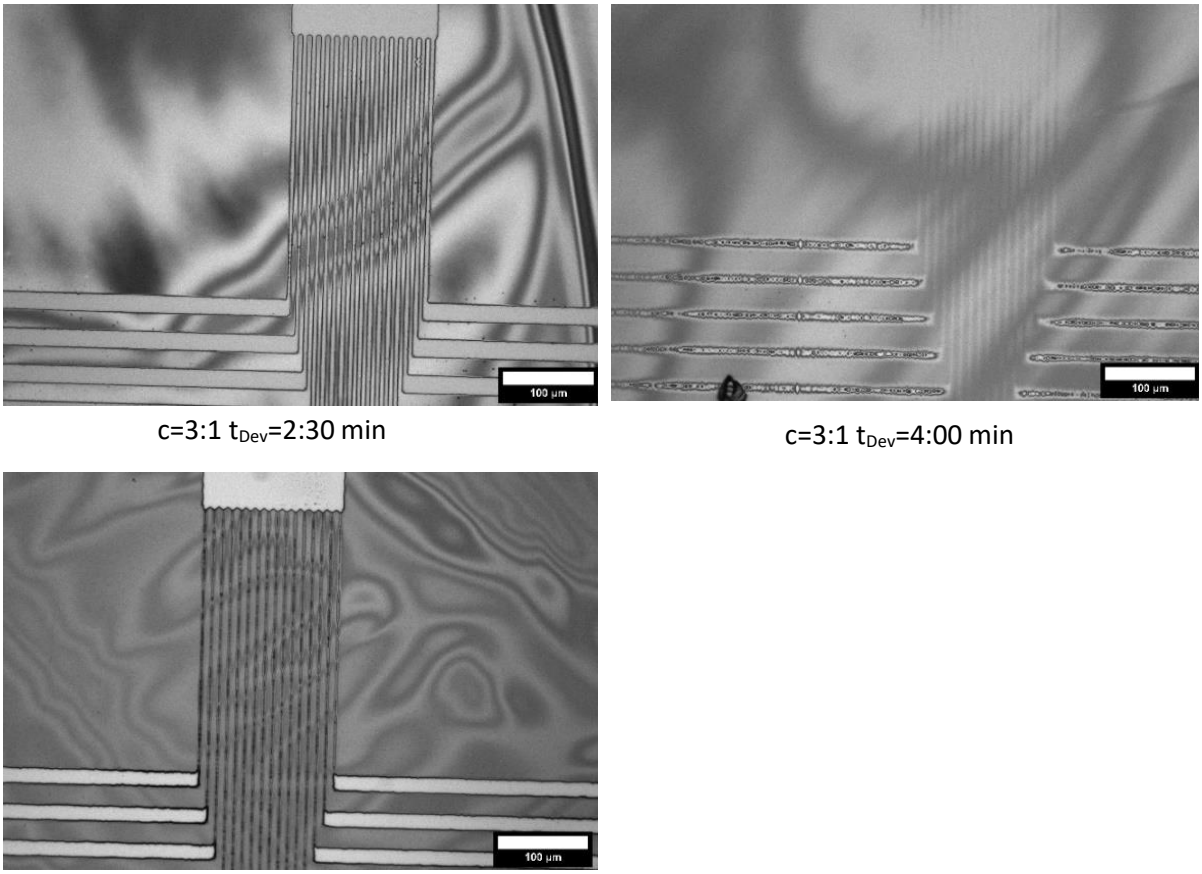

c=3:1 t_{Dev}=2:30 min

c=3:1 t_{Dev}=4:00 min

c=3:1 t_{Dev}=8:00 min

Figure 32: Development result for AR-N-4400-10 at t_{Dev}= 2 min 30 s, 4 min, and 8 min.

AR-P-3110

As a result of the previous experiment with AR-N-4600-10 the dose for AR-P-3110 was increased from the recommended 70 mJ/cm^2 to 250 mJ/cm^2. The manufacturer recommends AR 300-47 as the developer diluted 6:1 with deionized water and 60 s development time [48].We started at a dilution of 5:1 and raised the development time from 30 s to 75 s. Results can be compared in Figure 33. While 30 s and 45 s were too short to remove any excess resist, 75 s was too long and attacked the edges of the structure. The lines of all 4 samples show defects. Line width d of 5 rows originating from sample 1 at 30 s was measured over 60 µm as shown in Figure 34. Variations from d_{Min}=7,0 µm up to d_{Max}=8,8 µm were measured with an

average of d_{avg}=8,0±0,3 µm. Linewidths are at least 2 µm wider than that of the mask. The reason for this is the overcut of the positive resist (compare Figure 4 on page - 6 -). The UV dose was not sufficient enough to ensure proper development of the bottom part of the resist resulting in line widening. Line width measurements for each sample showed normal distribution according to Shapiro-Wilk test and ANOVA with a significant level of α=0,05 revealed significantly different variances with p=0,0003. Results are presented in Figure 35. 60 s t_{Dev} resulted in accurate and uniform linewidth with d_{avg}=5,0±0,1 µm. As it turned out this 5:1 dilution and a development time of 60 s showed very good results and complies with the manufacture's recommendation It would be expected that increasing t_{Dev} results in decreased line width for a positive resist. However, an increased line width of 6,2±0,2 µm for t_{Dev}=75 s was found. Profilometric measurement confirmed no significant difference in resist height. Possible explanations for this result are either a reduced localized concentration and activity of the developer or increased absorption at the top of the resist layer. This decreases the development rate of the bottom part of the resist resulting in an overcut (see Figure 4).

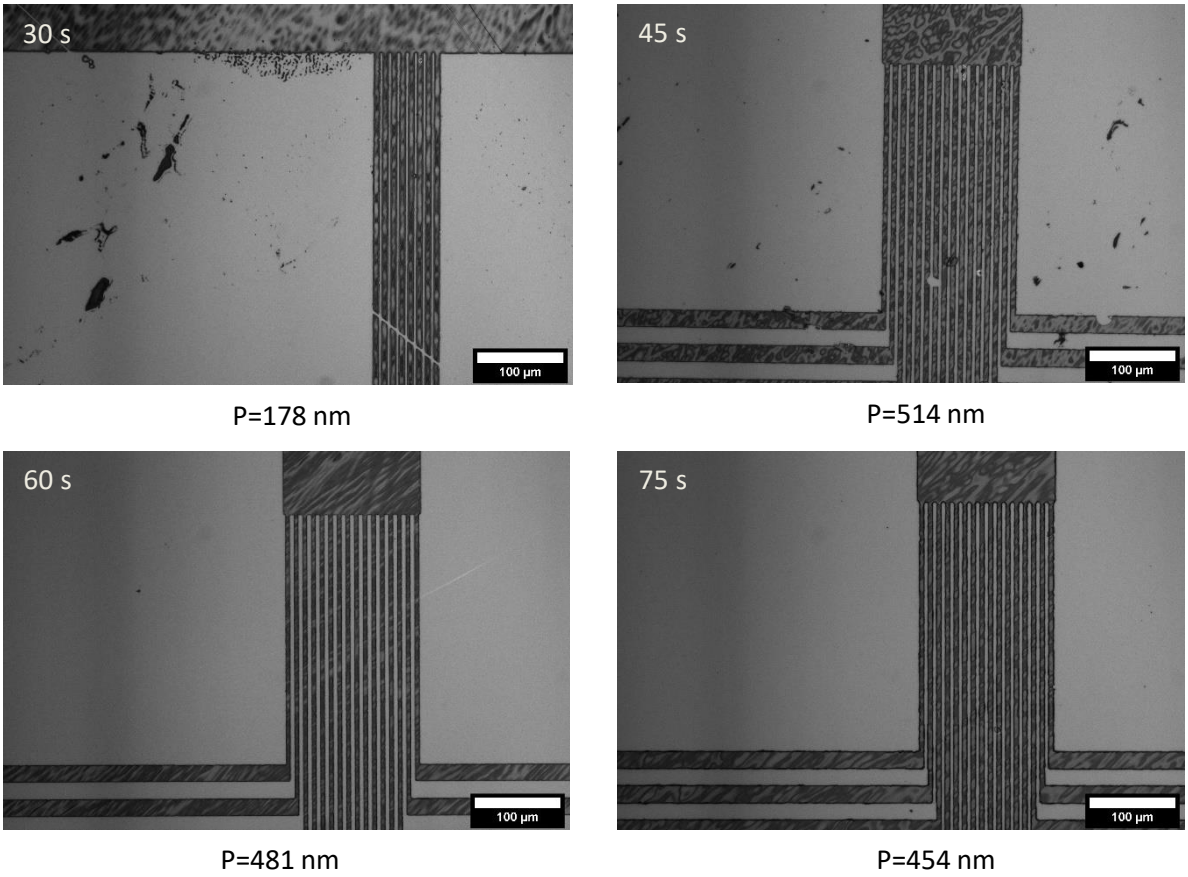

Figure 33: Development of AR-P-3110 in AR-300-47 5:1 after t_{Dev} =30 s, 45 s, 60 s and 75 s.

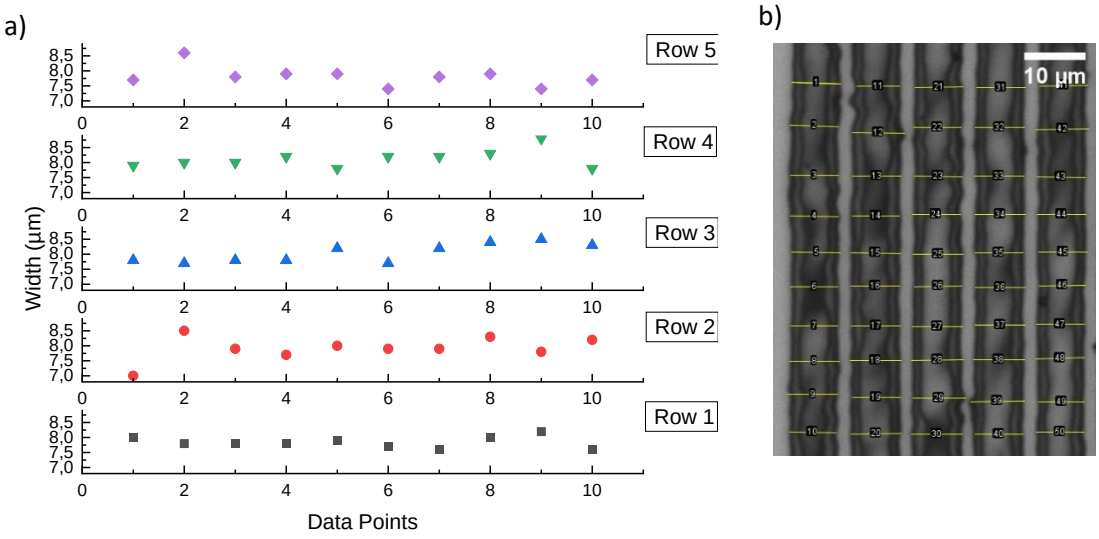

Figure 34: a) Line width measurement of row 1 to 5. b) measurement spots on row 1 to 5(left to right) of sample 1 with AR-P-3110.

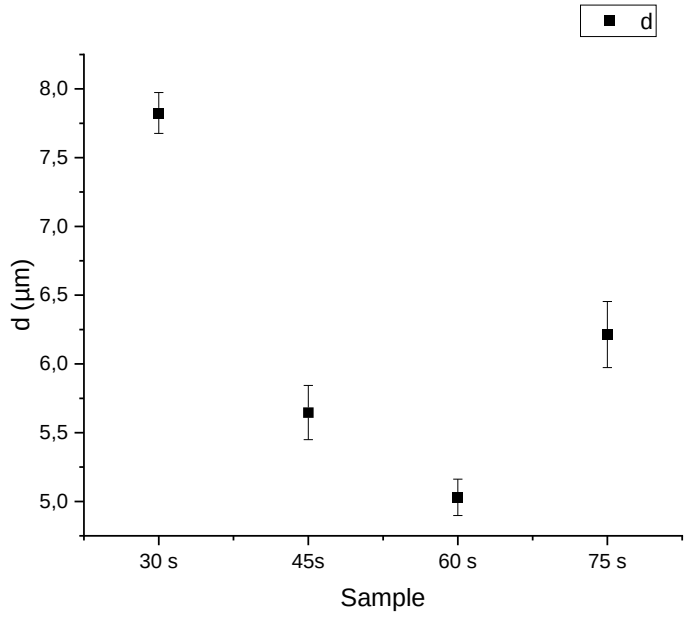

Figure 35: Average line width d of AR-P-3110 at varying t_{Dev}

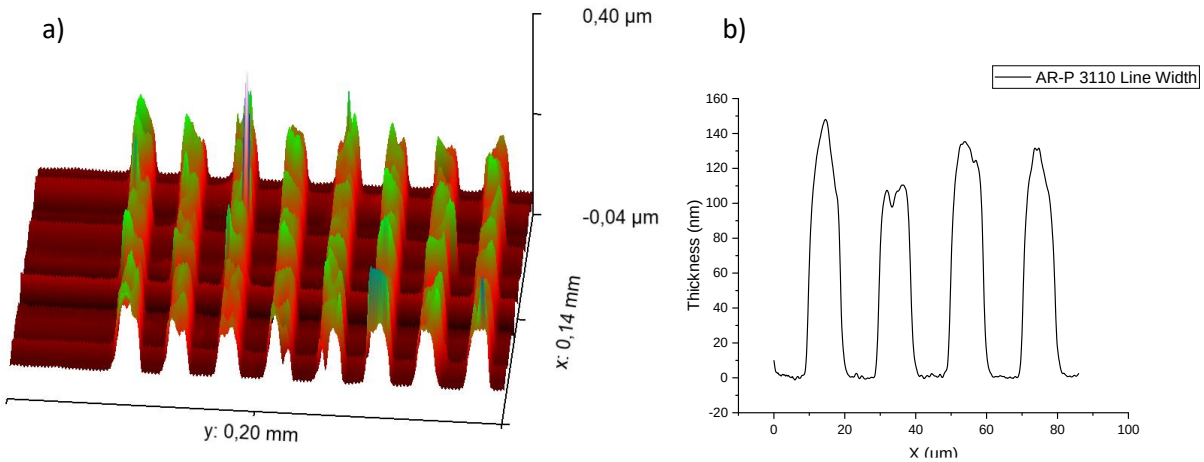

Figure 36: 3D Plot and derived line profile of lines fabricated by UV-Lithography of AR-P-3110.

The uniformity of the lines from sample 1 was confirmed by creating a 3D map with profilometry. No correlation between line height and width was found. However, line widening was observed.

The resolution of each resist was derived from the smallest achieved structure. Best resolution was observed for AR-P 3110 with 2,3±0,4 µm, followed by AR-N-4400-10 (2,8±0,3 µm), AR-N-4600-10 (2,9±0,3 µm), and AR-N-4400-05 (3,3±0,3 µm). Resolution values given by Allresist were not achieved.

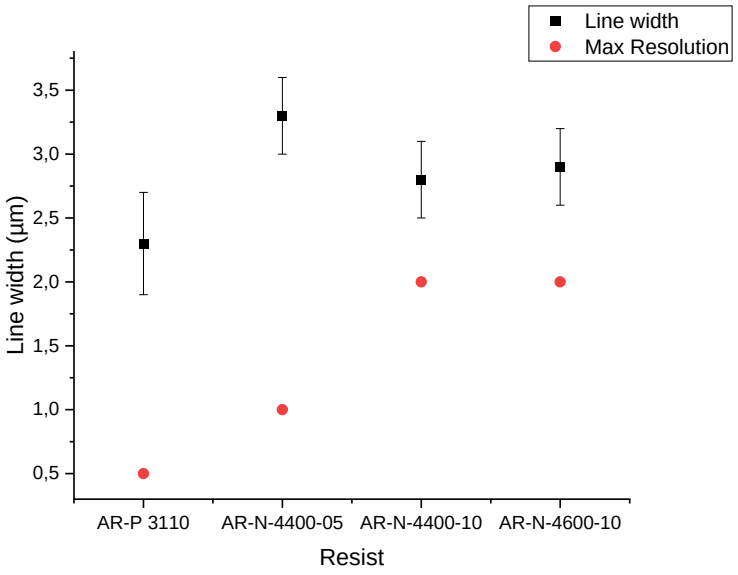

Figure 37: Smallest achieved structure for each resist and maximum resolution according to Allresist [48].

4.3 Characterization of the film formation under various conditions

In 4.1 capabilities of FTM coated photoresist for UV-Lithography were discussed. These resist films and possibilities in manipulating the film generation process are now investigated. Methodology for sample characterization was described in 3.6 and will be applied to samples prepared as presented in 3.4.

4.3.1 Temperature influence

4-inch Si wafers were FTM coated and UV-Lithography was performed as described in 3.4.1 . The results can be seen in Figure 38 a) and b). Both samples show interference rings indicating a difference in resist thickness distribution. It must be noted that only a fraction of the film is transferred to the substrate. The injection zone mustn't be in the center or even on the substrate.) Sample 1 coated at 22 °C water temperature shows a smooth surface over the entire wafer like it is depictured in Figure 39 a), while the 40 °C sample 2 is covered in sprinkles and has visible surface roughness. Figure 39 b) shows the remains of the cast drop and wave-like spreading formations. Secondary drops smaller in size near and partially connected with the injection zone were observed. Larger portions of the resist split from the original drop. Spreading originating from these secondary drops occurred. Height P_{Avg} measurements performed by Profilometry as shown in Figure 39 c) and d) revealed circular-shaped thickness distributions for both samples. At 22 °C the resist seems to spread evenly and only thins out at the outer edges of the film. Thinning is expected with an increasing radius of the film since the resists must cover an increasing area. Sample 2 reveals the in 4.1 mentioned three zones as highlighted in Figure 38 b). The thin zone inside the yellow circle corresponds to the inner zone. High Marangoni flow transferred most of the polymer out of the injection respective inner zone, resulting in a thin resist film in the middle. Simultaneously bigger formations of resist in form of secondary drops were present in the inner zone decreasing the average resist size even further. Resist accumulated near the border of the outer and inner zone due to low Marangoni flow and only thinned out towards the edge due to an increasing radius.

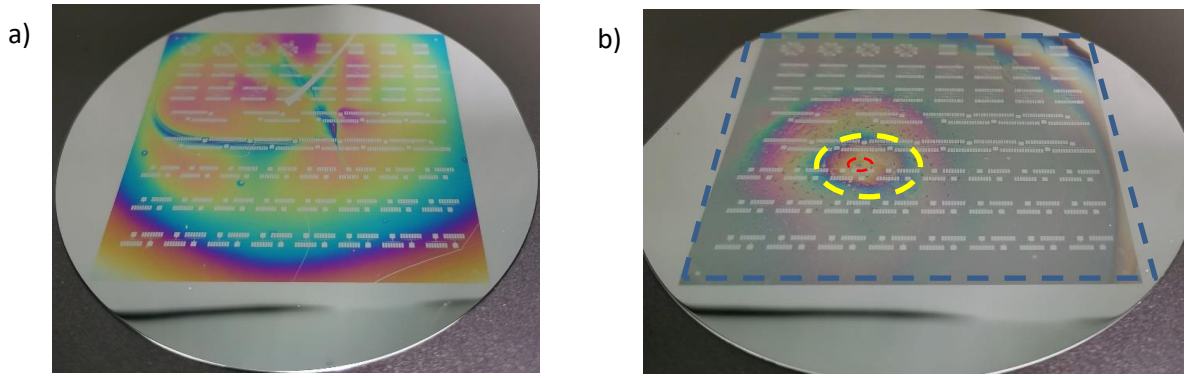

Figure 38: Si wafer FTM coated with AR-N-4600-10 at a) T_{H2O}=21 °C and b) T_{H2O}=40 °C. Red circle injection zone, yellow circle inner zone blue square outer zone.

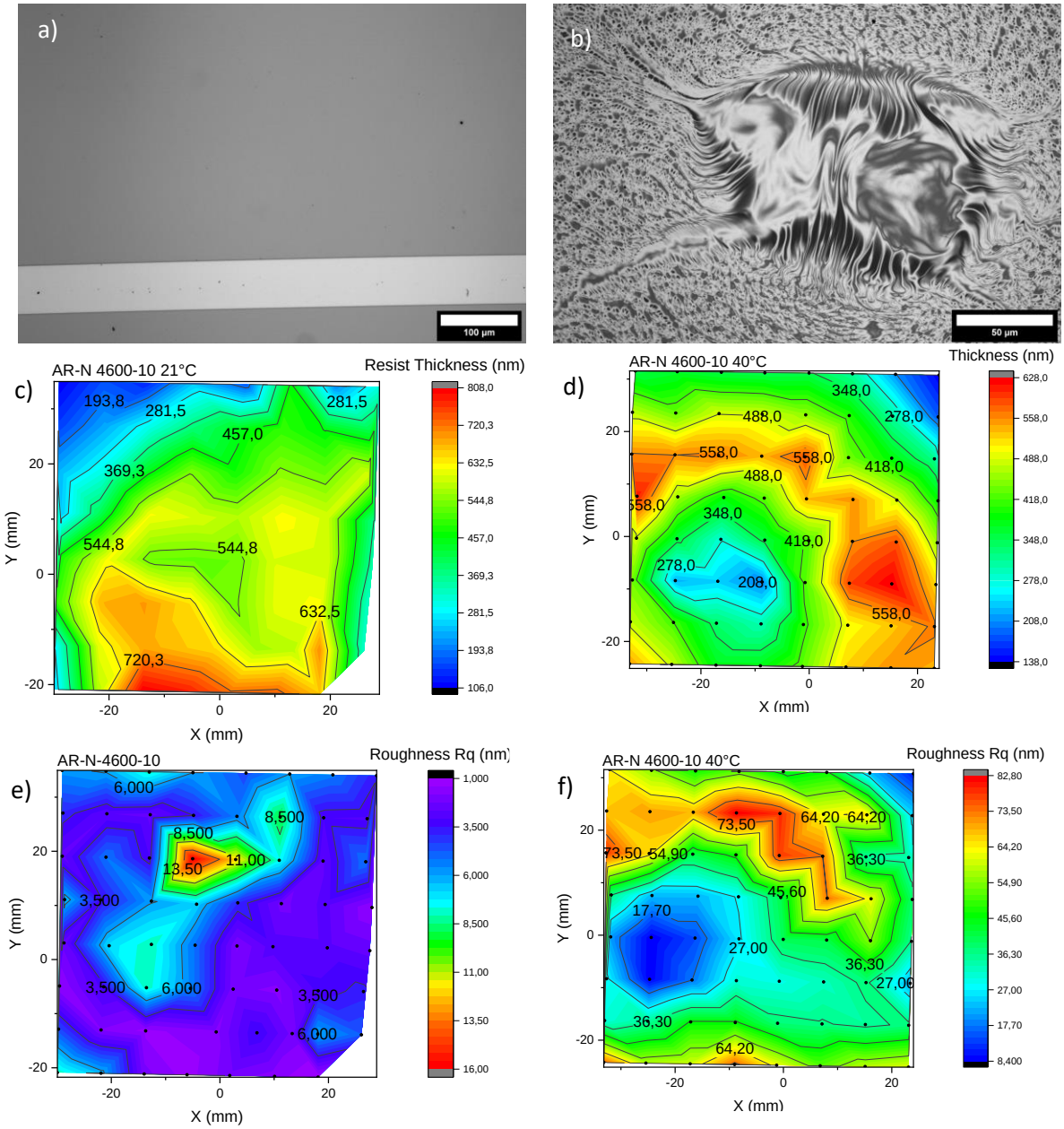

Figure 39: Microscopic images of a) sample 1 and b) sample 2. c) and d) are and contour plots derived from profilometric measurements for each temperature T_{H2O} and e) and f) show the corresponding roughness plots.

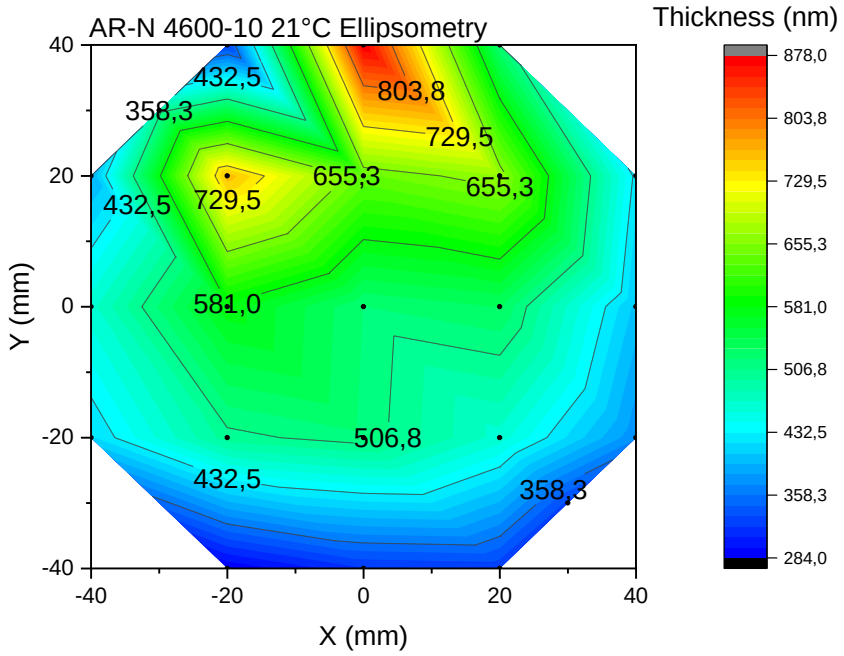

Figure 40: Thickness distribution of AR-N-4600-10 at T_{H2O}=21°C measured by ellipsometry without UV-Lithography.

Figure 40 pictures the thickness of an unprocessed wafer with AR-N-4600-10 measured by ellipsometry. Compared to the result in Figure 39 a similar distribution pattern and resist thicknesses were measured. Dark erosion cannot be excluded but is believed to be minimal. The average thickness was determined to 484 nm compared to 472 nm of the sample processed by UV-Lithography. Ellipsometry could not be conducted on the 40 °C sample due to poor surface roughness.

Topographic profiles for both samples derived from profilometry measurements are shown in Figure 41. While FTM coating at room temperature resulted in smooth surfaces over the length of 1 mm with an average roughness R_q=4,3 nm an increase in surface roughness up to 45 nm was observed at 40 °C T_{H2O}. In comparison the roughness of a spin-coated wafer with AR-N-4600-10 is 1,9 nm. Not only is the thickness distribution nonuniform but also high roughness was observed at higher water temperatures resulting in poor topographical properties.

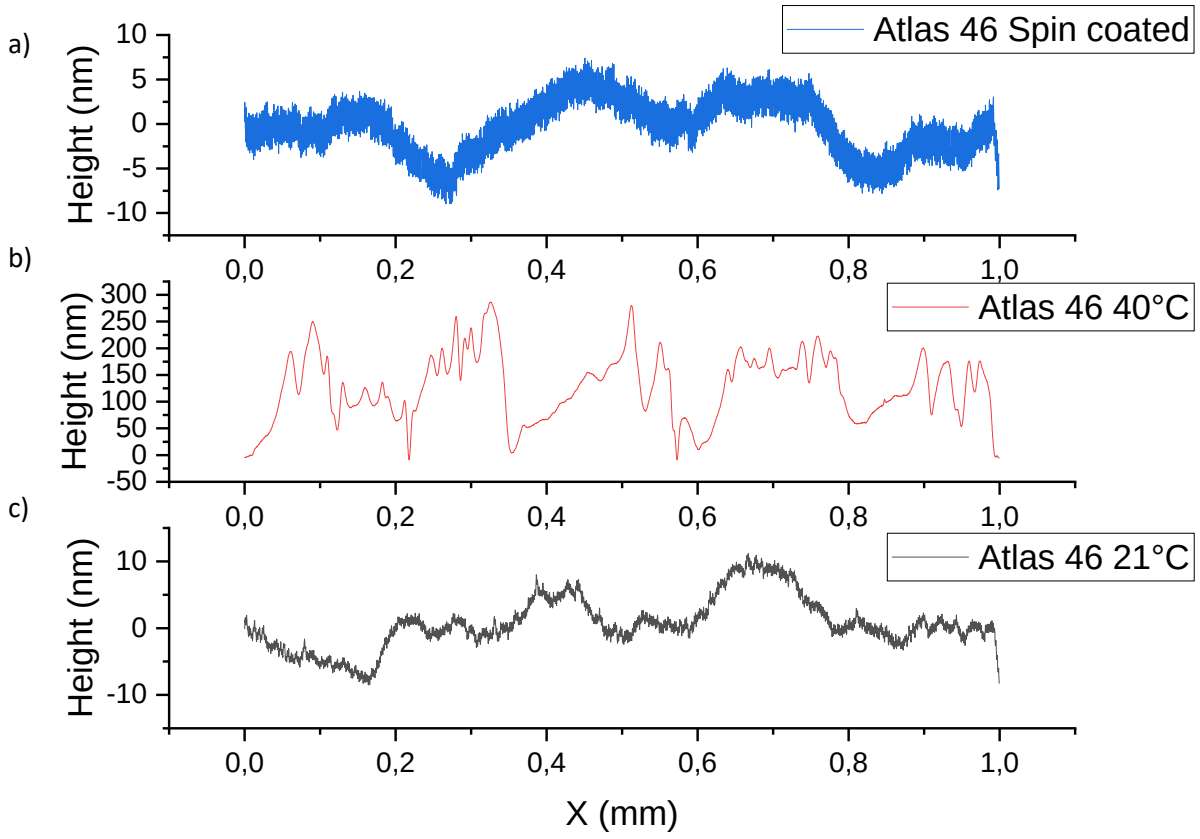

Figure 41: Topographic profile a) spin coated AR-N-4600-10 as well as b) FTM coated AR-N-4600-10 at 21 °C and c) 40°C water temperature measured by profilometry.

In Figure 41 b) the thickness seems to oscillate. 64 datasets, used to generate the contour plot, were investigated and Fast Fourier Transformation was applied but no specific frequency was found. In [57] Kovalchuk describes the phenomenon of spontaneous surface tension oscillation caused by Marangoni instabilities. This oscillation corresponds to an oscillation in surface velocity (see Figure 42) and might be the reason for the observed surface profile. If this oscillation is present during the spreading process and enhanced due to higher dissolution of the solvent at higher temperatures, it is possible that fluctuations in surface velocity cause accumulations of resist during slow phases. Further research must be conducted to verify this

theory. Measuring the surface tension during the spreading process and recording it with a high speed camera might help to understand this process.

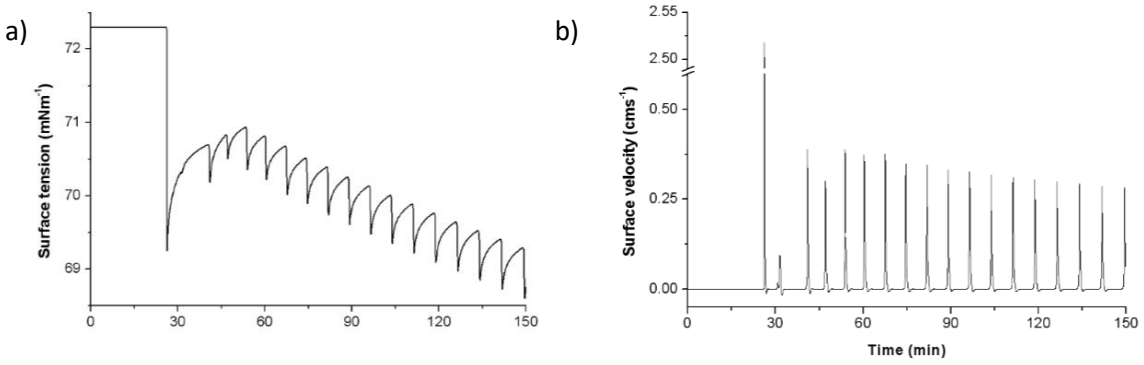

Figure 42: a) Surface tension oscillation and b) surface velocity oscillation over time caused by Marangoni instability (reproduced from [57, p. 1432])

4.3.2 Resist influence

Positive and negative resists possess different chemical compositions (see 2.1) and vary in viscosity. The impact of these parameters will be discussed here. Figure 43 displays three AR-N-4400-05 coated Si wafers all produced under the same conditions. Profilometer measurements show the thickness distribution at 64 points. Allthough all 3 samples show a different spreading pattern a general trend for thickness distribution can be observed. Thinner resist layers in the inner zone, followed by a steep thickness increase at the beginning of the outer zone and thinning towards the edge of the resist film was observed. Minimum, maximum, and average thickness is shown in Figure 44. Radial symmetric resist distribution was observed with minimal thickness of P_{Min}=65 nm and maximum thickness of P_{Max}=891 nm. Deviations in thickness of samples 1 to 3 were measured to 1%σ=41,5 %, 45 %, and 50 % respectively with an average thickness of P_{Avg}(#1)=331±138 µm, P_{Avg}(#2)=279±128 µm, and P_{Avg}(#3)=349±176 µm).

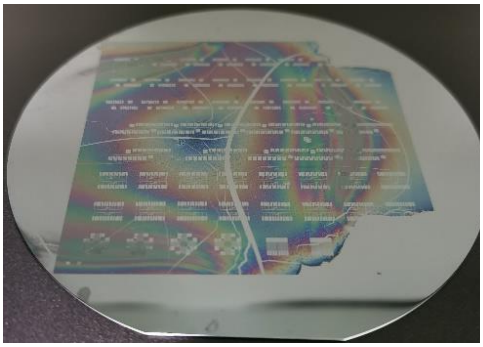

Sample #1

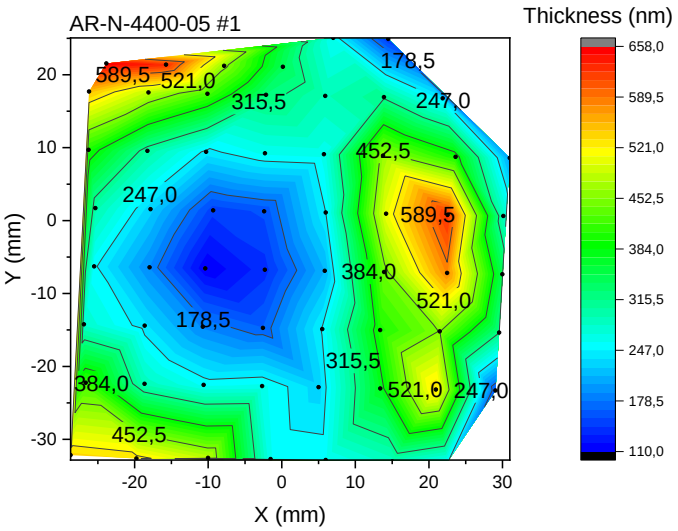

Sample #2

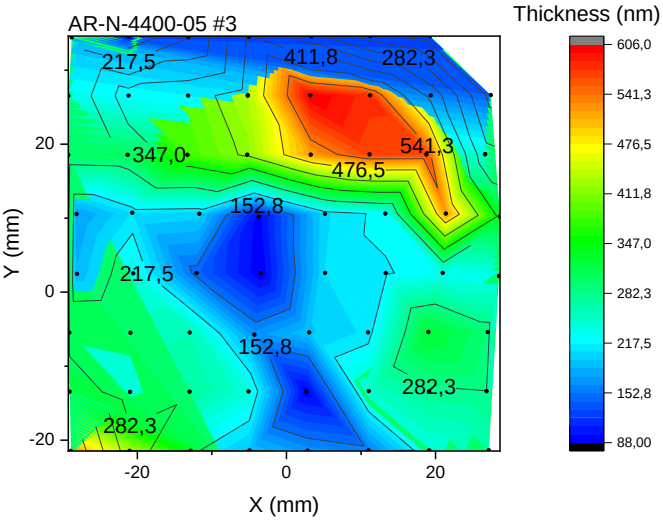

Sample #3

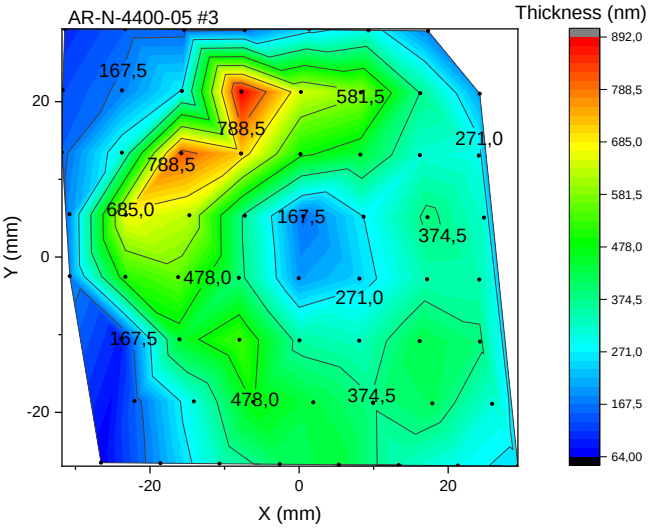

Figure 43: Images and thickness distribution of 3 FTM coated AR-N-4400-05 samples on 4" Si wafer.

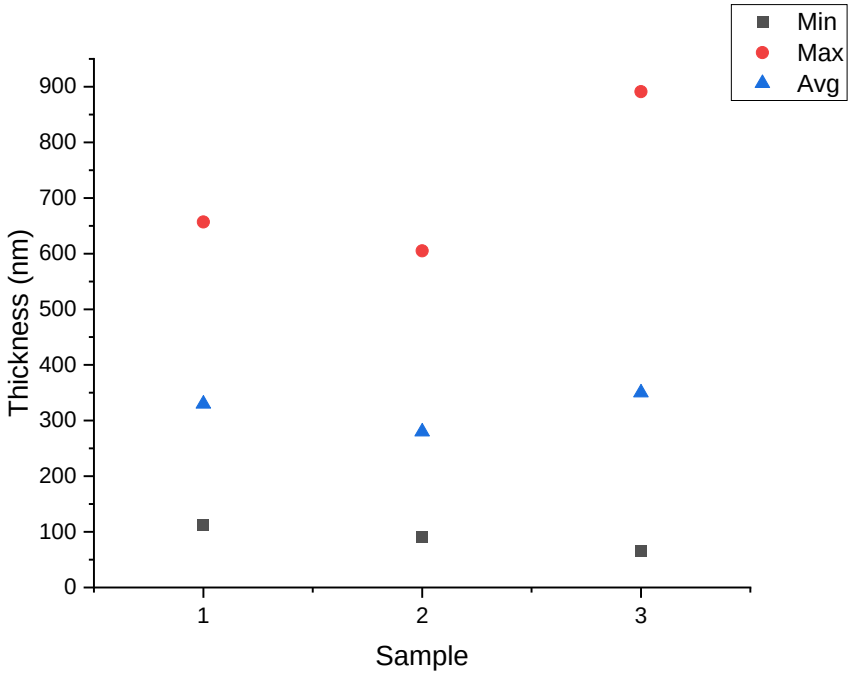

Figure 44: Minimum, maximum and average thickness of FTM coated AR-N-4400-05.

All 3 samples show a different resist spreading pattern which will be discussed now. The solvent concentration gradient after drop casting is believed to be inhomogeneous over time for various reasons. For one the drop causes motion on the water surface influencing the solvent diffusion and therefore the Marangoni flow. Secondly, fast solidification at the water resist interface was observed with liquid resist remaining on top of it. The liquid resist spreads on top of the solid resist until the solvent evaporated or it hits the water surface. From there secondary water resist spreading was observed. Furthermore, motion of the film towards the edge of the container during the spreading constraints the film and forces it to either compress or evade in other directions resulting in non-uniform distribution. This behavior can be seen in sample 2. The resist was free to spread towards the lower right corner resulting in reduced film thickness but was constrained by the wall of the container at the top. To ensure undisturbed spreading the size of the container must therefore be large enough and the injection zone must be located in the middle of the container.

The size of the inner zone was measured from the contour plot of samples 1 to 3 and amounts to 758 mm^2, 359 mm^2 ,and 165 mm^2 with an average thickness of 189 nm, 157 nm, and 219 nm respectively. The extreme variation in thickness over each sample impacts the

photolithographic process as was shown in 4.2.3. Thin portions of the resist were overexposed and thick areas were underdeveloped due to a short t_{Dev} resulting in inconsistent structures over the wafer.

Compared to AR-N-4600-10 more defects like cracks after drying were observed. No discrete pattern indicating the source of this behavior was found other than the overall decreased thickness. The solid content of AR-N-4400-05 is lower than the one of AR-N-4600-10 which explains the thinner and less robust film. It is also possible that the resin chains in AR-N-4400-05 form loose and less dense connections compared to the resin in AR-N-4600-10.

The effect of an increased solid content on the resulting film was investigated. AR-N-4400-10 containing a solid content of 45 % compared to 33 % of AR-N-4400-05 was processed. Samples and contour plots are presented in Figure 46. Immediately apparent in the images are large circular areas in the middle of the film attributed to an increase in the size of the inner zone. Profilometer data confirms the pattern to a lesser degree. Build-up of resist at the border between the inner and outer zone can be observed especially in samples #1 and #3. Measurements confirmed a higher thickness average (P_{Avg}(#1)=394±153 µm, P_{Avg}(#2)=460±173 µm, P_{Avg}(#3)= 578±354 µm). A correlation between solid content and thickness can therefore be assumed. It must be noted that an increase in solid content effects the spreading pattern. The thickness in a particular spot is much more dependent on the measuring position than on the solid content.

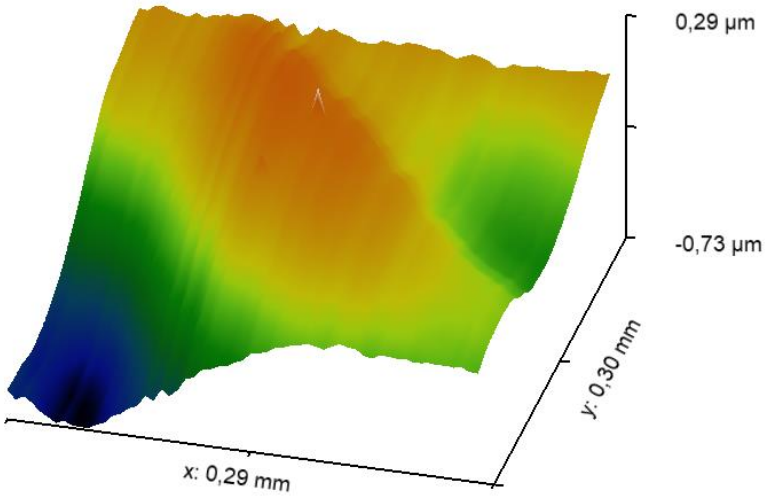

Figure 45: 3D Map of AR-N-400-10 measured by DektakXT. Area: 300x300µm resolution: 5µm/trace

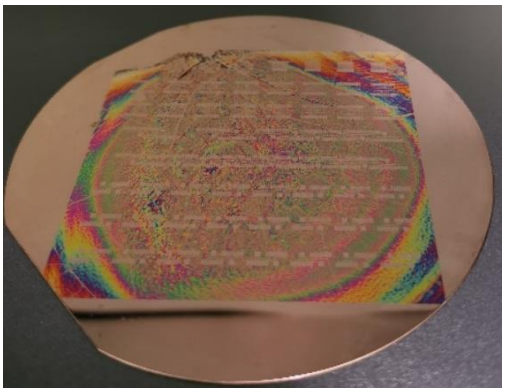

Sample #1

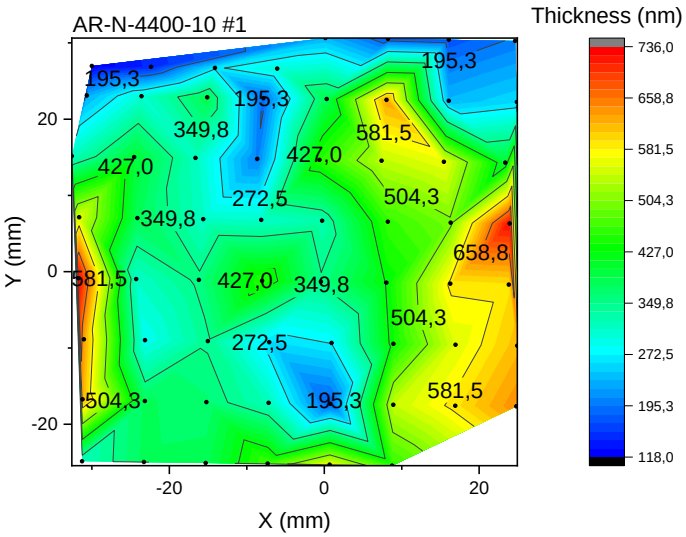

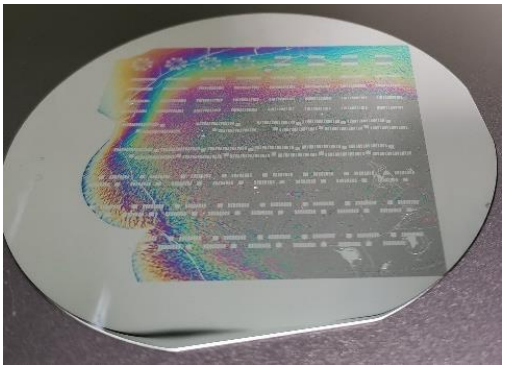

Sample #2

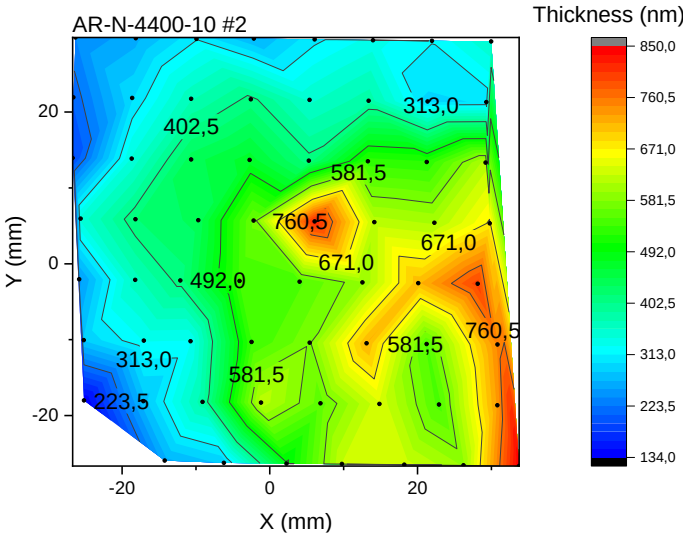

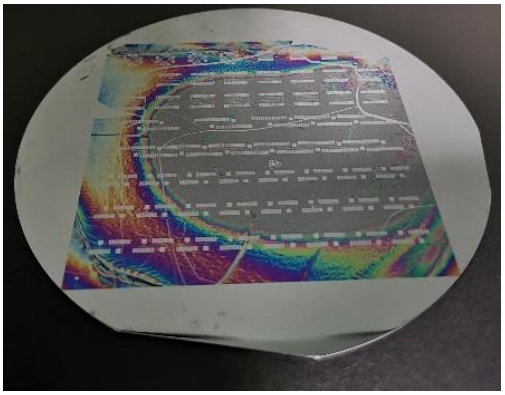

Sample #3

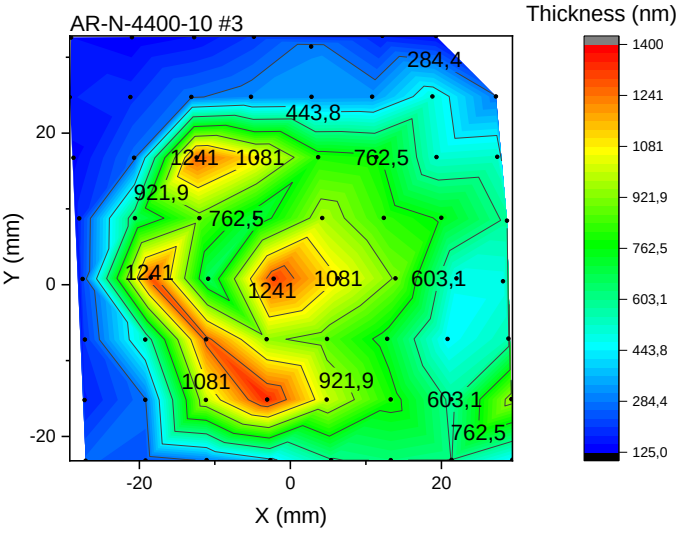

Figure 46: Images and thickness distribution of 3 FTM coated AR-N-4400-10 samples on 4" Si wafer.

So far the spreading occurred in a circular shape, but AR-P-3110 spread differently. Starting from the injection zone (1) the resist formed an inner (2) and outer zone (3). Additionally thin “arms” appeared connected to the outside but in random shapes and not interconnected. In comparison to AR-N-4400, the total area of the film is smaller. The size of the inner zone was measured to 472 mm^2 comparable to the size of AR-N-4400-05. The resist thickness near the border of the inner and outer zone showed only a marginal increase contributing to a low average of P_{Avg}= 223 nm. Even though the solid content is 5 % lower this is 50 to 110 nm less than that of AR-N-4400-05. Being a positive resist means that the resin has a different chain length and density impacting the solidification process. Roughness R_q in Figure 47 averaged 19,7 nm. Similar oscillations as described in 4.3.1 were observed. A 3D map Figure 49 over an extent of 300x300 µm confirmed a wavelike pattern with an overall roughness of S_q=34,0 nm.

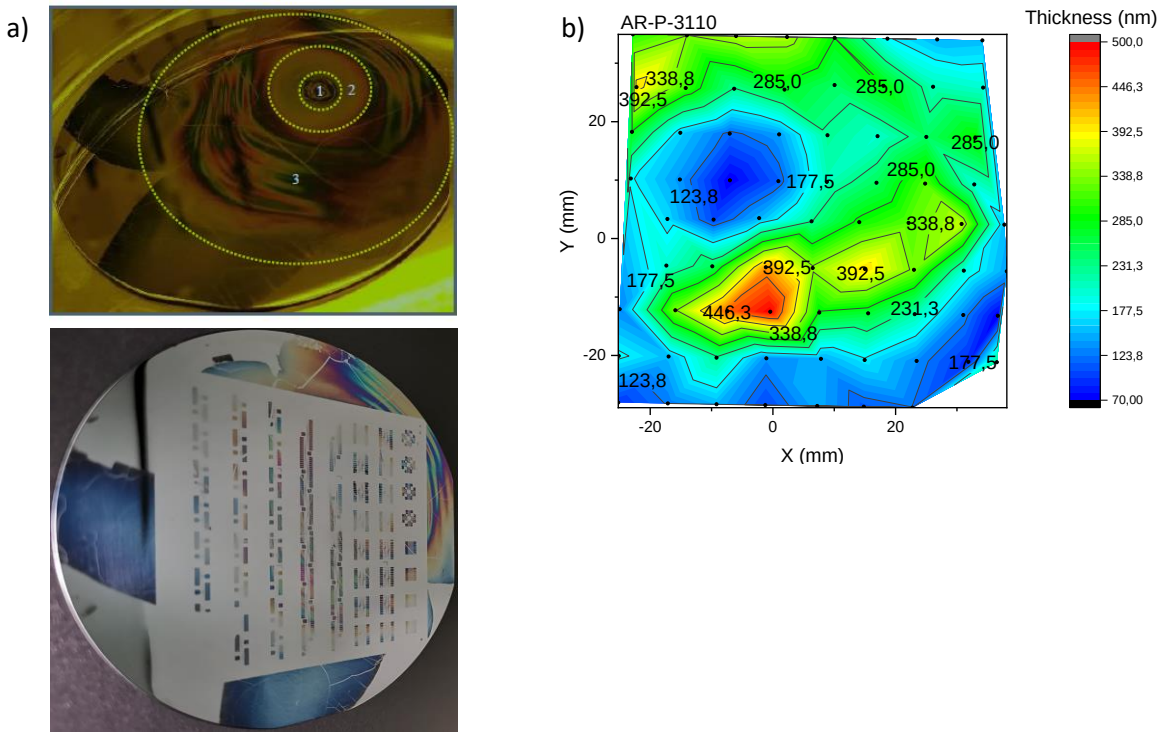

Figure 47:a) AR-P-3110 before and after UV-Lithography, b) contour plot derived from Dektak measurements

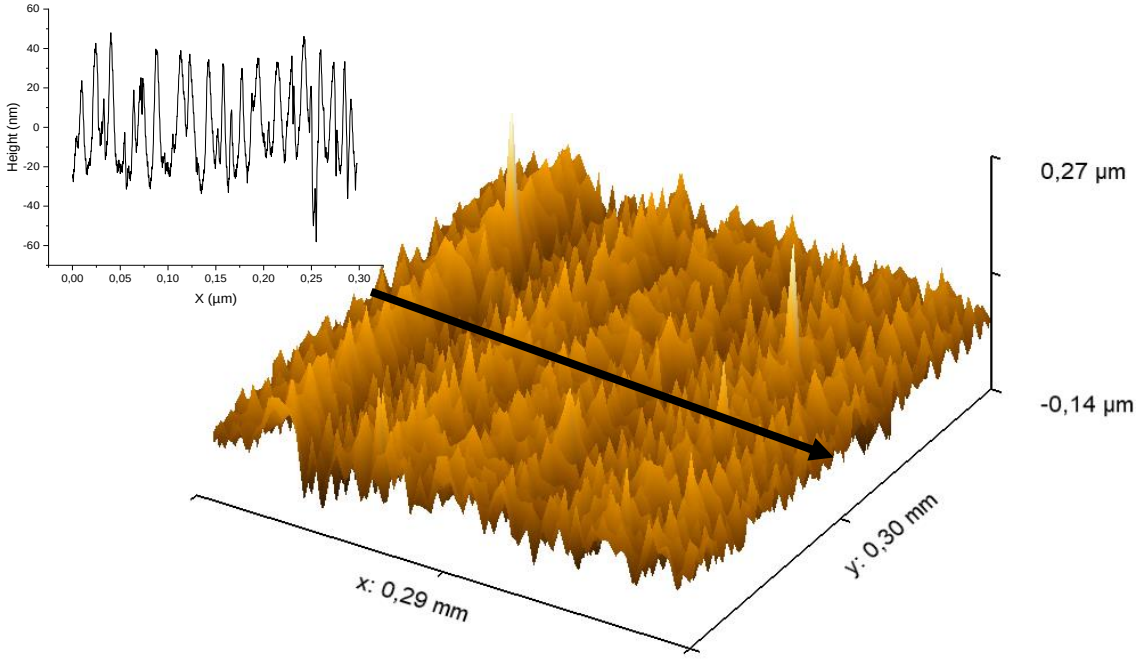

Figure 49: 3D-Map of AR-P-3110 and extracted line profile with visible oscillation.

4.3.3 Influence of Surfactants on the Film

Surface tension gradients as the driving force behind the mass transfer can be manipulated by adding surfactants to the liquid substrate. Adding dishwashing soap effectively reduces the surface tension of water [41]. Solvent from the resist solution, therefore, generates a smaller gradient and reduced spreading can be observed. The spreading can be completely oppressed by adding more surfactant to the liquid substrate. This behavior can be observed in Figure 50. Ellipsometry was performed to measure the resist thickness of the unprocessed samples 1 and 2 with 25 mg and 50 mg surfactant and profilometry to measure sample 3 with 50 mg surfactant after UV-Lithography. Ellipsometry could not be performed on sample 4 (100 mg surfactant). The spot size of the light source was too big covering an area of inhomogeneous resist distribution as indicated by the interference rings. An increase in surfactant resulted in a decrease in film size and inner zone and therefore increase in overall resist thickness. The distance between interference rings was reduced culminating in a perfect circular shape at 100 mg surfactant. Highest layer thickness was found in the inner zone due to slow Marangoni flow with decreasing thickness towards the edge of the film. Roughness of sample 3 was basically unchanged at R_q=4,6 nm compared to a sample without surfactant. Average thickness P_{Avg} increased to 950 nm with a maximum thickness of 2293 nm resulting from the decreased spreading area. The resist still proved to be processable by UV-Lithography. The resist

thickness can therefore be enlarged by lowering the surface tension of the liquid substrate at the cost of a reduced film area.

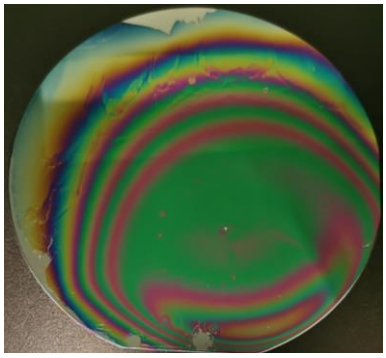

25 mg surfactant

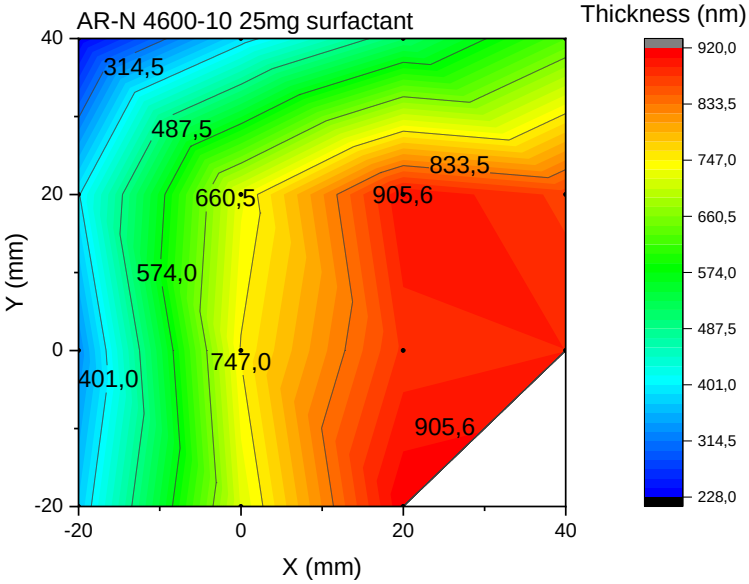

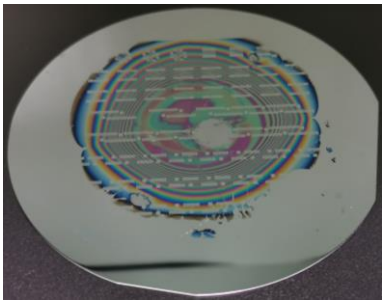

50 mg surfactant

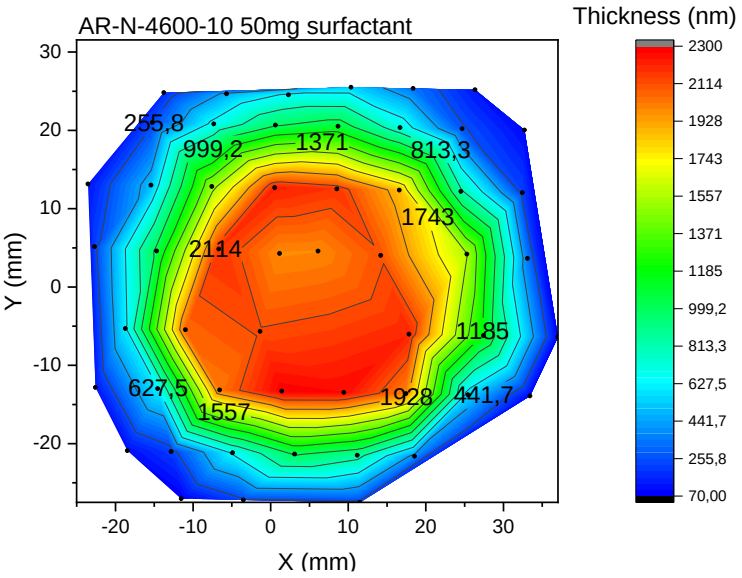

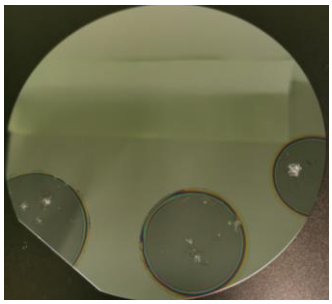

100 mg surfactant

Figure 50: Images and Height distribution gained from ellipsometric and profilometric measurement of FTM coated AR-N-4600-10 with surfactant ("Fit")..

4.3.4 Impact of the substrate surface energy on the coating mechanism

After drying, cracks of various lengths occurred, most likely due to water evaporating underneath the resist film. The goal of this experiment was to reduce the amount of water by manipulating the surface energy of the substrate. Dynasylan F8261 was coated on the wafer and chemically bonded to SiO_2 which is present in a thin layer on all Si wafers without special processing (see **Fehler! Verweisquelle konnte nicht gefunden werden.**) [15]. Fluoroalkyl functionalized silane significantly reduces the surface energy of the substrate and turns the surface hydrophobic. The contact angle was measured to 106,8 ° proofing the hydrophobic character of the sample. The sample was then FTM coated as described. It was assumed that the water is displaced by the resist film during the coating minimizing trapped water between the substrate and resist. Unfortunately, this was not observed. Samples showed smooth and intact surfaces after drying but after tempering at 95 °C visible defects were observed. Microscopic images in Figure 51 revealed the formation of droplets of varying sizes. The reason for this might be poor adhesion corresponding to the oleophobic character of Dynasylan F8261. Contact angles of diiodmethane were measured to 82,9 ° confirming this assumption. The glass transition temperature of AR-N-4600-10 with 33-44 °C was surpassed during the Tempering [47]. Poor adhesion coupled with resist flow on an oleophobic substrate then resulted in the observed drops.

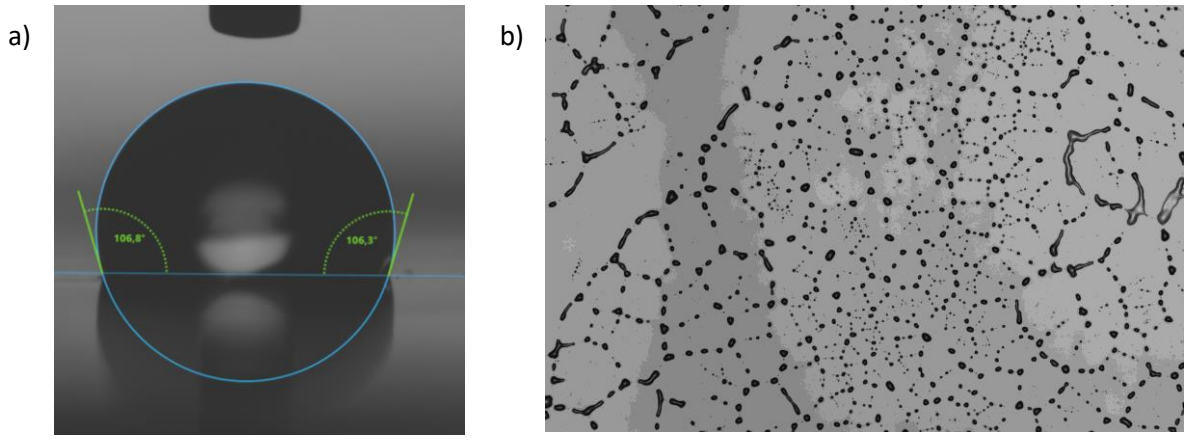

Figure 51: a) Contact angle measurement on Si with Dynasylan confirming the hydrophobic character. b) FTM coated AR-N-4600-10 on a Dynasylan coated Si substrate after tempering at 95 °C on a hotplate.

In contrast to the last experiment this time a superhydrophilic surface was examined. By exposing TiO_2 to UV light oxygen radicals are generated causing a hydrophilic character of the surface [58]. Contact angle measurements were conducted without UV and after 20 min exposure. Water spreads on the surface in a matter of milliseconds. Without UV water shows a contact angle of 60 °. After UV exposure the angle drops to 6 °. The water drop spreads so fast that a highspeed measurement was applied and the contact angle was recorded over time to measure the time it took to reach its minimum value. The contact angle fell below the threshold value of 5 ° in 360 ms. After 1 s the angle can be assumed to be 0 °.

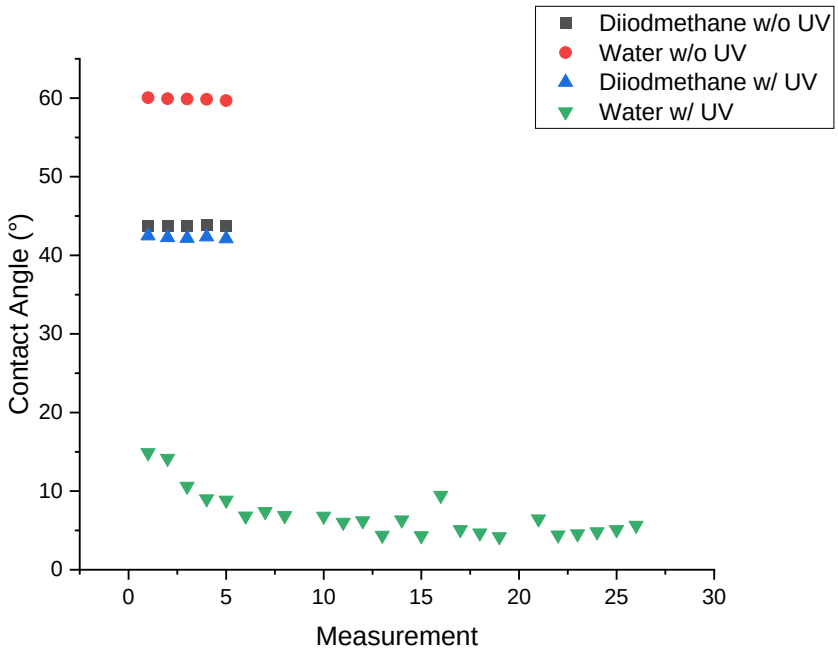

Figure 52: Contact angle measurement on a TiO_2 sample without UV exposure and after 20 min UV exposure.

The hydrophilic TiO_2 layer did not influence the coating mechanism. The resist adhered to the substrate but cracks were also present. The lithographic results in Figure 53 were comparable to samples without TiO_2.

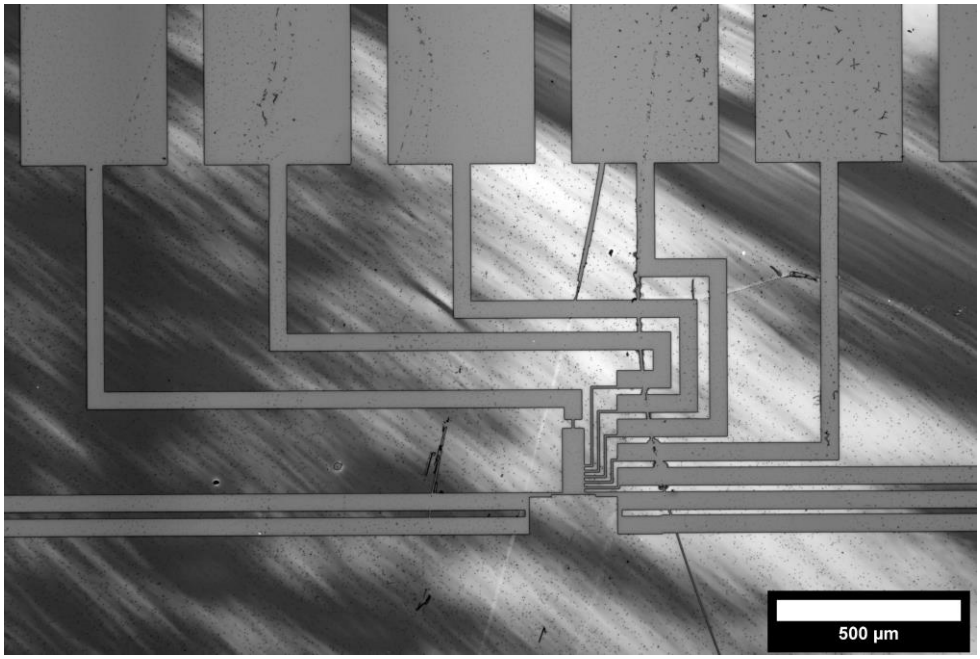

Figure 53: UV-exposed TiO_2 coated with AR-N-4600-10 after UV-Lithography.

4.4 FTM on nonplanar samples

The last chapter described the topology of different resists after FTM and UV-Lithography on planar substrates. Now experiments with the aim of FTM coating nonplanar and curved substrates with photoresists were conducted and will be presented in this chapter.

4.4.1 FTM coat as a protection layer

In this experiment, the capabilities of coating edges of microstructures were assessed. It is assumed that the thin film homogeneously covers the substrate as shown in Figure 54 since the film formation already happened on the liquid surface. Spray-coated samples in contrast show an inhomogeneous coverage as is depictured in *Figure 9* with thin parts at the top and resist accumulations on the bottom part of a wall. Obtaining images in the sideview to evaluate the results would have required difficult sample preparation. Instead, a different approach was chosen. A microstructured positive resist was coated with a negative resist and exposed to an excessive amount of UV. By doing so the positive resist should turn solvable while the negative resist becomes unsolvable. Defects in the negative resist can be made visible by development

in AZ-351. Both defect and defect-free structures were found on the wafer. The height of the sidewall was measured with profilometry (see Figure 56) to 10,4 µm with a slope of 86,7 %. Edges in Figure 55 a) were completely covered in negative resist protecting the underlaying positive resist whereas defects in the negative resist layer in Figure 55 b) created weak points open for development. With the knowledge of previous chapters, it can be assumed that cracks in the negative resist or weak spots due to thin resist layers are responsible for these defects.

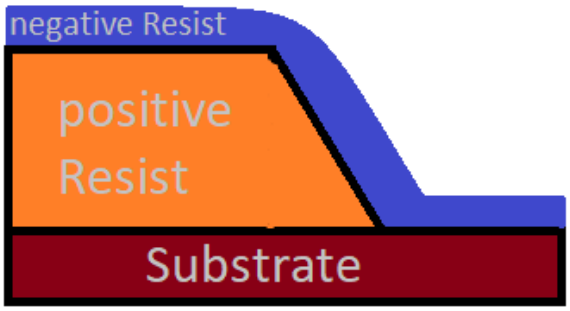

Figure 54: Proposed mechanism of coating edges with FTM resulting in a uniform coat

a)

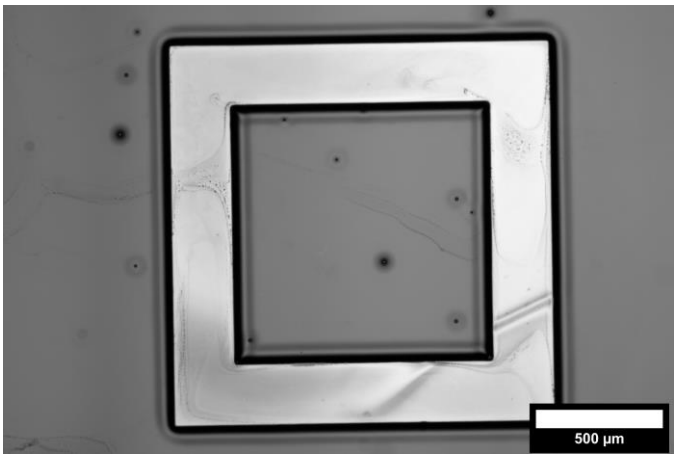

b)

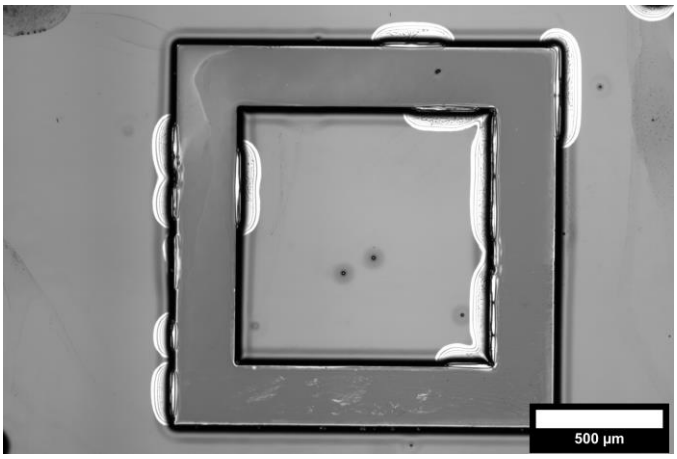

Figure 55: Microstructure in AR-P-3220 coated with AR-N-4600-10 after exposure and development, a) without defects caused by the developer and b) structure with visible development.

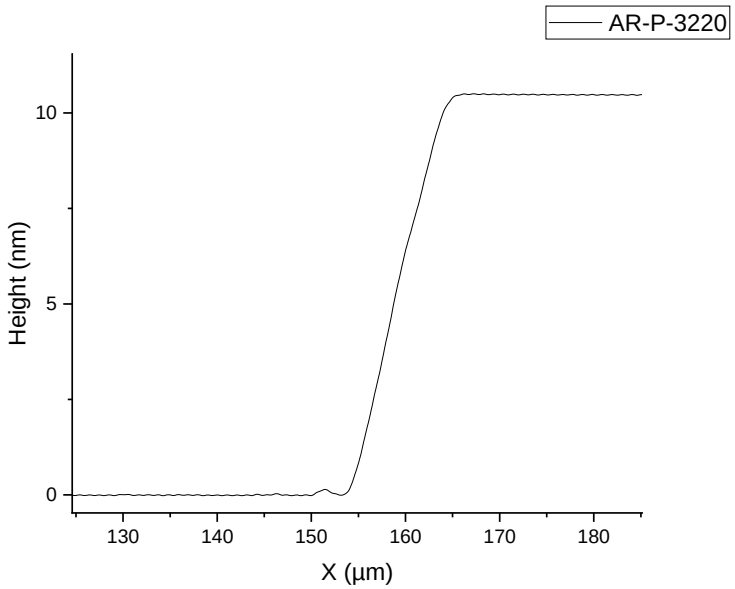

Figure 56: Topology of the wall of the square structure with 10,4 µm thick AR-P 3220.

4.4.2 NIL on nonplanar surfaces

In previous experiments it could be observed that the resist was strong enough to cover the side of the wafer and even the holes of the steel container without tearing, indicating the possibility to coat nonplanar surfaces. In [56] the curved surface of a vial was successfully coated with PTB7:$PC_{71}BM$[3]. Glass lenses of various shapes were therefore FTM coated with AR-N-4600-10 and AR-N-4400-10.

According to the datasheet AR-N-4600-10 is processable by t-NIL [47]. To test the effect of the FTM coating on the t-NIL process a wafer slice was coated with AR-N-4600-10 and a test structure with a pitch of 1,5 µm was transferred by NIL. The rainbow effect as seen in Figure 57 a) indicates a successful transfer. Profilometer measurement was conducted and a periodic pattern (Figure 57 b) with Δ=1,5 µm was found. The depth of the pattern could not be measured owing to the limitation of the profilometer and the tip size of 2 µm.

[3] Poly[[4,8-bis[(2-ethylhexyl)oxy]benzo[1,2-b:4,5-b']dithiophene-2,6-diyl][3-fluoro-2-[(2-ethylhexyl)carbonyl]thieno[3,4-b]thiophenediyl]] (PTB7):[6,6]-Phenyl C71-butyric acid methyl ester ($PC_{71}BM$)

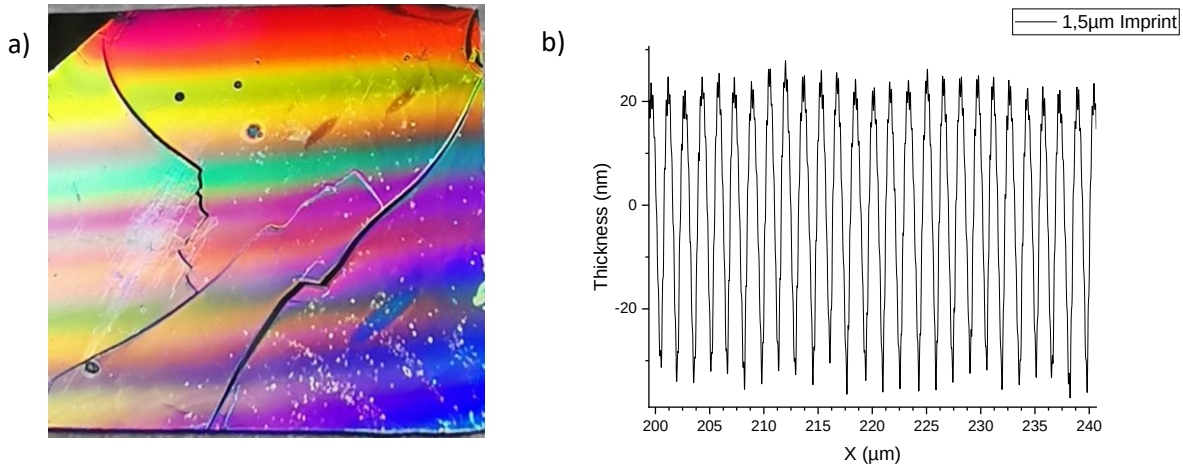

Figure 57: a) Nanoimprinted Si wafer with 1,5µm pitch and visible rainbow effect caused by the pattern. b) Profilometer measurement confirming a 1,5 µm pattern.

The resist proved to be capable of t-NIL so further experiments with nonplanar substrates were conducted.

A glass lens with a radius r=4 mm was coated with AR-N-4600-10. The curvature of the lens was measured to R=6,6 mm resulting in a ratio of r/R=0,6. Double-sided tape was used to fix the position of the lens during the coating process. Figure 58 shows that the film covers approximately 2/3 of the substrate creating a hollow space around it. The curved part however was fully coated. Wrinkles at the edge of the lens indicate stress caused by deformation during the coating process and a relatively stiff film. The lens was processed by NIL as described in 3.5.2. Holographic structures were successfully transferred to the lens. Figure 59 a) shows the combined image of 8 individually stacked darkfield images. Image stacking was necessary due to the curvature of the lens. The black circle in the middle is caused by the transparency and optical properties of the lens paired with the darkfield method only reflecting light in a donut shape. The structure was uniformly transferred in the visible areas with only minor defects which can be traced back to defects in the resist and impurities in the glass. The pattern in Figure 59 b) should represent a cross pattern after the transmission of green light from a laser. Instead, overlapping spots are visible. The curvature of the lens alternates the interference pattern of the holographic structure which is tuned for a flat substrate and distorts the image.

Figure 60 compares the master and the imprint. Structures were transferred 1 to 1. The master itself though was not perfect and showed signs of aging which negatively impacts the resulting pattern even more. Furthermore, non-uniform height distribution of the resist indicated by brighter and darker areas in

Figure *60* b) decrease the image quality of the hologram.

Figure 58: FTM coated Glass lens with AR-N-4600-10. The resist is strong enough to create a hollow space over several mm without tearing. Wrinkles are visible indicating stress caused by deformation.

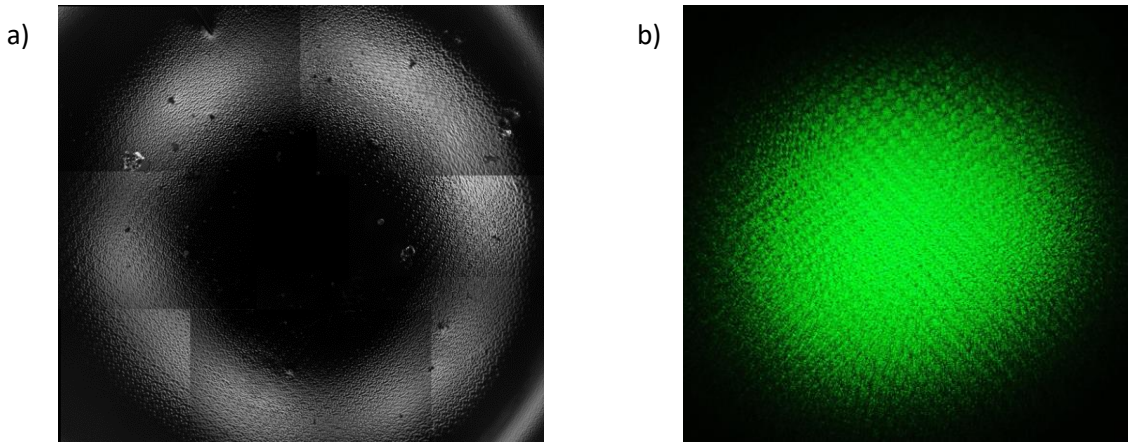

Figure 59: a) Lens coated with AR-N-4600-10 imprinted with holographic structure. Image is stitched together from eight pictures at 5-x magnification. b) Distorted dot pattern after radiating through the lens with a green laser beam.

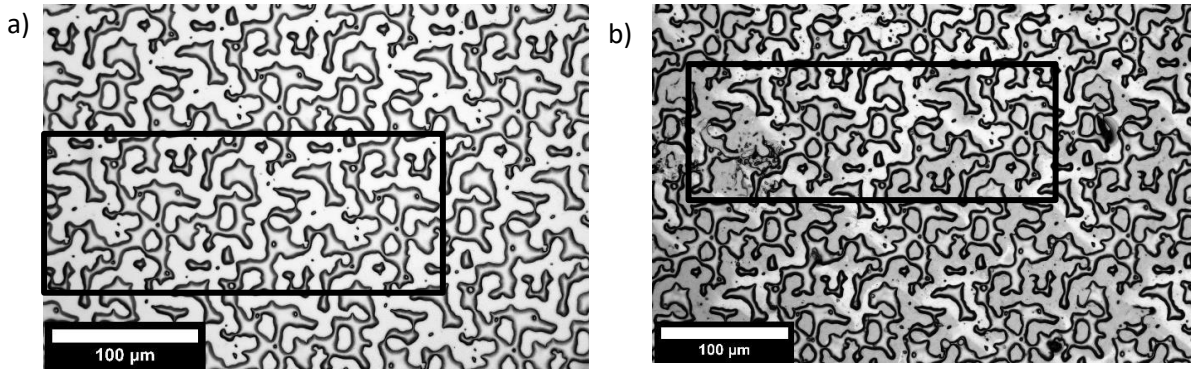

Figure 60: a) PDMS master stamp with a holographic pattern. b) Imprinted pattern in AR-N-4600-10. Black rectangles show the same pattern.

Two less curved lens arrays were coated with AR-N-4400-10 and imprinted, one with the 1,5 µm pitch and one with the holographic structures. The results of the coat and the imprint

are shown in Figure 61 a) and b). The film tore near the border of two smaller lenses of the array where the height difference was too tall. Additionally, the PDMS was not flexible enough to imprint the groove between two lenses. Otherwise, structures were successfully transferred over the entire sample. Both the holographic image of the Bessy logo as well as the dot grid were made visible by the green laser. Bright spots in the middle corresponding to the zero order of the interference pattern can be observed. These indicate poor quality of the holographic structure probably caused by the nonuniform resist thickness, optical properties of the lens, the geometry of the lens distorting the image and bad quality of the master (see Figure 60 a).

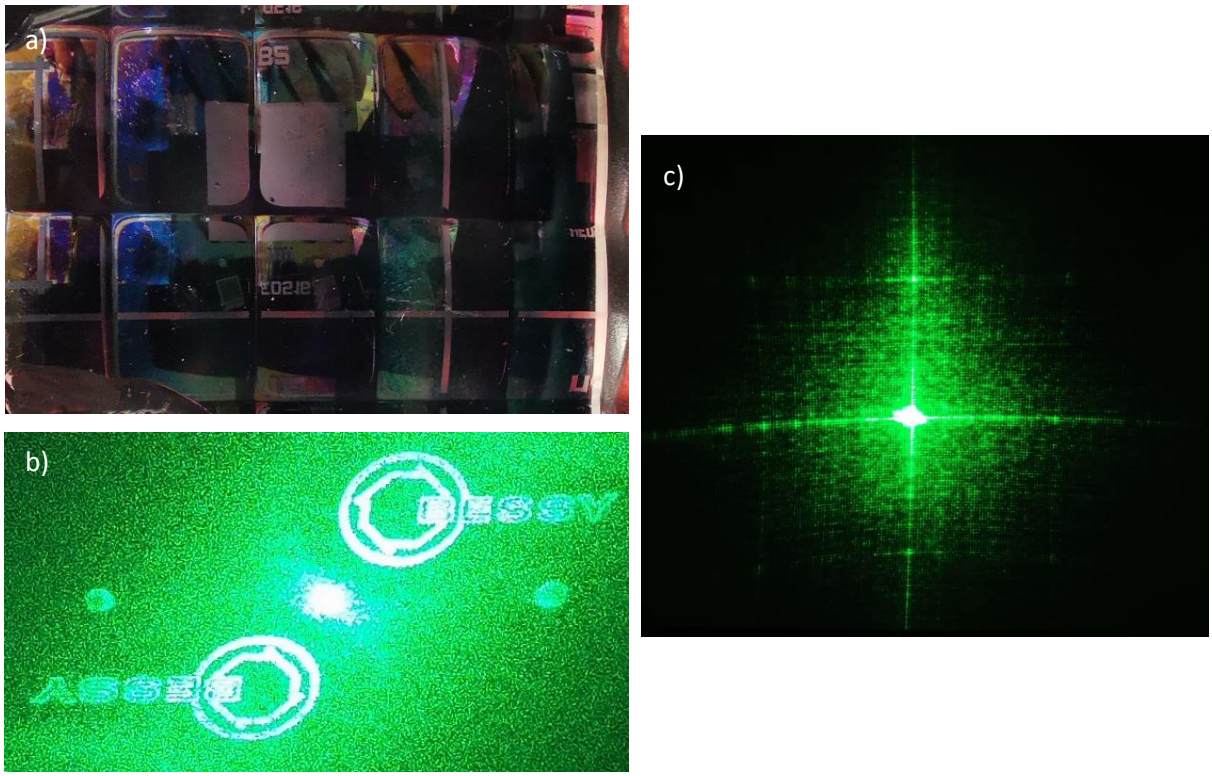

Figure 61: Lens array coated with AR-N-4400-10 and visible imprinted hologram. b) Bessy Logo and c) dot grid visualized by radiating through the lens with a green laser beam.

The second lens imprinted with a 1,5µm pitched structure showed interference up to the 2nd order (see

Figure *62* b). Profilometry was conducted to confirm the existence of the structures over a length of 2 mm with a 0,4 mm height difference. By fitting a circle function to the data in Figure 62 c) a curvature of 5,8 mm was obtained and a ratio of r/R=0,34 can be calculated. After curvature

subtraction, the plot shows the surface profile. The difference in minimum and maximum height was measured to 1,6 µm. Fluctuations can be attributed to the inhomogeneous resist thickness as it was shown in Figure 45 and imperfections of the lens present before coating. The transfer of the periodic pattern was confirmed over 2 mm and additionally in the x and y axes by a 400x400 µm 3D map in Figure 64.

Profilometer measurement of structures with pitches below the diameter of the measuring tip is not reliable. The direction of the measurement must be perpendicular to the pitch. Otherwise, an increased distance would be measured. Therefore, light microscopic images were made (Figure 62 a). As a result of the curvature, the images had to be stacked. However, stacking introduced slight deviations in the line continuity and straightness which does not reflect the real pattern. The stacked image was Fast Fourier transformed to exactly measure the distance between two plateaus. A pitch of 1,51 µm was calculated confirming the profilometer measurement.

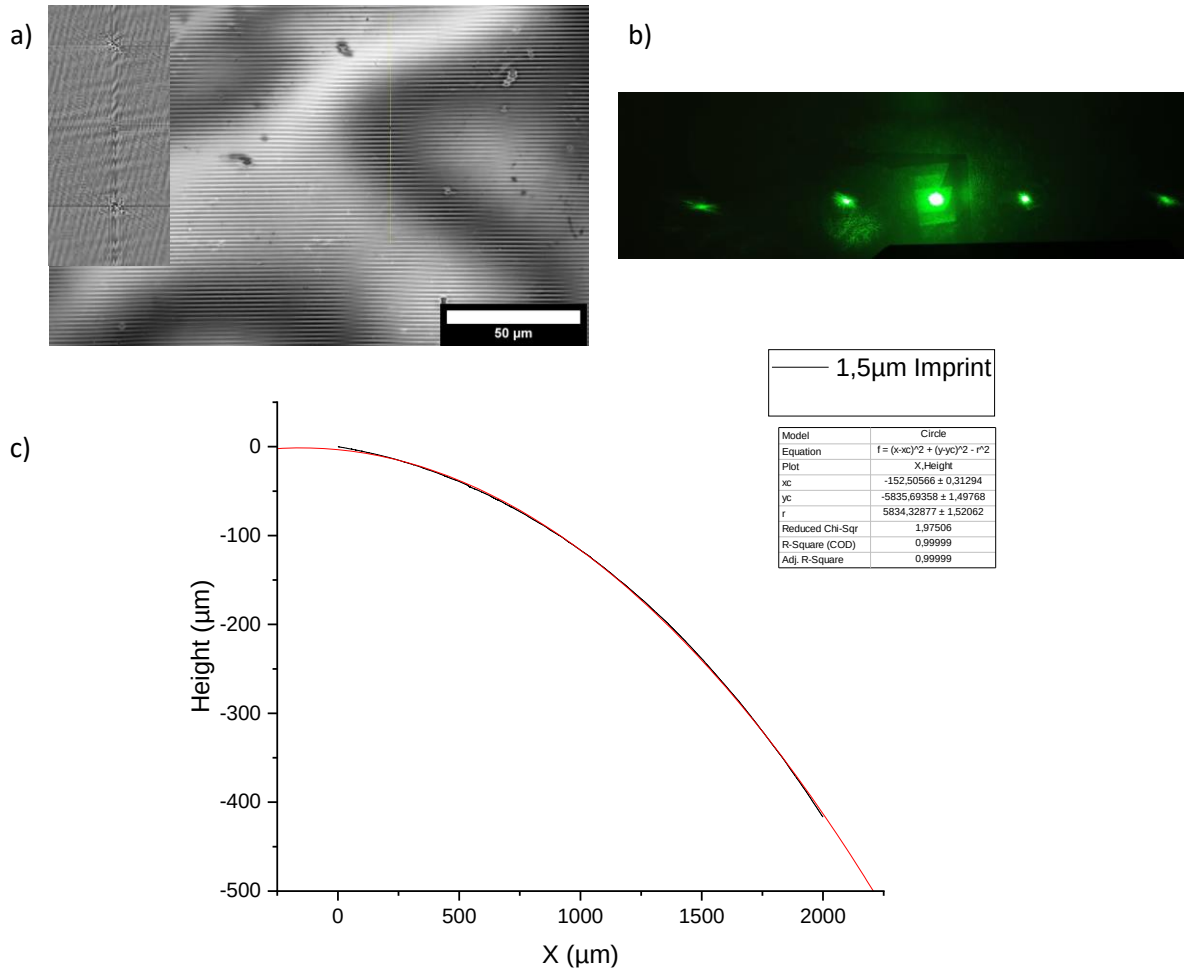

Figure 62: a) Stacked microscopic image showing the periodic pattern in AR-N-4400-10. The inlet image displays the FFT of the image used to measure the pitch to 1,51 µm. b) Interference pattern after radiating through the lens with a green laser beam. c) Original height data acquired by profilometry and circle fit to determine the radius of the lens. d)

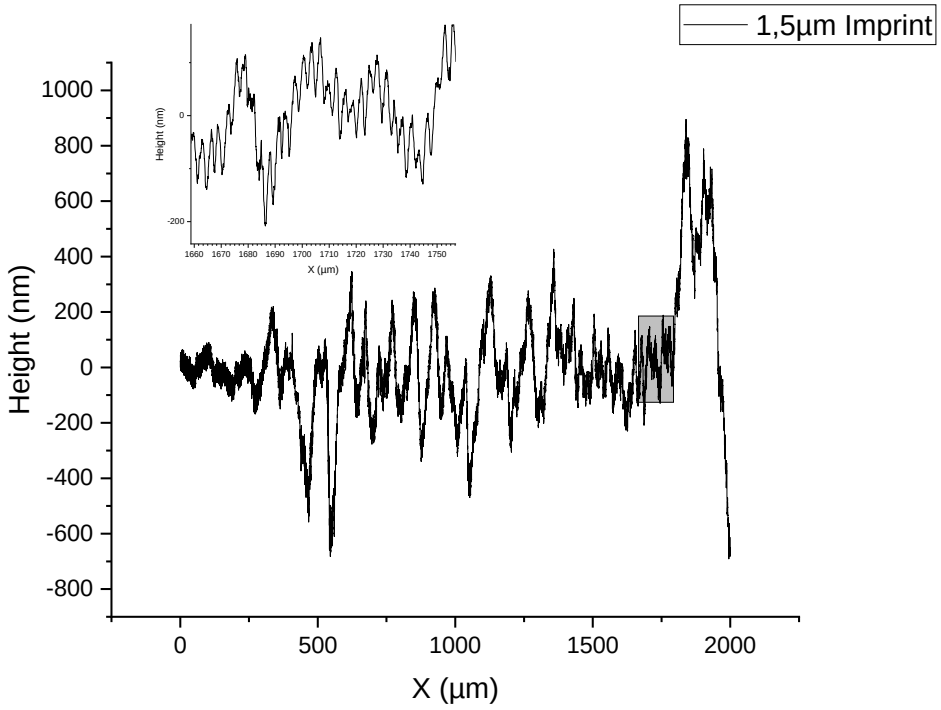

Figure 63: Height profile after curvature subtraction derived from Figure 62 c). The inlet shows the periodic pattern observable over the entire length.

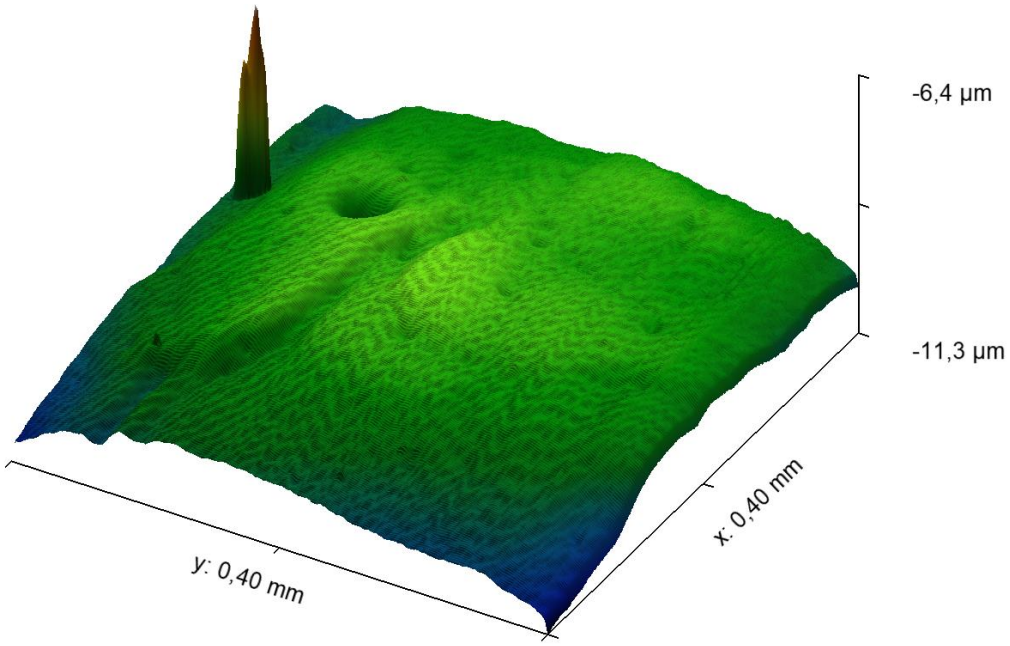

Figure 64: 3D Map of the lens array FTM coated with AR-N-4400-10 and imprinted with a periodic 1,5 µm pattern. (Pattern might not be visible in the printed version)

4.4.3 UV lithography on nonplanar substrates

This experiment was conducted as a proof of concept. Conventional contact mode UV-Lithography was performed with FTM coated nonplanar substrates. To no surprise the results were not great (see *Figure 65*). Only some portions of the lens were in contact with the mask. Areas with no contact were exposed to a broader angle of incidence hence exposing unwanted regions of the substrate. Reflections and scattering caused by the substrate could also have led to defects. To circumvent this laser direct writing was performed. AZ MIR 701 was successfully coated on an amber glass vial and processed. With no optimization fairly straight lines with approximately 1 mm width, spread over a length of 14,2 mm were achieved. The r/R ratio was calculated to 0,52 with a lot of headroom for improvements. Nonetheless it was shown that UV-Lithography can be performed on curved substrates coated by the new FTM method, opening up new possibilities in micro- and nanostructuring curved nonplanar substrates.

a) b)

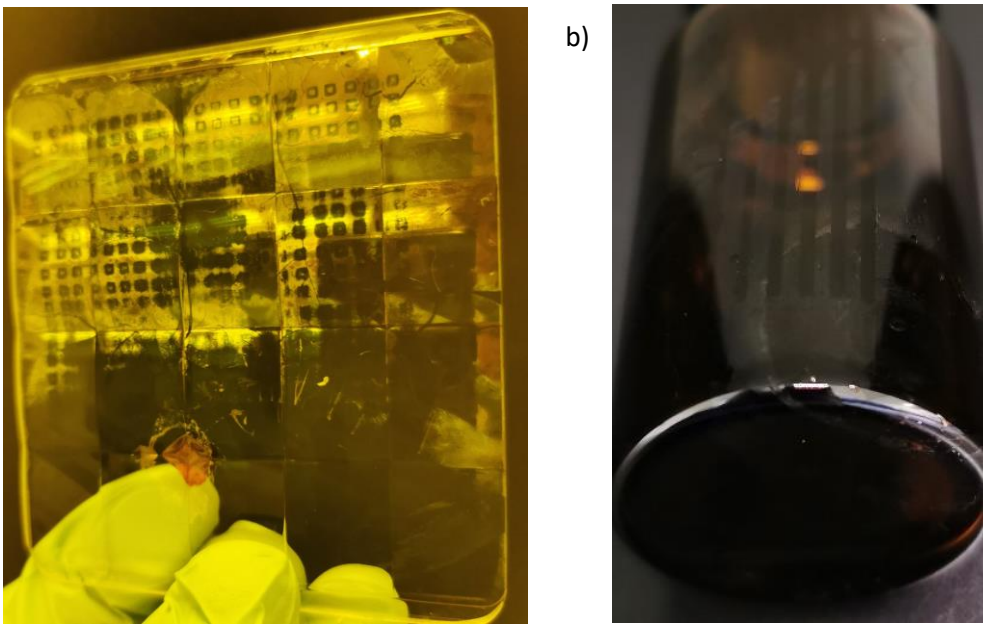

Figure 65: a) AR-P 3110 FTM coated on a lens array and processed by UV-Lithography in contact mode. b) Amber glass vial FTM coated with AZ MIR 701 and processed by Direct Laser writing.

5 Summary

This chapter will summarize the observation and information gained by the conducted experiments.

5.1 FTM film morphology

The FTM method was applied to coat planar and nonplanar substrates. A workflow was presented including the following steps:

1. Cleaning the substrate in alkali based washing solution, acetone and propan-2-ol.

2. Substrate immersion into deionized water with and without additive and optional heating depending on the resist and desired thickness.

3. Drop casting of the photoresist with a fine dosing micro syringe in the middle of a large enough container.

4. Film transfer by lowering the water level with subsequent drying in a vacuum oven for 2-3 h at moderate temperatures of 40-50 °C

5. Optional patterning method: UV-Lithography, Direct Laser Writing or NIL

Flat 4” Si wafer were coated with several photoresists by this method. For all applied photoresists a wave like distribution was observed. The thickness distribution derived from profilometer measurements of all resists and coating conditions is presented in Table 8. The non-uniformitiy in resist distribution effected the quality of the fabricated structures.

A correlation between solid content and resist thickness P_{Avg} as well as roughness R_q was found for AR-N-4400. However, resist distribution was different for samples fabricated with the same process parameters and sample size was low.

Table 8: Min, Max and Avg Thickness and Roughness of each Resist.

Resist	AR-N-4600-10 T_{H2O}=20 °C	AR-N-4600-10 T_{H2O}=40 °C	AR-N-4600-10 50 mg surfactant	AR-N-4400-05	AR-N-4400-10	AR-P-3110
P_{Min} (nm)	107	140	75	112 90 65	119 135 129	71
P_{Max} (nm)	807	628	2293	657 605 891	735 849 1348	498
P_{Avg} (nm)	479	432	948	331 280 349	394 460 578	223
1%σ	37,2 %	26,6 %	83,4 %	41,7 % 46,1 % 50,4 %	38,4 % 38,7 % 61,1 %	43,9 %
R_q (nm)	4	45	5	37 45 45	7 9 9	19

Manipulating the Marangoni flow heavily impacted the achieved resist film. It was found that an increase in water temperature led to increased surface roughness for AR-N-4600-10 and an oscillating pattern that was also found in AR-P-3110. The addition of surfactant effectively reduced the size of the resist film and thereby increased the thickness. Preparing the sample with Dynasylan F8261 to minimize trapped water between the wafer and the film effectively turned the wafer hydrophobic but also resulted in the destruction of the resist film. UV-activated TiO_2 had no effect on the coating mechanism.

5.2 UV-Lithography and NIL

UV-Lithography with FTM coated resists was performed successfully. Positive as well as negative resists proofed to be processable after coating with resolutions as low as 2,3±0,4 µm for AR-P-3110. The positive resist showed overcut resulting in line widening. An amber glass vial was FTM coated with AZ MIR 701 and processed with a laser direct writer resulting in 1 mm lines (r/R=0,52). Non planar surfaces e.g. glass lenses were FTM coated with imprintable negative resists AR-N-4400-10 and AR-N-4600-10. Holographic and periodic pattern were successfully imprinted on these substrates with r/R ratios as low as 0,6.

5.3 Advantages and Disadvantages

Advantages of the new method include:

- Very low resist usage of around 10 µL for 4” wafer
- Minimal waste of resist if the substrate size and film size match
- Coating of nonplanar and microstructured substrates is possible
- Good surface roughness for AR-N-4600-10 and AR-N-4400-10 at T_{H2O}=21 °C

Disadvantages:

- Poor uniformity for all resists
- Poor surface roughness for AR-N-4400-05 and AR-P-3110 with wavelike oscillations of resist thickness
- Defects and tearing after drying observed on all resists
- Limited resist choice
- Multiple coats necessary for µm thick resist films coupled with increased processing time for each run

6 Outlook

The aim of this work was to show the adaptation of the Floating Film Transfer Method as a new way of coating planar and non planar substrates with photoresist. It was shown that FTM coats can be applied for UV-Lithography and NIL. This opens up possibilities for new process. But first questions that occurred during this work need answers.

Further research needs to be conducted to better understand the spreading process. Surface tension measurement during the spreading is suggested to explore the origin of the oscillation in resist thickness. There is also need for theoretical and experimental studies on the Marangoni flow of photoresist solutions on liquid substrates which is believed to be key in fabricating a more uniform resist film. Furthermore studies on the impact of the chemical composition of the resist (e.g. chain length of the resin, different solvents at various concentrations, etc.), different liquid substrates and the addition of surfactants should be conducted to optimize the method.

There is room for improvement of the UV-Lithography process parameters to achieve smaller structures either by optimizing the here conducted experiments or by investigating into new resist materials, fine tuned to the FTM method.

There are plenty of possible applications for FTM coated photoresist like:

- Coating of deep grooves and structures in MEMS fabrication
- Improving optical properties like transmission or reflectivity of lenses of by patterning the surface [18,21].
- 3D traces on PCBs over electrical components
- Self cleaning surfaces on curved substrates through nanopatterning

References

[1] Ghodssi R, Lin P. MEMS Materials and Processes Handbook. Boston, MA: Springer US; 2011.

[2] Willson CG, Dammel RR, Reiser A. Photoresist materials: a historical perspective. In: Advances in Resist Technology XIV, Vol. 3049.p. 28–41.

[3] Manouras T, Argitis P. High Sensitivity Resists for EUV Lithography: A Review of Material Design Strategies and Performance Results. Nanomaterials (Basel) 2020;10(8).

[4] Sun E. TSMC Details Impact of Fab 14B Photoresist Material Incident, Updates 1Q'19 Guidance; Available from: https://pr.tsmc.com/system/files/newspdf/PGWQISTHTH/NEWS_FILE_EN.pdf (25 April 2022).

[5] Feng X-G, Sun L-C. Mathematical model of spin-coated photoresist on a spherical substrate. Opt Express 2005;13(18):7070–5.

[6] Eun D-S, Kim D-W, Seo C-T, Lee J-H, Bae Y-H, Yu I-S, Suk C-G. Photoresist Spray Coating for Resist Film Performance of Deep Silicon Cavities. J. Korean Phys. Soc. 2007;50(6):1947.

[7] Pham NP, Boellaard E, Burghartz JN, Sarro PM. Photoresist Coating Methods for the Integration of Novel 3-D RF Microstructures. J. Microelectromech. Syst. 2004;13(3):491–9.

[8] Pham NP, Tezcan DS, Ruythooren W, Moor P de, Majeed B, Baert K, Swinnen B. Photoresist coating and patterning for through-silicon via technology. J. Micromech. Microeng. 2008;18(12):125008.

[9] Kosbar LL. Multicomponent Langmuir–Blodgett resists for optical lithography. J. Vac. Sci. Technol. B 1990;8(6):1441.

[10] Roberts GG, Pitt CW. Langmuir–Blodgett Films, 1982. Elsevier; 1983.

[11] Biolinscientific. Langmuir and Langmuir-Blodgett; Available from: https://www.biolinscientific.com/measurements/langmuir-and-langmuir-blodgett (14 April 2022).

[12] Morita T, Singh V, Nagamatsu S, Oku S, Takashima W, Kaneto K. Enhancement of Transport Characteristics in Poly(3-hexylthiophene) Films Deposited with Floating Film Transfer Method. Appl. Phys. Express 2009;2(11):111502.

[13] Pandey M, Singh V, Kumar C, Pandey SS, Nakamura M. Recent progress in the macroscopic orientation of semiconducting polymers by floating film transfer method. Jpn. J. Appl. Phys. 2022;61(SB):SB0801.

[14] Tiwari S, Takashima W, Nagamatsu S, Balasubramanian SK, Prakash R. A comparative study of spin coated and floating film transfer method coated poly (3-hexylthiophene)/poly (3-hexylthiophene)-nanofibers based field effect transistors. Journal of Applied Physics 2014;116(9):94306.

[15] Koch C, Rinke TJ. Fotolithografie: Theorie und Anwendung von Fotolacken Entwicklern, Ätzchemikalien und Lösemittel. Microchemicals; 2012.

[16] ASML. The science behind the chip; Available from: https://www.asml.com/en/technology/lithography-principles (14 April 2022).

[17] Versolato OO. Physics of laser-driven tin plasma sources of EUV radiation for nanolithography. Plasma Sources Sci. Technol. 2019;28(8):83001.

[18] Jacobo-Martín A, Jost N, Hernández JJ, Domínguez C, Vallerotto G, Askins S, Antón I, Rodríguez I. Roll-to-roll nanoimprint lithography of high efficiency Fresnel lenses for micro-concentrator photovoltaics. Opt Express 2021;29(21):34135–49.

[19] Shin YJ, Shin MJ, Guo LJ, Shin JS. Fabrication of contact lens containing high-performance wire grid polarizer. Polym. Int. 2017;66(9):1269–74.

[20] Ocier CR, Richards CA, Bacon-Brown DA, Ding Q, Kumar R, Garcia TJ, van de Groep J, Song J-H, Cyphersmith AJ, Rhode A, Perry AN, Littlefield AJ, Zhu J, Xie D, Gao H, Messinger JF, Brongersma ML, Toussaint KC, Goddard LL, Braun PV. Direct laser writing of volumetric gradient index lenses and waveguides. Light Sci Appl 2020;9(1):196.

[21] AlQattan B, Yetisen AK, Butt H. Direct Laser Writing of Nanophotonic Structures on Contact Lenses. ACS Nano 2018;12(6):5130–40.

[22] Kirchner R, Guzenko VA, Schift H. Single-digit 6-nm multilevel patterns by electron beam grayscale lithography. Advanced Optical Technologies 2019;8(3-4):175–80.

[23] MOON S, KIM J. Chemistry of photolithographic imaging materials based on the chemical amplification concept. Journal of Photochemistry and Photobiology C: Photochemistry Reviews 2008.

[24] Schirmer M, Kaiser C, Perseke D. Resist Wiki; Available from: https://www.allresist.de/wp-content/uploads/2015/07/allresist_resistwiki_druckversion.pdf (25 April 2022).

[25] Hilleringmann U. Silizium-Halbleitertechnologie. Wiesbaden: Springer Fachmedien Wiesbaden; 2014.

[26] Norrman K, Ghanbari-Siahkali A, Larsen NB. 6 Studies of spin-coated polymer films. Annu. Rep. Prog. Chem., Sect. C 2005;101:174.

[27] Weber D. Optimierung der Prozessstabilität für die Herstellung von nanoskaligen Strukturen durch Laserinterferenzlithographie. Masterarbeit. Zwickau; 2017 (16 June 2016).

[28] Krebs FC. Fabrication and processing of polymer solar cells: A review of printing and coating techniques. Solar Energy Materials and Solar Cells 2009;93(4):394–412.

[29] Chen BT. Investigation of the solvent-evaporation effect on spin coating of thin films. Polym. Eng. Sci. 1983;23(7):399–403.

[30] Das R, Chanda A. Fabrication and Properties of Spin-Coated Polymer Films. In: Fakirov S (editor). Nano-size Polymers. Cham: Springer International Publishing; 2016.p. 283–306.

[31] Yu L, Lee YY, Tay FEH, Iliescu C. Spray Coating of Photoresist for 3D Microstructures with Different Geometries. J. Phys.: Conf. Ser. 2006;34:937–42.

[32] Fowler M, Bai D, Planje C, Shao X. High-Aspect Ratio Planarization using Self-Leveling Materials. Additional Conferences (Device Packaging, HiTEC, HiTEN, and CICMT) 2012;2012(DPC):2567–86.

[33] Kayaku Advanced Materials I. SU-8 Permanent Negative Epoxy Photoresist: Technical Datasheet; 2020; Available from: https://kayakuam.com/wp-content/uploads/2020/09/KAM-SU-8-50-100-Datasheet-9.3.20-Final.pdf (18 June 2021).

[34] Grund T, Fischer K. Optimizing Spray Coating Yield and Throughput. In: SUSS Report, 1/2014.p. 1–4.

[35] Pham NP, Scholtes TL, Klerk R, Wieder B, Sarro PM, Burghartz JN. Direct spray coating of photoresist for MEMS applications. In: Karam JM, Yasaitis JA (editors). Micromachining and Microfabrication Process Technology VII. SPIE; 2001.p. 312–9.

[36] Michel A. Aegerter., Martin Mennig (editors). Sol-Gel Technologies for Glass Producers and Users. Boston, MA, s.l.: Springer US; 2004.

[37] Griffin J, O´Kane M. Dip Coating: Practical Guide to Theory and Troubleshooting; Available from: https://www.ossila.com/en-eu/pages/dip-coating (25 April 2022).

[38] Fahrner W. Nanotechnologie und Nanoprozesse. Berlin, Heidelberg: Springer Berlin Heidelberg; 2017.

[39] Handrea-Dragan M, Botiz I. Multifunctional Structured Platforms: From Patterning of Polymer-Based Films to Their Subsequent Filling with Various Nanomaterials. Polymers (Basel) 2021;13(3).

[40] Fu N, Liu Y, Ma X, Chen Z. EUV Lithography: State-of-the-Art Review. Journal of Microelectronic Manufacturing 2019;2(2):1–6.

[41] Lauth GJ, Kowalczyk J. Einführung in die Physik und Chemie der Grenzflächen und Kolloide. Berlin, Heidelberg: Springer Berlin Heidelberg; 2016.

[42] Thomson J. XLII. On certain curious motions observable at the surfaces of wine and other alcoholic liquors. The London, Edinburgh, and Dublin Philosophical Magazine and Journal of Science 1855;10(67):330–3.

[43] Mandsberg NK, Boi S, Bunckenburg DA, Zhang M, Pastorino L, Boisen A. Marangoni-induced pepper-patterns: Transition from circle to star shape. Surfaces and Interfaces 2021;26:101443.

[44] Yadav N, Kumari N, Ando Y, Pandey SS, Singh V. Development of High-Sensitivity Poly(2,7-(9,9-dioctylfluorene)- alt -5,5-(4′,7′-di-2-thienylbenzo [c][1,2,5]thiadiazole)) Thin-Film-Based Phototransistors by the Ribbon-Floating Film Transfer Method. Phys. Status Solidi RRL 2021;15(8):2100185.

[45] Pandey M, Gowda A, Nagamatsu S, Kumar S, Takashima W, Hayase S, Pandey SS. Rapid Formation and Macroscopic Self-Assembly of Liquid-Crystalline, High-Mobility, Semiconducting Thienothiophene. Adv. Mater. Interfaces 2018;5(6):1700875.

[46] Pandey M. Controlling the Orientation of Semiconducting Polymers in Floating Film for Anisotropic Charge Transport inOrganic Field Effect Transistor; 2017.

[47] Allresist. AR-N4600 Atlas46 Produktinformationen; Available from: https://www.allresist.de/wp-content/uploads/2020/03/AR-N4600_Atlas46_Deutsch_Allresist_Produktinformationen.pdf (24 March 2022).

[48] Allresist. Parametersammlung AR-Resists; Available from: https://www.allresist.de/wp-content/uploads/2016/03/parametersammlung_ar-resists.pdf (25 April 2022).

[49] Roché M, Li Z, Griffiths IM, Le Roux S, Cantat I, Saint-Jalmes A, Stone HA. Marangoni Flow of Soluble Amphiphiles. Phys. Rev. Lett. 2014;112(20).

[50] Rasouli SA. Fabrication of Superhydrophobic-Superoleophilic Membranes for Oil-Water Separation Applications. St. John’s, Newfoundland and Labrador, Canada; 2021.

[51] Wang R, Hashimoto K, Fujishima A, Chikuni M, Kojima E, Kitamura A, Shimohigoshi M, Watanabe T. Light-induced amphiphilic surfaces. Nature 1997;388(6641):431–2.

[52] Tompkins HG, Irene EA. Handbook of ellipsometry. Norwich NY, Heidelberg Germany: William Andrew Pub; Springer; 2005.

[53] SENTECH Instruments GmbH. SE 800 Short Manual; Available from: https://www.sentech.com/en/site__305/ (25 April 2022).

[54] Wlodek J, Gofron KJ, Cai YQ. Achieving 3D imaging through focus stacking. In: AIP Conference Proceedings (2019), Vol. 2054.p. 50001.

[55] FRANZIS Verlag GmbH. FOCUS Projects 3 Professional - Handbuch.

[56] Noh J, Jeong S, Lee J-Y. Ultrafast formation of air-processable and high-quality polymer films on an aqueous substrate. Nat Commun 2016;7:12374.

[57] Kovalchuk N. Spontaneous oscillations due to solutal Marangoni instability: air/water interface. Open Chemistry 2012;10(5):1423–41.

[58] Janczarek M, Hupka J, Kisch H. Hydrophilicity of TiO2 exposed to UV and VIS Radiation. Physicochemical Problems of Mineral Processing;2006(40):287–92.

Declaration of Originality

I hereby declare that the present thesis and the work reported herein was composed by and originated entirely from me without any help.

All sources used from published or unpublished work of others are reported in the list of references. All parts of my work that are based on others' work are cited as such.

This thesis has not been submitted for any degree or other purposes, neither at the Westsächsische Hochschule Zwickau nor at any other university or college.

Date _____ Signature _____